Dissertation

submitted to the

Combined Faculty of Natural Sciences and Mathematics

of the Ruperto-Carola University Heidelberg, Germany

for the degree of

Doctor of Natural Sciences

presented by

M.Sc. Sandra Katharina Specht

born in Staßfurt, Germany

Oral examination: 10.12.2018

Structure-function analysis and membrane association of *Leishmania tarentolae* and *Plasmodium falciparum* Erv

Referees: Prof. Dr. Michael Lanzer

Prof. Dr. Marcel Deponte

Table of contents

Acknowledgements

I would like to pay my gratitude to Prof. Dr. Marcel Deponte for giving me the opportunity to perform my PhD in his lab and on this project. Thank you for the supervision, the teaching and the many experiences I have gained thanks to you.

Further I would like to thank Prof. Dr. Michael Lanzer for the opportunity to work at the parasitology department. Thank you for the discussions on this project and the consulting in the “TAC” meetings.

Thank you, Prof. Dr. Christine Clayton and PhD Silvia Portugal, for the suggestions on this project, your advice during the “TAC” meetings and for reviewing my thesis.

I would also like to thank Margarida Duarte and Kai Hell and their labs for the collaboration on the research paper.

I am grateful to Marcel Deponte, Linda Liedgens, Verena Staudacher, Gino Turra, Natalie Schneider, Kristoffer Rauch, Franz Hoffmann and Sabine Johnson-Daum for the proofreading and suggestions on this thesis.

A very special thank you goes to all the gladiators who have joined me in battle! Thank you, Linda Liedgens, Verena Staudacher, Cletus Wezena, Kristina Feld, Johannes Krafczyk, Gino Turra, Robin Schumann, Fabian Geissel, Mirko Höhn, and Maryam Talebi Haghighi for the warm welcome in the lab; the action, happy times and strange singing you brought with you to the lab, and for the shared adventures outside the lab exploring the beautiful sides of Heidelberg and the Pfalz. Thank you all for the work-related input and your great ideas during coffee breaks or seminars. But thank you even more for “the loveliness” (to quote Cletus), all your encouragement and the hilarious moments. It was amazing to have you around me every day!

A big thank you to my shared flat mates in Heidelberg and Kaiserslautern. To the “Brückenstreet Gang”, Anja Thomas, Franz Hoffmann, and Hendrick Wulfken for all the lovely times, your encouragement and your friendship even after I have left town. To Tim Schöndube and Matthias Blum for giving me a home and making me feel at home in Kaiserslautern.

Ich danke auch meinen Eltern, meinem Bruder und Oma und Opa für den Rückhalt während der Doktorarbeit und eigentlich immer!

Zu Letzt möchte ich mich noch bei Natalie Schneider und Kristoffer Rauch bedanken. Vielen Dank, Natalie und Hasi, für die ganze seelische Unterstützung, das Anfeuern, Mitjubeln; Liebhaben und Aufbauen, wenn alles furchtbar war!

Summary

Throughout evolution most of the mitochondrial genes have been transferred to the nuclear genome. Thus, proteins targeting one of the four mitochondrial compartments have to be translocated after their synthesis in the cytosol. This process is essential for mitochondrial biogenesis in all eukaryotes. Nevertheless, mitochondrial protein import machineries of parasitic protists differ significantly from the established models in opisthokonts (e.g. mammals and yeast), although import signals are functionally conserved.

In yeast and mammals, Mia40/CHCHD4 and the sulfhydryl electron transferase Erv1/ALR are the essential components for the import and oxidative folding of sulphur-containing proteins in the mitochondrial intermembrane space. Substrates of this pathway carry conserved cysteine motifs that are recognised by Mia40 and subsequently oxidized to the formation of intramolecular disulphide bonds. In a disulphide relay system, electrons are transported from Mia40 to Erv1 and on to cytochrome *c*, which finally introduces them into the respiratory chain. However, a Mia40 homologue could not be identified in the genome of important apicomplexan and kinetoplastid parasites, while Erv1 is ubiquitously conserved. Both the Erv homologues from the kinetoplastid parasite *Leishmania tarentolae* (*Lt*Erv) and the malaria parasite *Plasmodium falciparum* (*Pf*Erv) were imported into yeast mitochondria but failed to replace their yeast counterpart.

Here I analyse structure-function relationships of *Lt*Erv in the endogenous as well as the opisthokont model system *Saccharomyces cerevisiae*. I characterise particularities of the overall structure and the cysteine motifs that distinguish the protein from other homologues that actually interact with Mia40. The most obvious features comprise an additional C-terminal domain (KISS) restricted to this group of parasites and a partially conserved cysteine residue close to the N-terminus (C17). Yeast complementation assays suggest that the presence of the KISS domain does not inactivate the protein in the yeast system. In contrast, *Lt*Erv gained functionality when C17 was removed or the yeast shuttle arm was N-terminally fused to the protein. Residue C17 is therefore most likely the reason why *Lt*Erv does not interact with yeast Mia40 and interrupts the oxidative protein folding machinery in yeast. However, the translocation of *Lt*Erv itself into yeast mitochondria is not affected. Unlike soluble *Sc*Erv1, the protist protein is presumably imported due to its membrane association. Whether the translocation of *Lt*Erv is structurally connected to its dysfunction in yeast and controlled by a conserved *trans* side receptor or by protein-lipid interactions remains to be further investigated. Additionally, the data strongly support the existence of a Mia40 replacement in parasitic protists because both *Lt*Erv and *Pf*Erv were unable to initiate substrate import on their own in yeast mitochondria. Potential replacement candidates were enriched by trapping mixed disulphide intermediates with a model substrate and have to be evaluated in the future.

Zusammenfassung

Im Laufe der Evolution wurden die meisten mitochondrialen Gene in das nukleare Genom überführt. So müssen Proteine, die für die Mitochondrien bestimmt sind, nach ihrer Synthese im Cytosol in die jeweiligen Kompartimente transloziert werden. Dieser Prozess ist für die Biogenese aller eukaryotischen Mitochondrien unerlässlich. Dennoch unterscheiden sich die parasitären Proteinimport Maschinerien deutlich von den etablierten Modellen der Opisthokonta (z.B. Säugetiere und Hefe). Die Importsignale der Proteine sind jedoch funktionell erhalten.

In Hefe und Säugetieren sind Mia40/CHCHD4 und die Sulfhydryl-Elektronentransferase Erv1/ALR die wesentlichen Komponenten für den Import und die oxidative Faltung von schwefelhaltigen Proteinen im mitochondrialen Intermembranraum. Substrate dieses Importweges tragen konservierte Cystein-Motive, die von Mia40 erkannt und anschließend zur Ausbildung intramolekularer Disulfidbrücken oxidiert werden. In einem „Disulfid Relay System“ werden Elektronen von Mia40 auf Erv1 und weiter auf Cytochrom *c* übertragen, welches diese schließlich in die Atmungskette einführt. Die Genome wichtiger parasitärer Eukaryoten (*Apicomplexa* und *Kinetoplastida*) kodieren jedoch kein Mia40 Homolog, während Erv1 durchgehend konserviert ist. Die Erv-Proteine des parasitären *Kinetoplastida Leishmania tarentolae* (*Lt*Erv) und des Malariaparasiten *Plasmodium falciparum* (*P*fErv) wurden in Hefemitochondrien importiert, konnten dort aber das Hefependant nicht ersetzen.

In dieser Arbeit untersuche ich Struktur-Funktionsbeziehungen von *Lt*Erv im endogenen sowie im heterologen Modellsystem *Saccharomyces cerevisiae*. Dabei werden die Besonderheiten der gesamten Proteinstruktur und der Cystein-Motive charakterisiert, welche das Protein von jenen Homologen unterscheidet, die mit Mia40 interagieren. Die offensichtlichsten Strukturmerkmale von *Lt*Erv sind eine zusätzliche C-terminale Domäne (KISS), die ausschließlich bei dieser Gruppe von Parasiten vorkommt und ein teilweise konservierter Cysteinrest in der Nähe des N-Terminus (C17). Komplementationsstudien deuten darauf hin, dass die KISS-Domäne keinen Einfluss auf die Inaktivität des Proteins im Hefesystem hat. Im Gegensatz dazu gewann *Lt*Erv an Funktionalität, wenn C17 entfernt oder der Hefeshuttlearm N-Terminal mit dem Protein fusioniert wurde. C17 ist daher höchstwahrscheinlich der Grund, warum *Lt*Erv nicht mit *Sc*Mia40 interagiert und die oxidative Proteinfaltungsmaschinerie in Hefe stört. Die Translokation von *Lt*Erv selbst ist dabei jedoch nicht betroffen. Im Gegensatz zu frei löslichem *Sc*Erv1 wird *Lt*Erv vermutlich aufgrund seiner Membranassoziation importiert. Ob die Translokation von *Lt*Erv strukturell an die Inaktivität in Hefe gekoppelt ist und über einen konservierten transseitigen Rezeptor oder über Protein-Lipid-Interaktionen gesteuert wird, muss noch weiter untersucht werden. Darüber hinaus unterstützen die Daten nachdrücklich die Existenz eines Mia40-Ersatzes in diesen Protisten, da sowohl *Lt*Erv als auch *Pf*Erv nicht in der Lage waren, eigenständig den Substratimport in Hefemitochondrien einzuleiten. Potentielle Kandidaten für ein Ersatzprotein wurden

in Form von gemischten Disulfid-Zwischenprodukten über ein Modelsubstrat angereichert, bedürfen jedoch noch weiterer Auswertung.

List of Figures and Tables

Figures

Tables

List of Abbreviations and Symbols

#	number
%	per cent
α	anti
Δ	delta
° C	degree Celsius
×	times
× g	times gravitational force
µF	microfarad
µg	microgram
µL	microliter
µm	micrometre
µM	micromolar
A	absorbance
ad	advanced-decline volume percent
ALR	augmenter of liver regeneration
Amp	ampicillin
Amp^R	ampicillin resistant
approx.	approximately
APS	ammonium persulfate
AQ	atovaquone
as	antisense
ATP	adenosine triphosphate
BHI	brain heart infusion
β-ME	β-mercaptoethanol
bp	base pairs
BSA	bovine serum albumin
C	cytosine
Cas	CRISPR-associated
CHCHD4	human Mia40
CL	cutaneous leishmaniasis
cm	centimetre
Cmc1	COX assembly mitochondrial protein
CO_2	carbon dioxide
CRISPR	clustered regularly interspaced short palindromic repeats
C-terminal	carboxy terminal
CytC	cytochrome *c*
COX	cytochrome *c* oxidase
D	glucose/ dextrose
Da	Dalton
ddH_2O	double deionised water
DHFR	dihydrofolate reductase
DMSO	dimethyl sulfoxide
DNA	deoxyribonucleic acid
DNAse	deoxyribonuclease
dNTP	deoxyribonucleoside triphosphate
DTT	dithiothreitol
E. coli	*Escherichia coli*
ECL	enhanced chemiluminescence
EDTA	ethylenediamine tetra acetic acid
Ef1	guanine nucleotide exchange domain
e.g.	*exempli gratia* (for example)
ER	endoplasmic reticulum
Erv	essential for respiration and viability
et al.	*et alii* (and others)
ETC	electron transport chain
FAD	flavin adenine dinucleotide
FCS	foetal calf serum
FOA	5-fluoroorotic acid
fw	forward
g	gram
G	glycerol or guanine
G418	geneticin
Gal	galactose
gDNA	genomic DNA
gRNA	guide RNA
GSH	glutathione (reduced)
GSSH	glutathione disulphide
h	hours
HEPES	4-(2-hydroxyethyl)-1-piperazineethanesulfonic acid
HRP	horseradish peroxidase
IgG	immunoglobulin G
IM	inner mitochondrial membrane
IMS	intermembrane space
iRBC	*P. falciparum* infected red blood cell
ITS	intermembrane space targeting signal
Kan	kanamycin
Kan^R	kanamycin resistance
kb	kilo bases
kDa	kilo Dalton
KISS	kinetoplastida-specific second
KO	knock out
kV	kilo Volt
L	litre
L.	*Leishmania*
LB	Luria-Bertani
Li	*Leishmania infantum*
Lt	*Leishmania tarentolae*
LiOAc	lithium acetate
M	molar
mA	milliampere
MCS	multiple cloning site
mg	milligram
MIA	mitochondrial IMS import and assembly
MiaN	N-terminal mitochondrial targeting signal with transmembrane domain of *Sc*Mia40
Mia40s	N-terminally truncated Mia40
min	minute
MISS	mitochondrial intermembrane space sorting signal
mL	millilitre
mM	millimolar
mm(PEG)24	methyl-PEG-maleimide

MOPS	3-(*N*-morpholino)propanesulfonic acid
MPI	mitochondrial protein import
ms	milliseconds
mtDNA	mitochondrial DNA
mut	mutation
N	number
N_2	nitrogen
NEB	New England Biolabs
NEM	*N*-ethylmaleimide
Neo	neomycin
Neo^R	neomycin resistance
nm	nanometre
N-terminal	amino terminal
O_2	oxygen
OD_{600}	optical density at 600 nm
OM	outer mitochondrial membrane
PAGE	polyacrylamide gel electrophoresis
PAM	protospacer adjacent motif *or* pre-sequence translocase-associated motor
PBS	phosphate-buffered saline
PCR	polymerase chain reaction
PEG	polyethylene glycol
P.	*Plasmodium*
Pf	*Plasmodium falciparum*
PFA	paraformaldehyde
Pfu	*Pyrococcus furiosus*
PI	protease inhibitor
pmol	picomole
PMSF	phenylmethylsulphonyl fluoride
PVDF	polyvinylidene fluoride
RBC	red blood cell
rev	reverse
RNA	ribonucleic acid
rpm	rounds per minute
RPMI	Rosewell Park Memorial Institute
rRNA	ribosomal RNA
RT	room temperature
s	sense
S medium	synthetic minimal medium
Sc	*Saccharomyces cerevisiae*
SAM	sorting and assembly machinery
SAR	Stramenopiles, Alveolata, Rhizaria
SD medium	synthetic minimal medium containing glucose
SDS	sodium dodecyl sulphate
sec	seconds
SG medium	synthetic minimal medium containing glycerol
SGal medium	synthetic minimal medium containing galactose
sgRNA	single guide RNA
SOC	super optimal broth
Sub	substrate
T	thymine
T.	*Trypanosoma or Toxoplasma*
TAE	Tris-acetate-EDTA-buffer
Taq	*Thermus aquaticus*
Tb	*Trypanosoma brucei*
TBS	Tris buffered saline
TCA	Trichloroacetic acid
TCEP	Tris(2-carboxyethyl)phosphine
TE	Tris-EDTA
TEMED	tetramethyl ethylenediamine
TIM	translocase of the inner mitochondrial membrane
T_m	melting temperature
TM	transmembrane domain
TOB	mitochondrial outer membrane beta-barrel protein
TOM	translocase of the outer mitochondrial membrane
Tris	Tris(hydroxymethyl)aminomethane
tRNA	transfer RNA
U	units
Ura	uracil
UV	ultraviolet
V	volt
VL	visceral leishmaniasis
v/v	volume per volume
w/v	weight per volume
WHO	World Health Organization
WR99210	1,6-Dihydro-6,6-dimethyl-1-[3-(2,4,5-trichlorophenoxy)propoxy]-1,3,5-triazine-2,4-diamine
WT	wildtype
x	any
YP	yeast extract peptone
YPD	yeast extract peptone containing glucose
YPG	yeast extract peptone containing glycerol
YPGal	yeast extract peptone containing galactose
YT	yeast extract tryptone
Zwf1	glucose-6-phosphate 1-dehydrogenase

Amino acids were abbreviated using the standard one or three letter code.

1 Introduction

1.1 Parasitic protists and their impact on public health

The paraphyletic group of protozoa comprises more than 200 000 named species of unicellular eukaryotes, of which ~10 000 were classified as parasites (Cox, 2002). Since they are not a coherent phylogenetic group, protists share biological properties and phylogenetic relationships with other eukaryotic lineages, which have distributed them throughout the evolutionary tree (Figure 1.1) (Simpson and Roger, 2004; Adl *et al.*, 2005; Ocana and Davila, 2011; Adl *et al.*, 2012). Phyla that contain parasitic protists include the *Alveolata* (apicomplexans, e.g. *Plasmodium, Cryptosporidium, Theileria, Toxoplasma, Babesia*) as a branch of *SAR*, *Discoba* (kinetoplastid flagellates, e.g. *Trypanosoma, Leishmania*) and *Metamonada* (intestinal flagellates, e.g. *Giardia, Trichomonas*) belonging to the supergroup of *Excavata*, and *Archamoebae* (Amoebae, e.g. *Entamoeba*) as a representative of the Amoebozoa (Cox, 2002; Adl *et al.*, 2012).

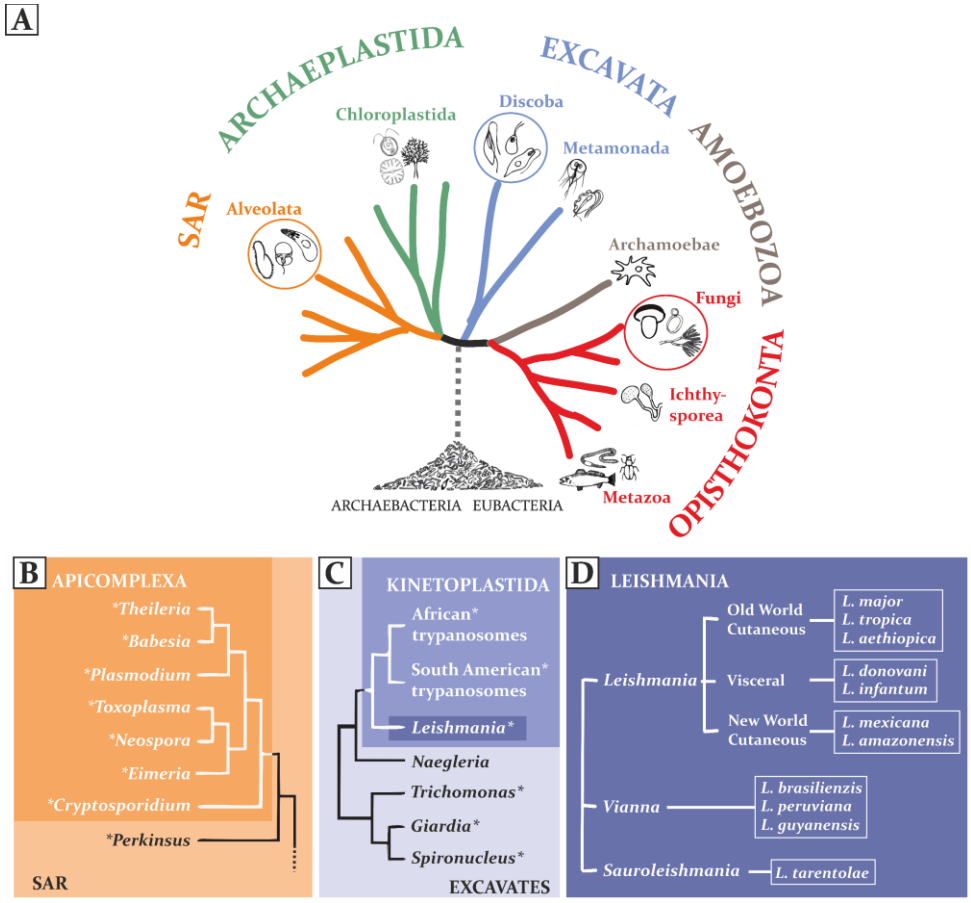

Figure 1.1 | Phylogenetic relationships among eukaryotes. (A) Eukaryotic tree of life indicating the five supergroups and in extracts subgroups of free living and parasitic representatives. SAR = Stramenopiles, Alveolata, Rhizaria. Tree was modified from Adl *et al.* (2012). **(B, C, D)** Phylogenetic relationships within the groups **(B)** SAR and the subgroup *Apicomplexa,* **(C)** *Excavates* and the subgroup *Kinetoplastida,* and **(D)** *Leishmania.* Asterisks indicate parasitic organisms. Figure was modified from Chaudhary and Roos (2005) and Bates (2007).

Protozoan parasites represent important human pathogens that are responsible for a major part of the global health burden and contribute significantly to morbidity and mortality in the developing world (Lozano *et al.*, 2012; Andrews *et al.*, 2014). Typically, they cause classical diseases of poverty which are hardly considered by the pharmaceutical industry, although many of them are targeted as research priorities by the World Health Organization (WHO) (Chaudhary and Roos, 2005; WHO, 2012a). Diarrhoeal diseases caused by the enteric protists *Entamoeba*, *Cryptosporidium*, and *Giardia* caused the death of 33 900 people in 2010 and rank among the most frequent causes of decease in children under the age of five (Liu *et al.*, 2012; Kotloff *et al.*, 2013; Torgerson *et al.*, 2015; Burgess *et al.*, 2017). Members of the kinetoplastid parasites are threatening the lives of billions of people in the tropics and subtropics causing leishmaniasis, Chagas disease or sleeping sickness (WHO, 2015, 2018). Together they were responsible for over 71 000 deaths in 2010 (Lozano *et al.*, 2012). The most severe tropical disease caused by a protist remains to be malaria with an estimated 216 million cases annually and approximately 445 000 deaths worldwide in the year 2016 (WHO, 2017b).

1.1.1 The apicomplexan parasite *P. falciparum* – the causative agent of malaria

Malaria is a vector-borne disease caused by parasitic protists of the genus *Plasmodium*. It is transmitted by female *Anopheles* mosquitoes in endemic regions of the tropical and subtropical parts of Africa, South-East Asia, Oceania, the Indian subcontinent, and Central and South America.

The disease severely affects the poorest population and the most marginalised communities having the least access to prevention, diagnosis, and treatment. Most affected are children under the age of five, who account for 78 % of all malaria-related deaths, pregnant women, and immunocompromised patients, e.g. co-infected with HIV (WHO, 2012a, 2014). Initial signs of an infection typically occur within an incubation period of 7-30 days and herald the disease with periodic fevers and non-specific flu-like symptoms, such as headaches, chills, muscle pain, and vomiting. Untreated patients may develop severe and potentially fatal illness within 24 hours. Complicated or severe malaria is associated with prostration, severe anaemia, and respiratory distress, which can lead to multiorgan failure or cerebral malaria (Greenwood *et al.*, 2008; CDC, 2015).

Within the superphylum *Alveolata*, *Plasmodium* species are part of the parasitic group of *Apicomplexa* (Adl *et al.*, 2012). Closely related veterinary pathogens, such as *Theileria parva*, causing east coast fever and theileriosis, *Babesia bovis* and *B. bigemina*, the cause of Texas cattle fever, and *Toxoplasma gondii* produce dangerous invasive diseases in livestock and humans (Figure 1.1B) (Esteban-Redondo and Innes, 1997; Chaudhary and Roos, 2005; Saadatnia and Golkar, 2012; Yusuf, 2017). *Plasmodium* further belongs to the order of *Haemosporoidia* and the family of *Plasmodiidae* (Adl *et al.*, 2012).

The parasite's complex life cycle alternates between the female *Anopheles* mosquito, for sexual reproduction, and a vertebrate host, in which it multiplies asexually. Roughly 200 *Plasmodium* species may cause malaria in vertebrates, such as primates, rodents, birds, or reptiles (Dhangadamajhi *et al.*, 2010). Six of them are capable of infecting the human host, while *Plasmodium falciparum* is the most virulent, accounting for 99 % of the infections in 2016 (Sutherland *et al.*, 2010; Cowman *et al.*, 2016; WHO, 2017b). Outside of the African continent, *P. vivax* is the predominant pathogen of complicated malaria (Naing *et al.*, 2014; WHO, 2017b).

To complete their life cycle, the parasites undergo several morphological transformations to form unique "zoite" forms that allow them to invade different types of cells (Cowman *et al.*, 2016). In short, sporozoite-staged parasites are injected into the dermis of a vertebrate host during the blood meal of an infected mosquito. The motile parasites travel to the blood stream to reach the liver, in which they infect hepatocytes (Yamauchi *et al.*, 2007). During this clinical silent stage, the parasites multiply within 5-16 days and the newly formed merozoites are released into the blood circulation to invade erythrocytes (Prudencio *et al.*, 2006). In the intraerythrocytic cycle, the parasite undergoes schizogony, in which it multiplies asexually and develops from the initial ring stage to trophozoites and schizonts. The schizonts burst under red cell rupture and release new merozoites for another round of invasion and multiplication (Bannister *et al.*, 2000; Bannister and Mitchell, 2003). The cycle closes within one day (*P. knowlesi*), two days (*P. falciparum*, *P. vivax*, *P. ovale*), or three days (*P. malariae*) leading to the periodic fevers each time the host cells burst to unleash a new flood of parasites. During the red blood cell cycle, a subset of merozoites are programmed to differentiate into gametocytes that are essential for sexual reproduction and can be absorbed by a feeding mosquito (Greenwood *et al.*, 2008; Dhangadamajhi *et al.*, 2010; Cowman *et al.*, 2016).

1.1.2 Neglected tropical diseases caused by kinetoplastid parasites

Chagas disease, sleeping sickness, and leishmaniasis represent three substantially different infectious diseases, all induced by kinetoplastid pathogens and geographically limited by the range and environment of their insect vectors (Figure 1.1C,D). These devastating yet neglected diseases are hard to treat and exert enormous socioeconomic impacts, affecting people and livestock alike (Flohe, 2012). The causative agent of Chagas disease, *Trypanosoma cruzi*, is naturally transmitted by the infective faeces of a triatomine bug ("kissing bug") but may also be received congenital or through infective transfusions or contaminated food (Pereira *et al.*, 2010; WHO, 2012b). The disease is endemic in 21 countries in Latin America with an estimated seven million people infected (WHO, 2012b).

Sleeping sickness or African trypanosomiasis is caused by either of the species *T. brucei gambiense* and *T. brucei rhodesiense* in Western and Eastern equatorial Africa, respectively, and affects both humans and livestock (Cross, 2005; Ponte-Sucre, 2016). The disease is spread by the bite of the tsetse fly, which

threatens the lives of 61 million people in 37 countries on the African continent (WHO, 2012b). However, with fewer than 3000 cases reported in 2015, WHO was encouraged to target the human disease for elimination by 2020 (Buscher *et al.*, 2017; WHO, 2017a).

Parasites of the genus *Leishmania* are another serious public health problem and responsible for a variety of clinical manifestations with invasive, disfiguring, or lethal consequences, depending on the infectious species and the immune response of the host (Herwaldt, 1999; Torres-Guerrero *et al.*, 2017). Worldwide, between 12 and 15 million people are suffering from leishmaniasis and over a billion people live exposed to the infectious bites of phlebotomine sand flies in 98 countries in the tropics, subtropics, and Southern Europe (Figure 1.2) (WHO, 2012b, 2016; Torres-Guerrero *et al.*, 2017). The high burden of disease leads to over 20 000 fatalities annually (WHO, 2012b).

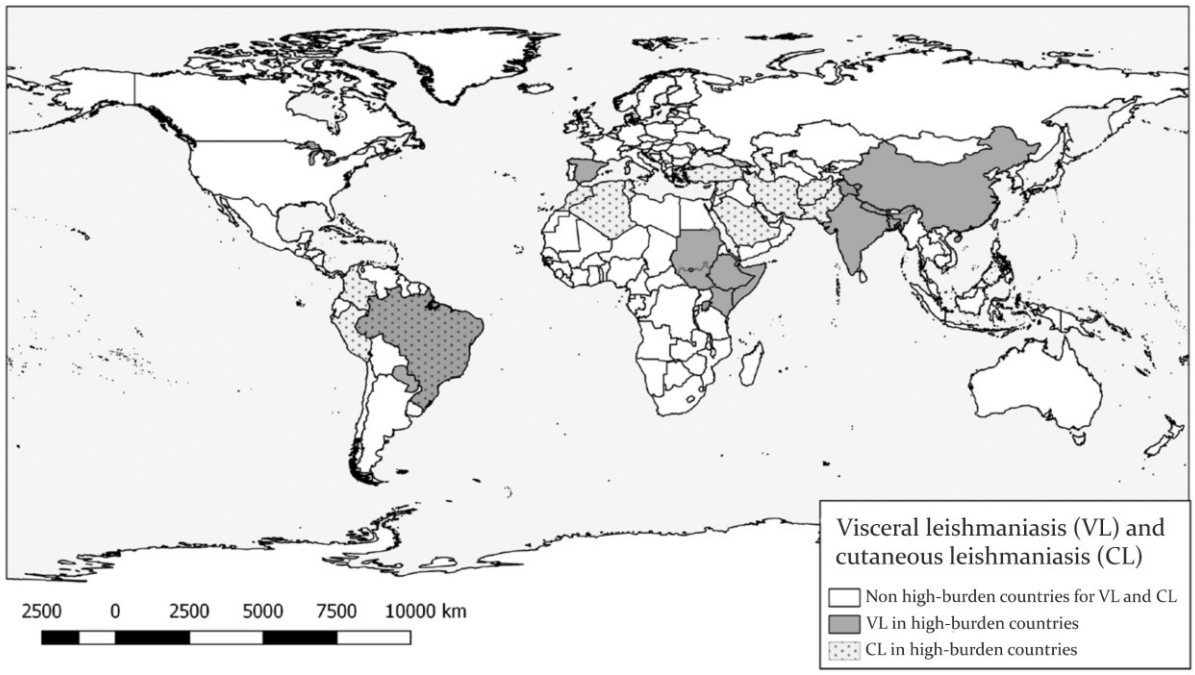

Figure 1.2 | Epidemiology of visceral and cutaneous leishmaniasis in high burden countries. Source: WHO (2016)

The WHO recognises four major clinical forms of the disease with varying severity resulting from parasite replication in macrophages of the mononuclear phagocyte system, the skin, and the naso-oropharyngeal mucosa (Herwaldt, 1999). Cutaneous leishmaniasis (CL), also known as oriental sore, is the most common clinical syndrome and associated with chronic skin ulcer. Causative agents are *L. tropica*, *L. braziliensis,* and *L. major*. As a metastatic complication, CL may lead to mucocutaneous leishmaniasis (*L. braziliensis*, *L. guyanensis*) having a highly defacing, mutilating, and potentially fatal outcome. Visceral leishmaniasis (VL) or *Kala-Azar* (Hindi for black fever) is the most severe clinical form and a systematic infection primarily of children in India and East Africa (*L. donovani*) as well as in Southern Europe and the new world (*L. infantum*). Patients suffer from fever, splenomegaly, weight loss, pallor, cough, hepatomegaly, asthenia, anorexia, and eventually die within two years if not

treated. Post kala-azar dermal leishmaniasis (*L. donovani*) is a dermatosis that develops in patients following VL treatment and ranges from single papules and nodules to a nodulo-papular rash (WHO, 2012b, 2015, 2016).

The treatment of these diseases often involves toxic or inefficient substances, which require extensive or prolonged administration. Due to the lack of available drugs for an efficient combination therapy, drug resistances are promoted, while vector control is hard to adequately maintain and useless to people with lifelong chronic infections. In addition, the parasites' sophisticated mechanisms of immune evasion are clouding the hope for a vaccine (WHO, 2012a). The identification of novel drug targets seems as important as ever and is craving for new discoveries on the parasites' biology on a cellular as well as biochemical basis.

Within the *Excavata*, protists of the genera *Leishmania* and *Trypanosoma* are euglenozoan *Discoba* belonging to the class of *Kinetoplastea* and the family of *Trypanosomatidae* (Adl *et al.*, 2012). The complex life cycle of *Leishmania* comprises two developmental stages and involves both the invertebrate and the vertebrate host. In the insect vector, the extracellular parasite is flagellated and resides in the intestinal tract of the female sand fly (Akhoundi *et al.*, 2016). These promastigotes are transmitted into the skin of the vertebrate host and absorbed by macrophages. There they transform into intracellular amastigotes that are ovoid and non-motile. Parasites remain in the amastigote stage during their entire inhabitation in the vertebrate host (Gossage *et al.*, 2003; Bates and Rogers, 2004).

About 53 different *Leishmania* species have been described that are able to infect a variety of mammalian, insect, or reptile host species (Akhoundi *et al.*, 2016). Among them, 30 are pathogenic for mammals and more than 20 are known human pathogens that can be transmitted by any of the 98 medically relevant sand fly species (Ashford, 2000; WHO, 2012b). Phylogenetic analyses have further subdivided the different *Leishmania* species (Figure 1.1D) into the three subgenera *Vianna*, *Leishmania* (consisting of the human infecting species), and *Sauroleishmania* (the reptile infecting species) (Gomez-Eichelmann *et al.*, 1988; Bates, 2007).

1.2 Mitochondria – the organelle and antiparasitic drug target

Mitochondria are oxygen-consuming "power organelles" that form a dynamic and interconnected network found in almost all eukaryotic cell types except for red blood cells (Rich and Marechal, 2010). Evolved from the endosymbiotic uptake of an aerobe α-proteobacterium by a primitive, heterotrophic eukaryote (Archibald, 2015), the organelle is surrounded by a double membrane generating four biochemically distinct compartments: The outer (OM) and the inner mitochondrial membrane (IM) and the two aqueous sections, the intermembrane space (IMS) and the matrix (Figure 1.3A). The OM separates the organelle from the cytosol but incorporates pore forming proteins for the interchange

of small molecules and the passage of cytoplasmically synthesised mitochondrial proteins (Walther and Rapaport, 2009; Rich and Marechal, 2010). The IM exhibits a large surface area that is organised in the inner boundary membrane as well as numerous invaginations or cristae and may adapt its morphology to the necessities of the eukaryotic cell (Heath-Engel and Shore, 2006; Scheibye-Knudsen *et al.*, 2015). The increased surface area is required to host the enzyme complexes of the electron transport chain (ETC) as well as the adenosine triphosphate (ATP)-synthase for oxidative phosphorylation (Sazanov, 2015).

In the course of evolution, most of the mitochondrial genes have been lost or transferred to the nuclear genome. In humans, the mitochondrial genome (mtDNA) consists of a small circular DNA molecule of about 16 kilobases (kb) that is inherited through the maternal lineage and located in the matrix (Mishra and Chan, 2014; Scheibye-Knudsen *et al.*, 2015). The mtDNA provides the genetic information for 13 proteins, 22 transfer RNAs (tRNAs), and two ribosomal genes (rRNAs) that are all critical for oxidative phosphorylation. The 13 polypeptides are part of the respiratory complexes I, III, IV, and V, which must be supplemented by the nuclear encoded subunits to be functional. At the same time, the encoded tRNAs and rRNAs are indispensable for the mitochondrial translation machinery that is required for the synthesis of the mitochondrial-encoded proteins (Friedman and Nunnari, 2014; Mishra and Chan, 2014; Scheibye-Knudsen *et al.*, 2015).

Besides their core function in ATP production, which is part of their prokaryotic heritage, mitochondria are involved in a range of cellular processes critical for cell function, health, cellular ageing, and apoptosis (Pellegrini and Scorrano, 2007; Larsson, 2010). The dynamic organelles constantly change in size and shape through fusion and fission incidences and are capable to move within the cell by association with the cytoskeleton (Okamoto and Shaw, 2005; Boldogh and Pon, 2006; Chan *et al.*, 2006; Hoppins and Nunnari, 2009; Roy *et al.*, 2015). Also, mitochondria execute important roles in biochemical processes, such as calcium homeostasis (De Stefani *et al.*, 2011), steroid metabolism (Miller, 2013), fatty acid oxidation (Adeva-Andany *et al.*, 2018), or haem and iron-sulphur cluster biosynthesis (Atamna, 2004). They depend on the import of proteins from the cytosol (Chacinska *et al.*, 2009) and lipids from the endoplasmic reticulum (ER) for cell survival and membrane formation (Flis and Daum, 2013; Scharwey *et al.*, 2013).

1.2.1 Special features of the parasites' mitochondria

Unicellular organisms are highly interesting not only from the evolutionary point of view but also regarding their cellular biology. They have a collection of special cytoplasmic structures and organelles with partially unique metabolic pathways. Among these, the mitochondrion is the most exciting

organelle, whose structure and tasks are of vital importance to the cell and in the main focus of both scientific fields (Gray *et al.*, 2004; Fidalgo and Gille, 2011).

Apicomplexan and kinetoplastid parasites usually rely on the proper function of a single, ramified mitochondrion, whose structure individually depends on the parasite species, but was generally described as peculiar in terms of matrix density as well as number and shape of cristae (Figure 1.3B,C) (de Souza *et al.*, 2009).

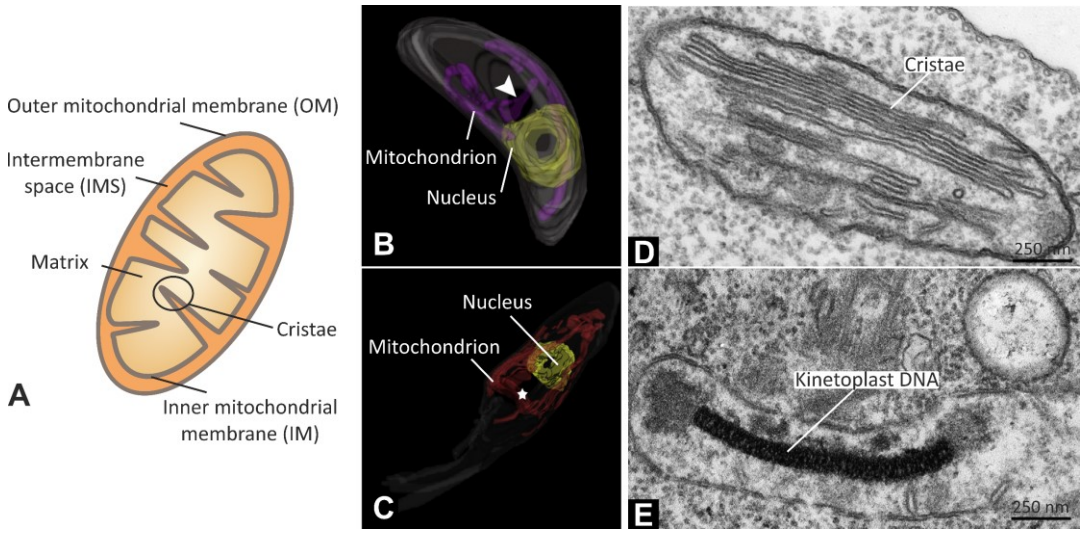

Figure 1.3 | Particularities of protist mitochondria. (A) Schematic summary of a mitochondrion. **(B)** Three-dimensional model of *Toxoplasma gondii* (*Apicomplexa*) shows the mitochondrion with two lateral branches that are intermediary connected (arrowhead). **(C)** Three-dimensional model of *Trypanosoma cruzi* (*Kinetoplastida*). The kinetoplast is marked with a star. **(D)** Electron microscopy picture of a *Leishmania* mitochondrion with a high metabolic activity showing many cristae. **(E)** Electron microscopy picture of an ultrathin section across the kinetoplast presenting the compact kinetoplast DNA network. Figure was modified from de Souza *et al.* (2009).

The smallest mitochondrial genome of about 6-7 kb was identified for apicomplexans, exhibiting a highly reduced gene content that encodes only three proteins of the ETC as well as fragments of rRNA (Vaidya *et al.*, 1989; de Souza *et al.*, 2009). All other mitochondrial proteins and tRNAs are nuclear encoded and must be imported from the cytosol. In *P. falciparum* blood stages, energy metabolism is primarily based on glycolysis while the ETC is lacking multiple subunits, such as components for proper ATP synthesis (Gardner *et al.*, 2002; Mather *et al.*, 2007; Vaidya and Mather, 2009; MacRae *et al.*, 2013; Jacot *et al.*, 2016). Yet, the ETC is crucial for parasite survival, accepting electrons that are produced during pyrimidine biosynthesis (Painter *et al.*, 2007).

The mitochondrion of trypanosomatids reacts highly sensitive to nutritional resources, which means it may present many cristae and claim up to 13 % (v/v) of the total cell volume under low glucose conditions (Figure 1.3D) (de Souza *et al.*, 2009). A special apomorphy of the class *Kinetoplastea* is the kinetoplast (Figure 1.3C), which is positioned in close proximity to the nucleus (Motta, 2008; Adl *et al.*, 2012; de Souza *et al.*, 2017). The kinetoplast is a dense structure within the mitochondrial matrix that

is made of a giant and complex network of circular DNA molecules called kinetoplast DNA (kDNA) (Figure 1.3E). The duplex kDNA molecules are arranged in 20-40 kb maxicircles of about 20-50 identical copies per network and several thousand minicircles that range in size between 0.5 and 2.5 kb, depending on the species (Lukes *et al.*, 2002; de Souza *et al.*, 2009). Maxicircles encode mitochondrial gene products, including rRNAs and subunits of the respiratory complexes, while minicircles contain the genetic information for guide RNAs that are needed to modify the cryptic maxicircle transcripts by insertion or deletion of uridine residues (Lukes *et al.*, 2002; Stuart and Panigrahi, 2002).

1.2.2 Mitochondrial targets and currently used antiparasitic drugs

Peculiarities of protist mitochondria have attracted much attention for antiparasitic therapies. Promising drug targets include the respiratory complexes, lipid metabolism, mtDNA content and mitochondrial protein synthesis, protists' alternative oxidases, or the transport systems importing tRNAs and proteins from the cytoplasm into the mitochondria (Kita et al., 2003; Mather et al., 2007; Sen and Majumder, 2008; Fidalgo and Gille, 2011; Goodman et al., 2017).

Several existing drugs are targeting the ETC by inhibiting the respiratory complexes or by excepting electrons in competition to the natural acceptors (Olszewska and Szewczyk, 2013), which in turn cause the mitochondrial membrane potential to collapse (Srivastava et al., 1997). The antimalarial artemisinin was suggested to be a competent inhibitor of the malaria parasite's alternative complex I NADH-quinone oxidoreductase (Li et al., 2005). Since this alternative complex does not encounter a match in humans, it appears to be a powerful target whose inhibition has been sought with several compounds (Abrahamsen *et al.*, 2004; Biagini *et al.*, 2006; Biagini *et al.*, 2012). The clinically approved hydroxynaphthoquinone atovaquone specifically targets the cytochrome *b* component of complex III by acting as a ubiquinone analogue (Fry and Pudney, 1992; Srivastava and Vaidya, 1999; Peters *et al.*, 2002). The compound was developed as an antimalarial but is also effective in treating trypanosomiasis and leishmaniasis (de Souza *et al.*, 2009). A combination therapy of atovaquone and proguanil, commercially available under the name Malarone™, indirectly arrests the biosynthesis of pyrimidines by disrupting the ubiquinone turnover and thereby eliminating the reducing power for the dihydroorotate dehydrogenase (Painter *et al.*, 2007). Another drug with multiple modes of action is the dicationic pentamidine, which has been used for the past 50 years to treat sleeping sickness or antimonial-resistant leishmaniasis (Sands *et al.*, 1985). It has been shown to unbalance the intracellular calcium content and block complex II of the ETC (Vercesi and Docampo, 1992). Additionally, it may induce apoptotic cell death in *L. donovani* and promotes linearisation of the kDNA minicircles (Shapiro *et al.*, 1989; Mehta and Shaha, 2004). Similar effects are achieved by agents targeting the

topoisomerase activity, which is essential for kDNA replication and can be dismissed by competitive inhibition or DNA breakage (Motta, 2008).

1.3 Mitochondrial machineries for protein import and assembly

Human mitochondria are composed of about 1500 different proteins, of which 1 % are synthesised in the mitochondrial matrix. The rest derives from nuclear-encoded genes that are translated on ribosomes in the cytosol, from which the proteins have to be translocated into the organelle by a multicomponent import machinery. Mitochondrial protein import (MPI), folding, and sorting machineries are strictly essential for cell viability and encompass at least six different pathways that are powered by the membrane potential, ATP metabolism, or redox reactions in the mitochondria (Chacinska *et al.*, 2009; Endo and Yamano, 2009; Gross and Bhattacharya, 2009; Dudek *et al.*, 2013; Harbauer *et al.*, 2014).

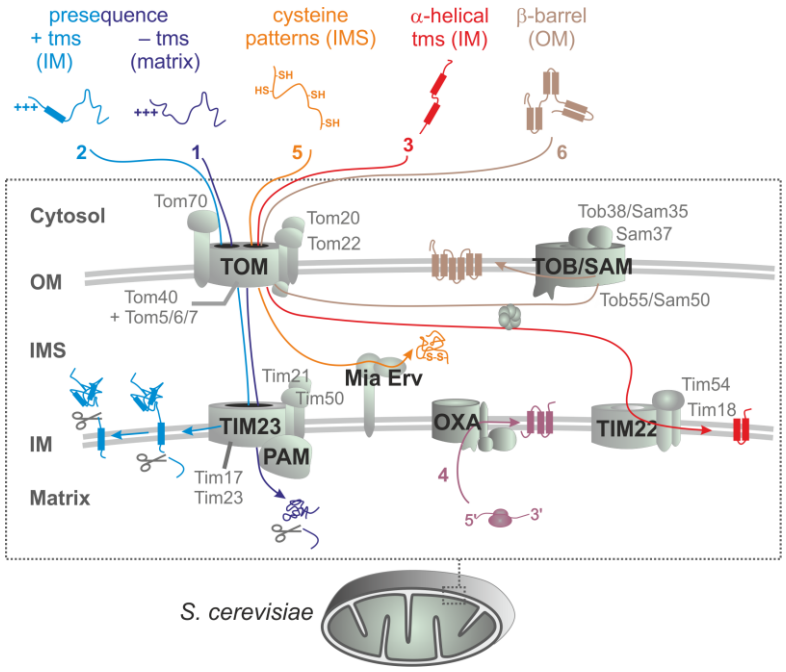

Figure 1.4 | Model of the mitochondrial protein import pathways and machineries in opisthokonts. **(1)** Pre-sequence pathway of matrix targeting proteins. **(2)** Stop-transfer pathway into the IM via TIM23. **(3)** Carrier pathway via TIM22 into the IM. **(4)** OXA pathway into the IM. **(5)** Oxidative folding pathway or MIA pathway of cysteine-rich proteins into the IMS. **(6)** Beta-barrel pathway into the OM. See text for details. OM = outer mitochondrial membrane, IM = inner mitochondrial membrane, IMS = intermembrane space. Figure was modified from Eckers *et al.* (2012) and Deponte (2013).

Precursor proteins may be scheduled for insertion into the mitochondrial OM or IM or reside soluble in the IMS or matrix (Figure 1.4). Independently on the mitochondrial compartment that will be the final destination of the proteins, they first have to pass the translocase of the outer mitochondrial membrane (TOM complex), whose largest subunit, Tom40, forms a hydrophilic channel through the

membrane (Hill *et al.*, 1998). Therefore, precursor proteins are either equipped with a cleavable pre-sequence or one of many internal targeting/sorting signals that bind to receptors of the TOM complex (Tom20, Tom22 and Tom70) prior to the translocation process (Brix *et al.*, 1997; van Wilpe *et al.*, 1999; Meisinger *et al.*, 2001; Chacinska *et al.*, 2009).

The classical MPI pathway (route 1) or pre-sequence pathway, guides proteins with a positively charged pre-sequence from the IMS to the translocase of the inner mitochondrial membrane (TIM23 complex). There, the IM potential and the pre-sequence translocase-associated motor (PAM) drive their translocation into the matrix (Martin *et al.*, 1991; Chacinska *et al.*, 2005). The two proteins Tim23 and Tim17 together form the pore of the complex, while Tim50 and Tim21 are receptors facing the IMS. The presence of a hydrophobic segment behind the pre-sequence (route 2; bipartite signal), causes a lateral release of the protein into the IM by the TIM23 stop-transfer pathway (Glick *et al.*, 1992; Meier *et al.*, 2005). Alternatively (route 4), proteins intended for the IM are translocated into the matrix and are secondarily inserted via the OXA export pathway. Substrates of this pathway usually have multiple transmembrane segments and include also mitochondrial-encoded proteins (Harbauer *et al.*, 2014). The carrier pathway (route 3) introduces proteins with multiple hydrophobic regions and internal targeting signals into the IM by small Tim chaperones and the carrier translocase of the inner membrane (TIM22 complex). Chaperones bind to the substrates in the IMS and guide them to the multiunit complex, consisting of the Tim22 channel and the associated receptor units Tim54 and Tim18 (Sirrenberg *et al.*, 1996; Koehler *et al.*, 1998; Sirrenberg *et al.*, 1998). Beta-barrel proteins (route 6) also bind to small Tim chaperones that transport them to the sorting and assembly machinery (SAM) or mitochondrial outer membrane β-barrel protein (TOB) for sorting into the OM (Wiedemann and Pfanner, 2017). Cysteine-rich IMS proteins (route 5) are imported and folded in a disulphide relay system via the mitochondrial import assembly (MIA) machinery (Chacinska *et al.*, 2004; Naoe *et al.*, 2004; Mesecke *et al.*, 2005).

1.3.1 Cysteine-rich proteins of the IMS

In accordance to their prokaryotic ancestors, mitochondria host fundamental different redox processes that have to be separated by kinetic barriers (Rozhkova *et al.*, 2004; Hell, 2008). The IMS is supposed to be separated from the reducing cytosol and mitochondrial matrix by two biological membranes. However, porins in the OM allow small molecules, such as reduced glutathione (GSH) to diffuse from the cytosol and establish a rather reducing environment in the IMS (Kojer *et al.*, 2012; Kojer *et al.*, 2015). Nevertheless, in contrast to the cytosol, in which efficient thioredoxin and glutathione/ glutaredoxin systems maintain cysteine-containing proteins in their thiol state, the narrow IMS catalyses the formation of disulphide bonds (Mesecke *et al.*, 2005; Herrmann and Kohl,

2007; Hell, 2008; Deponte and Hell, 2009). The oxidative protein folding pathway in the IMS is suggested to be kinetically uncoupled from the otherwise reducing environment (Hu *et al.*, 2008; Koehler and Tienson, 2009; Riemer *et al.*, 2009; Stojanovski *et al.*, 2012). Cysteine-rich proteins in the are organised in twin, disulphide-bridged Cx_3C or Cx_9C motifs (Frey and Mannella, 2000; Deponte and Hell, 2009). The family of small Tim chaperones is of a low molecular mass (<20 kDa) and has two Cx_3C segments juxtaposed in antiparallel α-helices that are stabilised by two disulphide bonds (Allen *et al.*, 2003; Webb *et al.*, 2006).

Mia40 is an import receptor essential for cell viability and contains six conserved cysteine residues, four of which form a twin Cx_9C motif. The other two are elements of the redox-active CPC motif (Stojanovski *et al.*, 2008; Terziyska *et al.*, 2009). The protein presents two redox-states in the IMS (Figure 1.5B). In the fully oxidized form, Mia40 is characterised by the presence of three disulphide bonds, one within the CPC motif and two linking the two α-helices of the Cx_9C-segment. Oxidized Mia40 is further the predominant species, also known as "active" conformation. In this conformation, the disulphide bond in the CPC segment is easily accessible to reducing agents. In contrast, partially reduced Mia40 has its first two cysteine residues (CPC) in the thiol state (Grumbt *et al.*, 2007). The fungal protein possesses a bipartite matrix targeting signal, which drives the import of the pre-sequence via the classical MPI pathway into the matrix. There, the targeting signal is removed, and the protein is laterally sorted into the IM facing the IMS (Naoe *et al.*, 2004; Terziyska *et al.*, 2005). Higher eukaryotes have shorter Mia40 homologues, in which the matrix targeting signal as well as the hydrophobic membrane anchor is missing and thus Mia40 is soluble inside the IMS (Hofmann *et al.*, 2005). Depletion of Mia40 is directly related to the abolished import of cysteine-containing proteins into the IMS (Chacinska *et al.*, 2004; Naoe *et al.*, 2004; Terziyska *et al.*, 2005).

1.3.2 The Mia40-Erv1 disulphide relay system

Proteins designated for the IMS of mitochondria reach their destination via one of three pathways (Figure 1.5): (I) they have pre-sequences and use the TIM23 complex for sorting, (II) they are rich in cysteine residues and trapped by oxidative folding, or (III) they associate with import receptors of the mitochondrial membranes (Herrmann and Hell, 2005; Erdogan and Riemer, 2017).

Class II proteins employ the oxidoreductase Mia40 and the flavoenzyme Erv1 (**e**ssential for **r**espiration and **v**egetative growth) or the respective mammalian homologues CHCHD4 and ALR (**a**ugmenter of **l**iver **r**egeneration). Reduced cysteine-containing proteins in the cytosol possess mitochondrial intermembrane space sorting signals (MISS) or intermembrane space targeting signals (ITS) that are recognised by the hydrophobic substrate binding cleft of Mia40 (Figure 1.5B) (Sideris *et al.*, 2009; Koch and Schmid, 2014b; Peleh *et al.*, 2014; Peleh *et al.*, 2016). The substrate passes the TOM complex and

forms a mixed disulphide intermediate with the oxidized CPC motif of Mia40 (Banci *et al.*, 2009). During this short-lived disulphide exchange reaction, an electron pair is passed onto Mia40, which introduces disulphide bridges in the substrate. The oxidized substrate folds into its functional conformation and is released into the IMS (Koch and Schmid, 2014a). It is not yet completely understood how the substrate's second disulphide bond is generated. A second interaction with a Mia40 molecule, molecular oxygen, glutathione (GSSG), or even Erv1 are conceivable. At the same time the substrate is oxidized, Mia40 is reduced and must be re-oxidized to maintain protein import. Therefore, the partially reduced Mia40 interacts with Erv1 in another transient disulphide intermediate. An electron pair is transferred to Erv1, leaving Mia40 in the oxidized state (Mesecke *et al.*, 2005; Banci *et al.*, 2011). The re-oxidation process is highly efficient, as can be read off the abundant amount of oxidized Mia40 (Terziyska *et al.*, 2009). The last step connects the disulphide relay system with cellular respiration, since Erv1 donates two single electrons to cytochrome *c* of the respiratory chain, in which molecular oxygen is finally reduced to water (Farrell and Thorpe, 2005; Bihlmaier *et al.*, 2007; Dabir *et al.*, 2007).

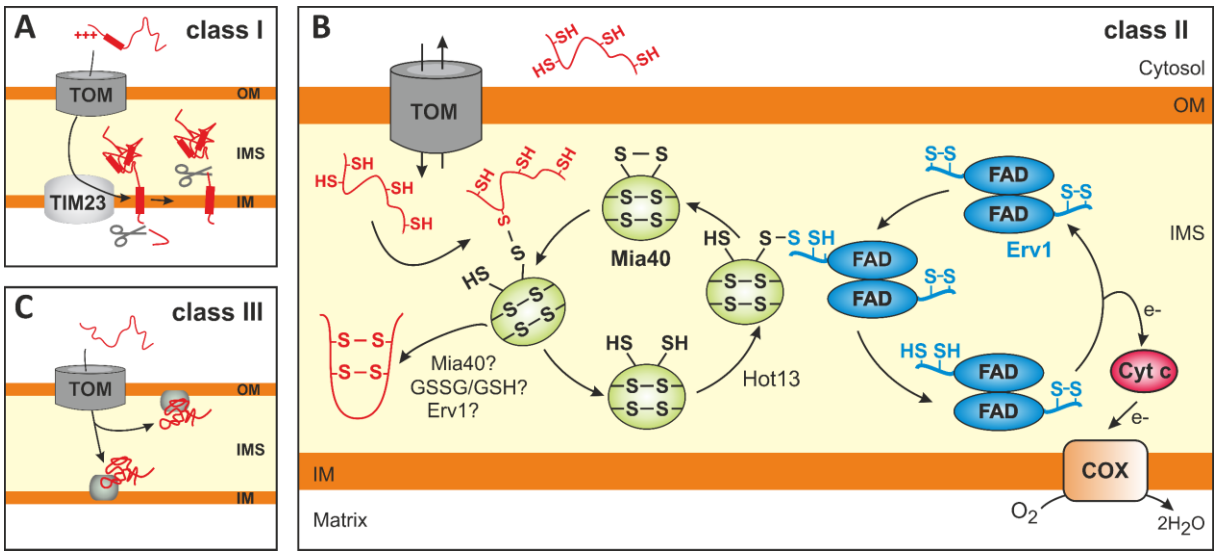

Figure 1.5 | Protein translocation pathways into the IMS. Proteins of the mitochondrial intermembrane space (IMS) are classified into three different groups according to their sorting pathways. **(A)** Class I proteins have a matrix targeting pre-sequence followed by a transmembrane segment and use the Tim23 complex for lateral sorting into the IMS. Matrix targeting signals are removed from the matrix side while soluble IMS proteins are released by another cleavage in the IMS. **(B)** Class II proteins are small and cysteine-rich and are imported via the Mia40-Erv1 disulphide relay system. See text for details. GSH/GSSG = glutathione, Cyt *c* = cytochrome *c*, COX = cytochrome *c* oxidase. **(C)** Class III proteins associate with binding sites at the outer (OM) or inner mitochondrial membrane (IM). Figure was modified from Herrmann and Hell (2005) and Deponte and Hell (2009).

1.3.3 Mitochondrial protein import of parasitic protists

Most of the knowledge concerning the MPI pathways have been collected over decades through extensive studies on yeast and other related opisthokonts (Neupert and Herrmann, 2007; Chacinska *et al.*, 2009; Endo and Yamano, 2009; Schmidt *et al.*, 2010; Dimmer and Rapaport, 2012; Dudek *et al.*,

2013; Peleh *et al.*, 2016). Data from other eukaryotic lineages just arrived during the last few years and illuminated the topic from a broader and evolutionary point of view. Studies, mainly on amoebae, apicomplexans and trypanosomes have shown that several components of the opisthokont system are altered or even absent (Dolezal *et al.*, 2010; Lithgow and Schneider, 2010; Pusnik *et al.*, 2011; Eckers *et al.*, 2012; Pusnik *et al.*, 2012; Singha *et al.*, 2012; Basu *et al.*, 2013).

The TOM complex as the main entrance gate into the mitochondria is expressed in almost all eukaryotes (Figure 1.6). However, in apicomplexans only the pore-forming Tom40 is conserved while the pre-sequence receptors are absent or significantly altered (Deponte *et al.*, 2012; Eckers *et al.*, 2012). Trypanosomes do not even possess a Tom40 homologue but employ an alternative translocase called "archaic TOM" (ATOM), which is a member of the Omp85 superfamily (Pusnik *et al.*, 2011). The presence of Tim17 and Tim23 homologues as well as several PAM components and chaperones in the apicomplexan genome indicate a rather conserved TIM23 complex and associated import pathway into the matrix and the IM (Deponte, 2013). In contrast, *in silico* data indicated the absence of Tim23 as well as several additional components of the complex in trypanosomes and leishmania (Schneider *et al.*, 2008; Singha *et al.*, 2008; Eckers *et al.*, 2012). Despite the compositional changes, the import machinery was functionally conserved for matrix-targeting and most likely also for laterally sorted proteins by the presence of Tim17 (Eckers *et al.*, 2012). Components of the OXA and β-barrel pathway were found in both apicomplexan and kinetoplastid parasites (Deponte *et al.*, 2012; Eckers *et al.*, 2012), while the multiunit TIM22 complex was roughly conserved in *Plasmodium* and completely absent in kinetoplastids. Nevertheless, substrates of the TIM22 pathway were successfully imported into both protist groups (Schneider *et al.*, 2008; Deponte *et al.*, 2012; Eckers *et al.*, 2012).

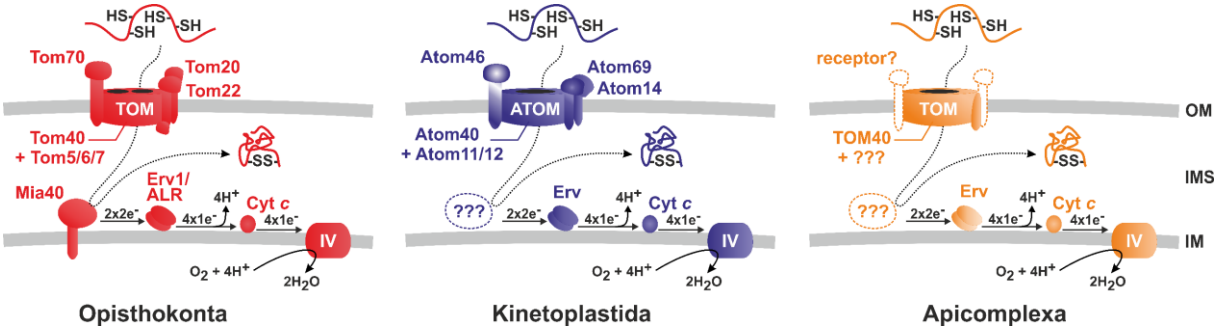

Figure 1.6 | Oxidative protein folding mechanism in different eukaryotic lineages. The oxidative protein folding in opisthokonts relies on the two proteins Mia40 and Erv1. In contrast, kinetoplastid and apicomplexan parasites only have a conserved Erv homologue. Components of the TOM complex are altered or missing (indicated with dashed lines or question marks). Figure was modified from Eckers *et al.* (2012) and contains additional data from Mani *et al.* (2015). OM = outer mitochondrial membrane, IM = inner mitochondrial membrane, IMS = intermembrane space.

MIA40 is expressed in fungi, amoebae, plants and animals. While the protein is essential in yeast but dispensable in plants, early branching eukaryotes, such as kinetoplastid and apicomplexan parasites,

do not contain a Mia40 homologue at all (Figure 1.6) (Allen *et al.*, 2008; Eckers *et al.*, 2012; Basu *et al.*, 2013; Eckers *et al.*, 2013). It is therefore controversially discussed whether the oxidative protein folding pathway that is now present in yeast and mammals, has gradually evolved from a one-component-system with only Erv1 (Allen *et al.*, 2008; Haindrich *et al.*, 2017; Peleh *et al.*, 2017) or whether an unknown component X replaces Mia40 in these early eukaryotes (Eckers *et al.*, 2013; Liedgens, 2018; Specht *et al.*, 2018).

In summary, the composition of MPI machineries were found to differ significantly between eukaryotes. Nevertheless protist proteins were successfully imported into yeast mitochondria and *vice versa* suggesting a functional conservation of the import pathways (Eckers *et al.*, 2012).

1.3.4 The FAD-dependent sulfhydryl electron transferase Erv

The flavoenzyme Erv1 is an essential protein of the IMS and was first identified in yeast (Lisowsky, 1992; Lange *et al.*, 2001). Mitochondria were observed to react sensitively on the loss or blockage of the protein, which was associated with the loss of the mitochondrial genome, impaired cellular respiration, and cell growth as well as defects in the overall mitochondrial morphology and distribution. Erv1 was further suggested to contribute to the biogenesis of cytosolic iron sulphur clusters, the maturation of haem, and the binding to cytochrome *c* and cytochrome *c* peroxidase. In general, the loss of Erv1 significantly reduces protein levels in mitochondria. This originates from reduced mitochondrial transcripts, impaired import and assembly of small Tim chaperones, and the related difficulties in the chaperone-depended import pathways (Lisowsky, 1992, 1994; Becher *et al.*, 1999; Lange *et al.*, 2001; Allen *et al.*, 2005; Rissler *et al.*, 2005; Dabir *et al.*, 2007).

In high contrast to Mia40, Erv1 is conserved throughout the eukaryotic phylogenetic tree with homologues in fungi, plants, animals, and parasitic protists (Figure 1.7) (Coppock and Thorpe, 2006; Allen *et al.*, 2008). Additionally, a distant homologue in the ER of fungi named Erv2 has been detected (Stein and Lisowsky, 1998). All homologues belong to the greater family of so-called sulfhydryl oxidases and reductases, which are known to connect thiol-disulphide-exchange reactions to the oxidation/ reduction of molecular oxygen or cytochrome *c*, as they fulfil both a reductive and an oxidative half-reaction. They further act as redox switches in intracellular compartments by accepting an electron pair and subsequently transferring two single electrons to the final electron acceptor (Fass, 2008; Deponte and Hell, 2009).

The homologues differ in sequence as well as size and composition (Fass, 2008). Probably the most obvious structural difference concerns the additional C-terminal domain of the kinetoplastid Erv that comprises almost 200 amino acids (Figure 1.7). The domain is restricted but variable within this parasitic group and was called Kinetoplastida-specific second (KISS) domain of Erv (Eckers *et al.*, 2013).

In contrast, all members bind a flavin adenine dinucleotide (FAD) in their active site and share several conserved cysteine residues (Cabibbo *et al.*, 2000; Lee *et al.*, 2000; Pagani *et al.*, 2000; Gerber *et al.*, 2001; Lisowsky *et al.*, 2001; Levitan *et al.*, 2004).

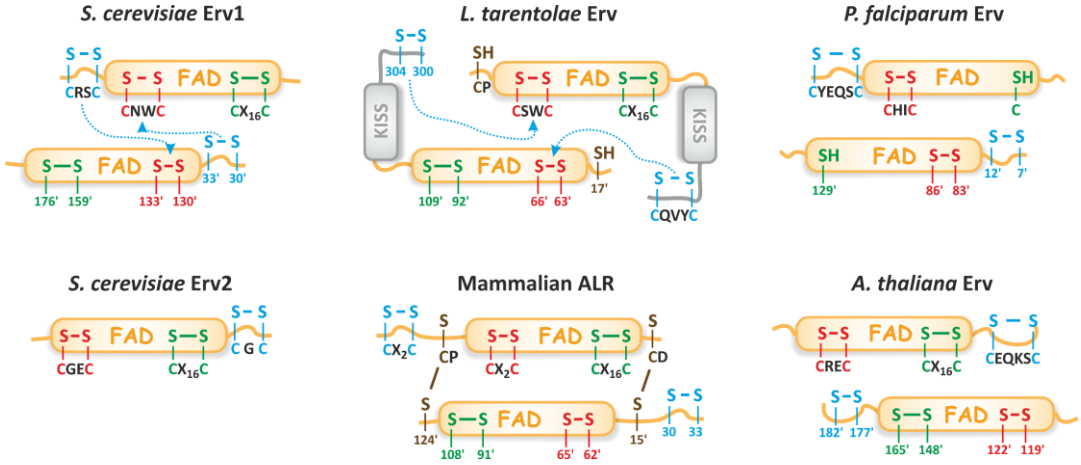

Figure 1.7 | Structural features of eukaryotic Erv homologues. Schematic representation of the Erv homologues from opisthokonts (*Sc*Erv1, *Sc*Erv2, ALR), kinetoplastida (*Lt*Erv), apicomplexans (*Pf*Erv), and plants (*At*Erv1). The N-terminal FAD-binding domain is conserved in all homologues while only the kinetoplastida Erv has an additional C-terminal KISS domain. The conserved cysteine motifs of the active site (red), the shuttle disulphide (blue), the structural pair (green), and the clamp-forming residue (brown) are highlighted and the positions are indicated. The electron transport is symbolised with a blue arrow. Figure is based on Fass (2008), Deponte and Hell (2009), and Eckers *et al.* (2013).

The cysteines are arranged in motifs and form up to four disulphide bonds to connect and stabilise the homodimer conformation (Gross *et al.*, 2002; Wu *et al.*, 2003; Vitu *et al.*, 2006; Deponte and Hell, 2009; Eckers *et al.*, 2013). The “distal” or “shuttle” pair is highly variable in the composition and location of the motif, ranging from a four-residues (opisthokonts) and six-residues motif (alveolates) at the N-terminal arm of the protein to a motif comprising three (Erv2), five (kinetoplastida), or six amino acids (plants) at the C-terminal arm. Both of the shuttle cysteines are required to interact with the dithiol substrate and relocate the electron pair from the protein surface to the redox centre of the second subunit (Gross *et al.*, 2002; Deponte and Hell, 2009; Farver *et al.*, 2009; Eckers *et al.*, 2013; Ang *et al.*, 2014). The redox active site is composed of a flavin and the “proximal” or “active site” cysteine pair, which is highly conserved and essential for the oxidase activity (Ang and Lu, 2009; Daithankar *et al.*, 2009; Farver *et al.*, 2009; Eckers *et al.*, 2013). Following the formation of an intermediate disulphide bond between the shuttle residue and the active site, electrons are transferred via the active site pair to the FAD, at the end of which disulphide bonds are restored within the distal cysteine pair (Figure 1.7). As electrons are used to reduce cytochrome *c* or, in case of Erv2, molecular oxygen, disulphide bonds are reintroduced into the proximal cysteine pair (Deponte and Hell, 2009). Another disulphide bond with a conserved $Cx_{16}C$ motif was found in almost all homologues, even in kinetoplastid parasites and Erv2, but was absent in apicomplexan parasites (Gross *et al.*, 2002; Wu *et al.*, 2003; Vitu *et al.*,

2006; Eckers *et al.*, 2013). This "structural disulphide bond" is located C-terminally within the flavodomain and in close proximity of the redox centre. Mutations concerning the participating cysteine residues affected protein function in yeast (*Sc*Erv1) as well as in *Arabidopsis thaliana* Erv1 (*At*Erv1) (Hofhaus *et al.*, 2003; Farver *et al.*, 2009). Meanwhile, the absence of the structural pair in the *P. falciparum* protein (*Pf*Erv) proposes a non-essential effect on proper folding (Eckers *et al.*, 2013). The mammalian ALR further holds an intermolecular disulphide bond. The so-called "disulphide camp" is generated between a single cysteine residue in a CP motif at the N-terminus of the flavodomain of one subunit and another single residue in the C-terminal region of the second subunit. The fully devolved clamp seems to be restricted to the mammalian homologue, but conserved N-terminal residues were found also in kinetoplastida, ciliates as well as many opisthokonts but not in plants, yeast or apicomplexans (Deponte and Hell, 2009; Eckers *et al.*, 2013).

Despite the long list of conserved patterns, minor structural differences within the homologues showed great impact on the protein function. This became clear as both the protist proteins *Lt*Erv and *Pf*Erv were imported into the IMS of yeast mitochondria but did not functionally replace the yeast protein (Eckers *et al.*, 2013). The same lack of complementation competence was found for the human ALR (Hofhaus *et al.*, 1999) as well as for *At*Erv1 (Peleh *et al.*, 2017). The incompatibility of the kinetoplastid and yeast systems may be due to the fact that *Lt*Erv does not interact with the Mia40 from yeast (*Sc*Mia40) and is membrane-associated in the IMS in strict contrast to soluble *Sc*Erv1 (Eckers *et al.*, 2013).

1.4 Aims of this study

The main objective of this thesis was to analyse structure-function relationships of the flavoenzyme Erv from the non-pathogenic kinetoplastid parasite *L. tarentolae*. The study was conducted on the basis of previous work by Elisabeth Eckers (Eckers *et al.*, 2012; Eckers *et al.*, 2013) and comprises data that have been published recently (Specht *et al.*, 2018).

The first aim was to determine a specific structure of the protist Erv, which causes incompatibility with *Sc*Mia40 resulting in a disrupted oxidative protein folding pathway in yeast. This pathway is functionally preserved in parasitic protists despite the lack of a Mia40 homologue. Nevertheless, protist Erv failed to functionally complement for *Sc*Erv1 in the yeast IMS and was unable to interact with *Sc*Mia40 (Eckers *et al.*, 2013). To achieve this goal chimeric constructs, in which *Lt*Erv properties were exchanged with those of yeast as well as structural mutants of *Lt*Erv were tested in *Sc*Erv1 complementation assays to identify a hindering structure.

The second objective concerned the unusual protein import and the membrane association of *Lt*Erv. I aimed to characterise the structural requirements as well as a redox-dependence of the membrane

association and the protein import process. In addition, it was of interest to determine to which mitochondrial membrane *Lt*Erv is associated. Since *Kinetoplastida* do not have a Mia40 homologue it is not surprising that *Lt*Erv does not cooperate with *Sc*Mia40. In addition, it was tested *in vivo* that *Lt*Erv is imported into yeast mitochondria independently of Mia40. If the protist Erv is not folding-trapped in the IMS by Mia40, how does it accumulate inside the mitochondrial compartment? According to the hypothesis to be tested, the tight membrane association of the endogenous and heterologous protein (Eckers *et al.*, 2012; Eckers *et al.*, 2013) triggers a class III pathway via a mitochondrial membrane binding site (Herrmann and Hell, 2005). Therefore, I performed differential fractionation assays to determine the membrane and the potential binding site to which *Lt*Erv is associated. Import and carbonate fractionation assays with mutant *Lt*Erv were conducted to find the property responsible for membrane-association and correct localisation inside the IMS of yeast and *Leishmania* mitochondria.

The third aim was to analyse the composition of the protist oxidative protein folding pathway. Without a Mia40 homologue in parasitic protists, the import pathway of small Tim proteins may include a Mia40 replacement or consists exclusively of an Erv performing the functions of both proteins in the folding trap mechanism (Haindrich *et al.*, 2017). I tested *Lt*Erv in yeast complementation assays for its ability to replace *Sc*Mia40. In addition, Linda Liedgens (2018) conducted an intensive and comprehensive search to find a Mia40 adapter replacement in *L. tarentolae.* There she tried to stabilise mixed disulphide intermediates between *Lt*Erv and the adapter replacement and between the replacement and a small Tim substrate. Unfortunately, the promising study had to be discontinued due to various difficulties with both chosen substrates. Here, I have tried to reactivate the search by using precisely selected substrates to overcome the known difficulties.

The last chapter of this work was intended to test whether Erv is essential in *P. falciparum*. The absence of Mia40 points towards an indispensable Erv protein that is crucial to maintain protein import into the IMS as demonstrated for *At*Erv1 (Carrie *et al.*, 2010; Peleh *et al.*, 2017). On the other hand, the potential existence of an import receptor in these parasites might overcome the need for this protein as well, and *PFERV* elimination might not affect parasite survival. Initial knock-out studies with Δ*pferv* were performed to test which of the hypotheses apply.

2 Materials and Methods

2.1 Materials

2.1.1 Technical equipment

Table 2.1 | List of equipment

Device	*Manufacturer*
Cell culture equipment	
Electroporator for *L. tarentolae* (Nucleofector 2b)	Lonza
Electroporator for *P. falciparum* (Gene Pulser)	Bio-Rad
Incubator for *L. tarentolae, P. falciparum* culture	Memmert
Incubator for yeast, solid culture	Heraeus; VWR
Laminar flow hood for *L. tarentolae, P. falciparum* (Safe 2020)	Thermo Scientific
Laminar flow hood for yeast	Flow Laboratories; Thermo Scientific
Light microscope for *L. tarentolae* (AE30)	Motic
Light microscope for *P. falciparum* (Axio)	Zeiss
Microplate reader (Infinite F200 Pro)	Tecan
Neubauer counting chamber (haemocytometer)	Roth
Rocking platform for *L. tarentolae* (Rotamax 120)	Heidolph
Shaking incubator for yeast, liquid culture (Innova 4000)	Infors AG; New Brunswick
Water bath for *L. tarentolae* culture (F12-ED)	JULABO
Water bath for *P. falciparum* culture (Aqualine AL5)	Lauda
Molecular biology equipment	
DNA electrophoresis apparatus	Bio-Rad; Biostep
Electrophoresis power supply (EPS 601; Mini 300)	GE Healthcare; Major Science
Gel documentation (E.A.S.Y 440K, UVT-28L)	Herolab
Heating block (Thermomixer)	Eppendorf
Incubator for bacteria, solid culture	Heraeus; VWR
Laminar flow hood for bacteria	Flow Laboratories; Thermo Scientific
Microwave	AEG
PCR cycler (Mastercycler gradient, Nexus gradient)	Eppendorf
Shaking incubator for bacteria, liquid culture (Innova 44, MaxQ4450)	New Brunswick, Thermo Scientific
Spectrophotometer (NanoDrop)	Thermo Fisher Scientific
Protein biochemistry equipment	
Film developer (Curix 60; Lumi-Imager)	Agfa; Roche

Device	*Manufacturer*
Heating block (MBT 250)	Kleinfeld Labortechnik
Power supply (PowerPac Basic; EPS 601)	Bio-Rad; Amersham Biosciences
Rocking platform (Duomax 1030)	Heidolph
SDS-PAGE electrophoresis system (Mini-PROTEAN Tetra Cell)	Bio-Rad
Western blot apparatus (PerfectBlue Semi-Dry Electro Blotter)	peqlab
Western blot apparatus (Mini Trans-Blot cell)	Bio-Rad
General equipment	
Autoclave (VX-95)	Systec
Analytical balance	Sartorius; Kern
Centrifuge (J-6B; J2-21M/E, Rotor JA-17, JA-10)	Beckman Coulter
Centrifuge Rotina 380 R	Hettich
Magnetic stirrer	Heidolph
Microcentrifuge (Mikro 220R, Mikro 200)	Hettich
Microcentrifuge SU1550	Sunlab
Microcentrifuge 5417R	Eppendorf
Multifuge 1 S-R	Heraeus
Multi-function rotator (PTR-30)	Grant-bio
pH meter (Basic Meter PB-11)	Sartorius
pH electrode (Blueline 56 Electrode)	SI Analytics
Pipette (Pipeteman P10-1000)	Gielson
Pipette controller (Accu-jet pro)	Brand
Portable spectrophotometer (Ultrospec 10)	Amersham Biosciences
Vortex-Mixer	Heidolph Instruments

2.1.2 Disposables

Table 2.2 | List of disposables

Disposable	*Source*
6 and 96 well plates (cell culture)	Greiner bio-one
Cell culture flasks for *L. tarentolae* (25 cm^2 T-flasks, 125 mL Erlenmeyer)	Corning
Cell culture flasks for *P. falciparum*	Greiner bio-one
Cryovials	Greiner bio-one
Cuvettes (single-use)	Sarstedt
Electroporation cuvettes for *P. falciparum* (Gene Pulser, 0.2 cm gap)	Bio-Rad
Microscope slides (SuperFrost)	Buddeberg
Needle (0.4 × 19 mm)	BD Mirolance
Nitrocellulose membrane	GE Healthcare

Disposable	*Source*
Parafilm	Sigma Aldrich
PCR reaction tubes	Sarstedt
Petri dishes (cell culture)	Greiner bio-one
Petri dishes	Sarstedt
Pipette tips	Steinbrenner
PVDF membrane	Millipore
Reaction tubes (1.5 and 2 mL, safe seal)	Sarstedt
Reaction tubes (15 and 50 mL)	Greiner bio-one
Scalpel	Braun
Serological pipettes (1, 5, 10 and 25 mL)	Sarstedt
Sterile syringe filters (0.2 µM)	Millipore
Sterile syringes	BD Plastipak
Sterile vacuum filter (0.22 µM, Stericup)	Millipore
Whatman paper	GE Healthcare
X-ray films (Super RX-N)	Fujifilm

2.1.3 Chemicals

Table 2.3 | List of chemicals

Chemical	*Source*
Acetic acid	Merck
Acetone	Honeywell
Acrylamide/Bis Solution, 37.5:1 (30 % w/v)	Serva
Adenine sulphate	Sigma Aldrich
Agar	Sigma Aldrich
Agarose	Serva
AlbuMax II	Life Technologies
Ammonium persulfate (APS)	Sigma Aldrich
Beta-Mercaptoethanol	Sigma Aldrich
Bradford reagent	Bio-Rad
Brain heart infusion (BHI)	BD
Bromophenol blue	Waldeck
BSA (Albumin bovine Fraction V, Fatty acid free)	Serva
Calcium chloride dihydrate	Merck
Complete protease inhibitor cocktail	Roche
Coomassie Brilliant Blue G 250	AppliChem
Diamide	Sigma Aldrich

Chemical	*Source*
Digitonin	AppliChem
Deoxyribonucleoside triphosphate (dNTPs)	Thermo Scientific
Dimethyl sulfoxide (DMSO)	Sigma Aldrich
Dithiothreitol (DTT)	Sigma Aldrich
DNA ladder (100 bp, 1kb)	New England Biolabs
Dnase I	Roche
Ethanol (absolute)	VWR
Ethylenediaminetetraacetic acid (EDTA)	Sigma Aldrich
Foetal calf serum (FCS heat inactivated)	Life Technologies
Folic acid	Sigma Aldrich
Galactose	Sigma Aldrich
Gel loading dye, purple 6×	New England Biolabs
Gentamicin	Life Technologies
Giemsa stock solution	Carl Roth
Glass beads 425-600 µm	Sigma Aldrich
Glucose monohydrate (D- Glucose)	Merck
Glycerol	AppliChem
Glycine	Merck
Hemin chloride	Calbiochem
HEPES [4-(2-hydroxyethyl)-1-piperazineethanesulfonic acid]	Merck
Histidine (L-His)	Sigma Aldrich
Hydrochloric acid (HCl)	VWR
Hypoxanthine	c.c.pro
Isopropanol	Sigma Aldrich
Leucine (L-Leu)	Sigma Aldrich
Lithium acetate	Sigma Aldrich
Luria Bertani (LB) agar	Carl Roth
Luria Bertani (LB) medium	Carl Roth
Lysine (L-Lys)	Sigma Aldrich
Manganese (II) chloride	Merck
Methanol	Honeywell
Methyl-PEG-maleimide (mm(PEG)24) reagent	Thermo Scientific
Midori Green Advance	Nippon Genetics
Milk powder (low-fat)	Carl Roth
MOPS (3-(*N*-morpholino)propane sulfonic acid)	Gerbu Biotechnik
N-ethylmaleimide (NEM)	Sigma Aldrich
Paraformaldehyde	Sigma Aldrich

Chemical	*Source*
Phenylmethylsulphonyl fluoride (PMSF)	Serva
Polyethylene glycol (PEG 3350)	Sigma Aldrich
PonceauS	Serva
Potassium acetate	Sigma Aldrich
Potassium chloride (KCl)	AppliChem
Potassium dihydrogen phosphate	Merck
Potassium monohydrogen phosphate	Merck
Prestained protein ladder	Thermo Scientific
Proteinase K	Roche
RNAse A	Sigma Aldrich
Roti Phenol/Chlorophorm/Isoamylalcohol	Carl Roth
RPMI 1640, HEPES	Life Technologies
Sodium acetate	Sigma Aldrich
Sodium chloride	Sigma Aldrich
Sodium dihydrogen phosphate	Merck
Sodium dodecyl sulphate (SDS)	Serva
Sodium hydroxide	Fischer Scientific
Sodium monohydrogen phosphate	Merck
Sorbitol (D-sorbitol)	Sigma Aldrich
TCEP (tris(2-carboxyethyl)phosphine)	Sigma Aldrich
Tetramethyl ethylenediamine (TEMED)	Serva
Trichloroacetic acid	Merck
Tris	Carl Roth
Tri-sodium citrate dihydrate	Merck
Triton X-100	Merck
Tryptone	BD
Tryptophan (L-Trp)	Sigma Aldrich
Tween-20	Sigma Aldrich
UltraPure Salmon Sperm DNA Solution	Invitrogen
Uracil	Sigma Aldrich
Urea	Serva
Yeast extract	BD
Yeast nitrogen base without amino acids	Sigma Aldrich

2.1.4 Enzymes

Table 2.4 | List of enzymes

Enzyme	*Operating conditions*	*Source*
Pfu DNA polymerase	72 °C (2 min/kb)	Promega
Phusion DNA polymerase	72 °C (15-30 sec/kb)	New England Biolabs
Proteinase K	RT – on ice	Roche
Restriction enzymes	37°C	New England Biolabs
T4 DNA ligase	16°C – RT	Thermo Scientific
Taq DNA polymerase	68°C (1 min/kb)	New England Biolabs

2.1.5 Antibodies

All antibodies were diluted in 5 % milk in TBS as indicated. Washing steps were applied at least three times for 10 min each in TBS. Antisera as used with α-*Sc*Erv1 and α-*Sc*Tim23 were washed off once in TBS, followed by three times in TBS-TT and once again in TBS to lose the detergent. Membranes that were decorated with the commercial antibody α-Flag were first washed once with TBS, then three times in TBS-T and finally with TBS. After the incubation of the secondary antibody, these membranes (α-Flag) were washed once in TBS, three times in TBS-TT and finally once in TBS.

TBS 10 mM Tris/HCl, 0.9 % (w/v) NaCl, pH 7.4

TBS-T TBS, 0.1 % (v/v) Tween 20

TBS-TT TBS, 0.1 % (v/v) Tween 20, 0.2 % (v/v) Triton X-100

Table 2.5 | List of antibodies used for western blot analysis

Name	*Origin*	*Dilution*	*Reference*
Leishmania (primary antibodies)			
α-Cytc	Rabbit	1:1000	Cell signalling technology
α-Ef1-alpha	Mouse	1:10000	Merck
α-Flag	Mouse	1:1000	Sigma Aldrich
α-*Lt*Erv	Rabbit	1:500	Eckers *et al.* 2012
α-*Lts*Tim1	Rabbit	1:500	Eckers *et al.* 2012
α-*Lt*Tim17	Rabbit	1:500	Eckers *et al.* 2012
α-*Lt*Tob55	Rabbit	1:250	Eckers *et al.* 2012
Yeast (primary antibodies)			
α-*Sc*Cmc1	Rabbit	1:250	Johannes Herrmann*
α-*Sc*Erv1	Rabbit	1:2000	Kai Hell**
α-*Sc*Tim23	Rabbit	1:500	Kai Hell**

Name	*Origin*	*Dilution*	*Reference*
α-*Sc*Tim44	Rabbit	1:250	Kai Hell**
α-*Sc*Tim50	Rabbit	1:250	Kai Hell**
α-*Sc*Tom70	Rabbit	1:250	Kai Hell**
α-*Sc*Zwf1	Rabbit	1:10 000	Buckau Lab***
Secondary antibodies			
α-Mouse IgG (H+L)-HRP conjugate	Goat	1:5000	Bio-Rad
α-Rabbit IgG (H+L)-HRP conjugate	Goat	1:10000	Bio-Rad

*Cell Biology, University of Kaiserslautern, Kaiserslautern, Germany
**Biomedical Center Munich, Ludwig-Maximilians University, Martinsried, Germany
***Center for Molecular Biology of Heidelberg University (ZMBH), Heidelberg, Germany

2.1.6 Oligonucleotides (Primers)

All oligonucleotide primers listed were purchased from Metabion. Restriction sites are underlined, and mutations introduced by mutagenesis primers are highlighted in red.

Table 2.6 | List of primers

Cloning L. tarentolae expression constructs	
Cloning MIA substrates	**Sequence 5' - 3'**
*Lt*Substrate1/s	ATGGCTCGCTCCCGTGCAGC
*Lt*Substrate1/as	CTACTGTGGAGGCTGCATCGG
*Lt*Substrate2/s	ATGATGAAGCCAACGTCCCCTAAC
*Lt*Substrate2/as	CTAGTACTCCACCTCCTGACCAG
*Lt*Substrate3/s	ATGGCGAACGGTGTGACGGC
*Lt*Substrate3/as	TCAGGCCCCCTTCTCCTTCTC
*Lt*Substrate4/s	ATGCAGGCTCCCAAGACAAGTAC
*Lt*Substrate4/as	CTACTGCGCCTTCATGCCCTTC
Mutagenesis primer	**Sequence 5' - 3'**
*Lt*Substrate2/C105S/s	GCGAGCAAAATGATG***TCT***TTCTACGAAGGTCTTCAG
*Lt*Substrate2/C105S/as	CTGAAGACCTTCGTAGAA***AGA***CATCATTTTGCTCGC
*Lt*Substrate2/C117S/s	GTTTCACAAATGGGGC***TCC***CTTCAGGACGACCTC
*Lt*Substrate2/C117S/as	GAGGTCGTCCTGAAG***GGA***GCCCCATTTGTGAAAC
*Lt*Substrate4/C122S/s	CCACGCCCATCTCG***TCT***TTTGGGCTGTTC
*Lt*Substrate4/C122S/as	GAACAGCCCAAA***AGA***CGAGATGGGCGTGG
*Lt*Substrate4/C132S/s	CATTTTCGCTGCAACA***TCC***ATGCAGATGCCGTAC
*Lt*Substrate4/C132S/as	GTACGGCATCTGCAT***GGA***TGTTGCAGCGAAAATG

Cloning Flag$_3$ and His$_8$ tags	**Sequence 5' - 3'**
pX-backbone/*FLAG*/s	GATCGGATCCTCTAGAAAGCTTGACTATAAGGACCACGACGGAG
pX-backbone/*FLAG*/as	GATCGCGGCCGCTTACTTATCGTCATCGTCTTTGTAATC
pX-backbone/*FLAG*+**His$_8$**/as	GATCGCGGCCGCTTA**GTGATGGTGATGATGGTGATGATG**CTTATCGTCA TCGTCTTTGTAATC
Subcloning into pX-Flag-(His)	**Sequence 5' - 3'**
*Lt*Substrat1/*Bam*HI/s	GATCGGATCCATGGCTCGCTCCCGTGCAGC
*Lt*Substrat1/*Hin*dIII/as	GATCAAGCTTCTGTGGAGGCTGCATCGGGTG
*Lt*Substrat2/*Bam*HI/s	GATCGGATCCATGATGAAGCCAACGTCCCC
*Lt*Substrat2/*Hin*dIII/as	GATCAAGCTTGTACTCCACCTCCTGACCAGC
*Lt*Substrat3/*Bam*HI/s	GATCGGATCCATGGCGAACGGTGTGACGGC
*Lt*Substrat3/*Hin*dIII/as	GATCAAGCTTGGCCCCCTTCTCCTTCTC
*Lt*Substrat4/*Xma*I/s	GATCCCCGGGATGCAGGCTCCCAAGACAAGTAC
*Lt*Substrat4/*Hin*dIII/as	GATCAAGCTTCTGCGCCTTCATGCCCTTCG
pX/*SCMIA40*/*Xma*I/s	GATCCCCGGGATGCTTCGCAACTTAGTCGTC
pX/*SCMIA40*/*Hin*dIII*/as	GATCAAGCTTAGGTTTGGATTCCTCATTCAATG
Subcloning into pX-backbone	***Sequence 5' - 3'***
pX/*LTERV*/*Bam*HI/rN/s	GATCGGATCCATGTCGGACGACGACGTAC
pX/*LTERV*/*Xba*I/rC/as	GATCTCTAGATTAGAGCTTGAGTTCTTCGTCC
pX/KISS/*Bam*HI/tN/s	GATCGGATCCATGGTGGTGCTGCGTCGG
pX/*LTERV*/*Xba*I/tC/as	GATCTCTAGATTATTGTTCCTCGATCGTTGGCG
Sequencing primer	**Sequence 5' - 3'**
pX-LS-s	CACCCTCAACCACCCCTC
pX-far-as	CACCCCAGGCTTTACACTT
Cloning E. coli expression constructs	
Subcloning into pET28	**Sequence 5' - 3'**
*Lt*Substrat1/*Nco*I/s	GATCCCATGGATGGCTCGCTCCCGTGCAGC
*Lt*Sub1/*Hin*dIII/*/as	GATCAAGCTTCTACTGTGGAGGCTGCATCGG
*Lt*Substrat2/*Nco*I/s	GATCCCATGGATGATGAAGCCAACGTCCCC
*Lt*Sub2/*Hin*dIII/*/as	GATCAAGCTTCTAGTACTCCACCTCCTGAC
*Lt*Substrat3/*Nco*I/s	GATCCCATGGATGGCGAACGGTGTGACGGC
*Lt*Sub3/*Hin*dIII/*/as	GATCAAGCTTTCAGGCCCCCTTCTCCTTCTC
*Lt*Substrat4/*Nco*I/s	GATCCCATGGATGCAGGCTCCCAAGACAAGTAC
*Lt*Sub4/*Hin*dIII/*/as	GATCAAGCTTCTACTGCGCCTTCATGCCCTTC

Cloning P. falciparum knock out plasmid pL7 and rescue plasmid	
Mutagenesis primer	**Sequence 5' - 3'**
PFERV/SDM3mis/fw	GCTTTTTCAAATTTATATCCT***TGCCACATC***TGTAAATTAGATTTATTAC
PFERV/SDM3mis/rw	GTAATAAATCTAATTTACA***GATGTGGCA***AGGATATAAATTTGAAAAAGC
Cloning primer	**Sequence 5' - 3'**
pL6/gRNA/*PFERV*/s	TAAGTATATAATATTTCTAATTTACAAATATGACAGTTTTAGAGCTAGAA
pL6/gRNA/*PFERV* /as	TTCTAGCTCTAAAACTGTCATATTTGTAAATTAGAAATATTATATACTTA
PFERV/5'MCS/*Sac*II/pL6/s	GATCCCGCGGTTATCTATCAAGTTGGAGGTTC
PFERV/5'MCS *Xba*I/pL6/as	GATCTCTAGACGTATGCTTTATTTTATCATATTC
PFERV/3'MCS/*Eco*RI/pL6/s	GATCGAATTCTTTACATAACATGATCAACCAAG
PFERV/3'MCS/*Nco*I/pL6/as	GATCCCATGGTGTATGATTTATATGCTGATTCC
pL6/gRNA/*PFTIM13*/s	TAAGTATATAATATTTAAAACTGTACACATGTAGAGTTTTAGAGCTAGAA
pL6/gRNA/*PFTIM13*/as	TTCTAGCTCTAAAACTCTACATGTGTACAGTTTTAAATATTATATACTTA
PFTIM13/5'MCS/*Sac*II/pL6/s	GATCCCGCGGAACATATTAAGAAGGAACAAGTTC
PFTIM13/5'MCS/*Xba*I/pL6/as	GATCTCTAGATACGATGGAATGTATAATATATTC
PFTIM13/3'MCS/*Eco*RI/pL6/s	GATCGAATTCGGCGCTTGGAACAGATGAC
PFTIM13/3'MCS/*Nco*I/pL6/as	GATCCCATGGCATATGTAACGGTATGTCTCC
PFERV/pHBIRH/*Not*I/fw	GATCGCGGCCGCATGATATTTATTGAAAAGTGCTATGAAC
PFERV/pHBIRH/*Sac*I/rw	GATCGAGCTCTTAATCAACTGTTTTGTACTTGTC
Analytical PCR primer	**Sequence 5' - 3'**
PFTIM13-check-PCR/s	TTTTCCCATCTTTTCCATTTTGG
PFTIM13-check-PCR/as	CAATGAAGGGTTATGTTAAATATAC
Sequencing primer	**Sequence 5' - 3'**
gRNA/LanzerLab-fw	GTAACCAAAATGCATAATTTTTCC
gRNA/LanzerLab	TAGGAAATAATAAAAAAGCACC
pL7/MCS1/s	TATATCCAATGGCCCCTTTC
pL7/MCS1/as	CAAAATGCTTAAGTCCTCCAC
pL7/MCS2/as	AACATTTGCTTTCTTGAAACGG
Seq0pBIRTH/Fw	TACCTACATACATATACAAACC
Cloning yeast plasmid shuffling constructs	
Mutagenesis primer	**Sequence 5' - 3'**
LTERV/C17S/s	CCCTGGTGAG***TCC***CCCACCCCGCTG
LTERV/C17S/as	CAGCGGGGTGGG***GGA***CTCACCAGGG
LTERV/C92S/s	TCTCACGCTACGTG***TCT***GAGATGCACAACAACG
LTERV/C92S/as	CGTTGTTGTGCATCTC***AGA***CACGTAGCGTGAGA
LTERV/C109S/s	CAAAGAACTCTTTGAT***TCC***ACCCCTAGCGTGGTGC
LTERV/C109S/as	GCACCACGCTAGGGGT**GGA**ATCAAAGAGTTCTTTG

Mutagenesis primer	**Sequence 5' - 3'**
pYX/*SCERV1*/*Lt*CxC/mut/s	GAAGATGGCAAACCT***TGTCAAGTGTACTGC***AACACCCTACTTGAC
pYX/*SCERV1*/*Lt*CxC/mut/as	GTCAAGTAGGGTGTT***GCAGTACACTTGACA***AGGTTTGCCATCTTC
Cloning primer for chimera	**Sequence 5' - 3'**
pYX232/*LTERV*/KissEnd/*Xho*I/as	GATCCTCGAGCTAACGCTTGAGACGTTTGAG
pYX232/*LTERV*/linker/*Xho*I/as	GATCCTCGAGCTACTCGATCGTTGGCGTATC
*SCERV*1Link/*Xho*I/as	GATCCTCGAGTTATTCGTCCCAGCC
pYX/*SCERV1*/C-T/*Eco*RI/s	GATCGAATTCATGAAAGCAATAGATAAAATGACG
overlap pYX/*Sc*CT/*Lt*FAD/s	CTCAAGAACATACAGGAAGGTTTGCCCCACCCCGCTGGAG
overlap pYX/*Sc*CT/*Lt*FAD/as	CTCCAGCGGGGTGGGGCAAACCTTCCTGTATGTTCTTGAG
pYX/*LTERV*/N-T/*Xho*I/as	GATCCTCGAGCTAGAGCTTGAGTTCTTCGTC
overlap pXY/*Sc*FAD/*Lt*Linker/s	GTAATTTCTGGGAAAAAAGATGGCACCCTGGGTACCCAAACAAG
overlap pXY/*Sc*FAD/*Lt*Linker/as	CTTGTTTGGGTACCCAGGGTGCCATCTTTTTTCCCAGAAATTAC
Subcloning into pYX232	**Sequence 5' - 3'**
pYX232/*LTERV*/*Eco*RI/rN/s	GATCGAATTCATGTCGGACGACGACGTACACG
pYX232/*LTERV*/*Xho*I/rC/as	GATCCTCGAGTTAGAGCTTGAGTTCTTCGTCC
pYX232/KISS/*Eco*RI/tN/s	GATCGAATTCATGGTGGTGCTGCGTCGGTGG
pYX232/*LTERV*/*Xho*I/tC/as	GATCCTCGAGTTATTGTTCCTCGATCGTTGGCG
Cloning Mia40-MTS constructs	**Sequence 5' - 3'**
pYX232/*MIA40*MTS/*Eco*RI/s	GATCGAATTCATGCTTCGCAACTTAGTCGTC
pYX232/*MIA40*MTS/as	AGGCTTCCTATTAGGAGCAATA
pYX232/*MIA40*MTS/*PFERV*/overlap/s	TATTGCTCCTAATAGGAAGCCTATGATATTTATTGAAAAGTGCTATGAAC
pYX232/*PFERV*/*Xho*I/as	GATCCTCGAGTTAATCAACTGTTTTGTACTTGTC
pYX232/*MIA40*MTS/*LTERV*/overlap/s	TATTGCTCCTAATAGGAAGCCTATGTCGGACGACGACGTACACG
pYX232/*MIA40*MTS/*LTERV*Cterm/overlap/s	TATTGCTCCTAATAGGAAGCCTATGGTGGTGCTGCGTCGGTGG
pYX232/*MIA40*MTS/*SCERV*Nterm/overlap/s	TATTGCTCCTAATAGGAAGCCTATGAAAGCAATAGATAAAATGACGGAT
Analytical PCR primer	**Sequence 5' - 3'**
*SCERV*CxxC/s	CTTGCCGATCATGTAACACCC
*SCERV*Linker/*Xho*I/as	CTCGAGTTATTCGTCCCAGCC
*SCERV*LtCxxxC/s	GTCAAGTGTACTGCAACACCC
*LTERV*Linker/*Xho*I/as	CTCGAGCTACTCGATCGTTGG
Sequencing primer	**Sequence 5' - 3'**
pYX232-fw	GCAGCATAATTTAGGAGTTTA
pYX232-rev	GATGTATCGGTCAGTCATTAATAC

2.1.7 Plasmids/constructs

Table 2.7 | List of plasmids and constructs

Name	*Characteristics/Application*	*Reference*
Vectors		
pDRIVE	Amp^R, Kan^R, T7 promoter, SP6 promoter; Subcloning in *E. coli*	Qiagen
pET28a	Kan^R, T7 promoter, C- and N-terminal His-Tag; Expression in *E. coli*	Novagen
pHBIRH	Amp^R, $BlasticidinS^R$, *RLUC;* Rescue *P. falciparum* knock out strains	Kristin Fürle*
pL6	Amp^R, hDHFR, *SCFCU1*; Guide RNA expression and homologous recombination in *P. falciparum* via CRISPR/Cas9	J.J. Lopez-Rubio**
pQE30	Amp^R, N-terminal MRGSH6GS-Tag, T5 promoter; Expression and subcloning in *E. coli*	Qiagen
pX-backbone	Amp^R, Neo^R, N-terminal His_8-Tag; Expression and pull-down assays in *L. tarentolae*	Linda Liedgens*
pX-Flag	Amp^R, Neo^R, C-terminal Flag-Tag; Expression in *L. tarentolae*	Mirko Höhn***
pX-Flag-His	Amp^R, Neo^R, C-terminal Flag-Tag, C-terminal His_8-Tag; Expression and pull-down assays in *L. tarentolae*	Mirko Höhn***
pYX232	Amp^R, 2µ, TRP, TPI promoter; Plasmid shuffling in *S. cerevisiae*	Eckers *et al.* 2013
TOPO-TA	Amp^R, Kan^R, T7 promoter; Subcloning in *E. coli*	Life Technologies
E. coli cloning and expression plasmids		
pDRIVE/ Sub 1	Putative MIA substrate 1 [LtaP04.0660]	Mirko Höhn***
pDRIVE/ Sub 2	Putative MIA substrate 2 [LtaP35.0210]	Mirko Höhn***
pDRIVE/ Sub 2/ C105S	Putative MIA substrate 2, point mutation C105S	Mirko Höhn***
pDRIVE/ Sub 2/ C117S	Putative MIA substrate 2, point mutation C117S	Mirko Höhn***
pDRIVE/ Sub 3	Putative MIA substrate 3 [LtaP19.1110]	Mirko Höhn***

Name	***Characteristics/Application***	***Reference***
pDRIVE/ Sub 4	Putative MIA substrate 4 [LtaP09.1390]	Mirko Höhn***
pDRIVE/ Sub 4/ C122S	Putative MIA substrate 4, point mutation C122S	Mirko Höhn***
pET28/ Sub 1	Putative MIA substrate 1 (*Nco*I /*Hin*dIII)	Mirko Höhn***
pET28/ Sub 2	Putative MIA substrate 2 (*Nco*I/*Hin*dIII)	Mirko Höhn***
pET28/ Sub 2/ C105S	Putative MIA substrate 2 (*Nco*I/*Hin*dIII), point mutation C105S	This work
pET28/ Sub 2/ C117S	Putative MIA substrate 2 (*Nco*I/*Hin*dIII), point mutation C117S	This work
pET28/ Sub 3	Putative MIA substrate 3 (*Nco*I/*Hin*dIII)	Mirko Höhn***
pET28/ Sub 4	Putative MIA substrate 4 (*Nco*I/*Hin*dIII)	Mirko Höhn***
pL6/ gRNA/ *PFERV*	*PFERV* guide RNA	This work
pL6/ gRNA/ *PFTIM13*	*PFTIM13* guide RNA	This work
pL7/ gRNA/ 3'/ *PFERV*	*PFERV* guide RNA and 3' homologous region (*Eco*RI/*Nco*I)	This work
pL7/ gRNA/ 3'/ *PFTIM13*	*PFTIM13* guide RNA and 3' homologous region (*Eco*RI/*Nco*I)	This work
pQE30/ #1 *LTERV*/ C-term	*LTERV* residues 123-314 (*Bam*HI/*Hin*dIII)	Eckers (2012)
pQE30/ #2 *LTERV*/ N-term	*LTERV* residues 1-119 (*Bam*HI/*Hin*dIII)	Eckers (2012)
pQE30/ #2 *LTERV*/ N-term/C17S	*LTERV* residues 1-119 (*Bam*HI/*Hin*dIII), point mutation C17S	Specht *et al.* 2018
pQE30/ #3 *LTERV*/ C300S/ C304S	*LTERV* (*Bam*HI/*Hin*dIII), point mutation C300S and C304S	Eckers *et al.* 2013
pQE30/ #3 *LTERV*/ C17S/ C300S/ C304S	*LTERV* (*Bam*HI/*Hin*dIII), point mutation C17S, C300S and C304S	Specht et al., 2018
pQE30/ #4 *LTERV*/ C63S	*LTERV* (*Bam*HI/*Hin*dIII), point mutation C63S	Eckers *et al.* 2013
pQE30/ #4 *LTERV*/ C17S/ C63S	*LTERV* (*Bam*HI/*Hin*dIII), point mutation C17S and C63S	Specht *et al.* 2018
pQE30/ #5 *LTERV*/ C300S	*LTERV* (*Bam*HI/*Hin*dIII), point mutation C300S	Eckers *et al.* 2013
pQE30/ #5 *LTERV*/ C17S/ C300S	*LTERV* (*Bam*HI/*Hin*dIII), point mutation C17S and C300S	Specht *et al.* 2018

Name	***Characteristics/Application***	***Reference***
pQE30/ #6 *LTERV*/ C17S	*LTERV* (*Bam*HI/*Hin*dIII), point mutation C17S	Eckers *et al.* 2013
pQE30/ #7 *LTERV*/ C92S/ C109S	*LTERV* (*Bam*HI/*Hin*dIII), point mutation C92S and C109S	Specht *et al.* 2018
pQE30/ #7 *LTERV*/ C17S/ C92S/ C109S	*LTERV* (*Bam*HI/*Hin*dIII), point mutation C17S, C92S and C109S	Specht *et al.* 2018
pQE30/ *PFERV*	*PFERV* (*Bam*HI/*Hin*dIII)	Eckers *et al.* 2013
pQE30/ *PFERV*/ 3mismatch	*PFERV* (*Bam*HI/*Hin*dIII), silent point mutations T249C, T252C and T255C	This work
TOPO-TA/ *PFERV*/ *3'*	*PFERV* 3' homologous region	This work
TOPO-TA/ *PFERV*/ *5'*	*PFERV* 5' homologous region	This work
TOPO-TA/ *PFTIM13*/ *3'*	*PFTIM13* 3' homologous region	This work
TOPO-TA/ *PFTIM13*/ *5'*	*PFTIM13* 5' homologous region	This work
L. tarentolae expression constructs		
pX/ *LTERV*	*LTERV* (*Bam*HI/*Hin*dIII)	Linda Liedgens*
pX/ #1 *LTERV*/ C-term	*LTERV* residues 123-314 (*Bam*HI/*Xba*I)	This work
pX/ #2 *LTERV*/ N-term	*LTERV* residues 1-119 (*Bam*HI/*Xba*I)	This work
pX/ #3 *LTERV*/ C300S/ C304S	*LTERV* (*Bam*HI/*Xba*I), point mutation C300S and C304S	This work
pX/ #4 *LTERV*/ C63S	*LTERV* (*Bam*HI/*Xba*I), point mutation C63S	This work
pX/ #5 *LTERV*/ C300S	*LTERV* (*Bam*HI/*Xba*I), point mutation C300S	This work
pX/ #6 *LTERV*/ C17S	*LTERV* (*Bam*HI/*Xba*I), point mutation C17S	This work
pX/ #7 *LTERV*/ C92S/ C109S	*LTERV* (*Bam*HI/*Xba*I), point mutation C92S and C109S	This work
pX-Flag-His/ *MIA40s*	*MIA40* residues 1-70 and 284-403 (*Xma*I/*Hin*dIII)	This work
pX-Flag-His/ *MIA40s*/ SPS	*MIA40* residues 1-70 and 284-403 (*Xma*I/*Hin*dIII), point mutation C85S and C87S	This work
pX-Flag-His/ Sub 1	Putative MIA substrate 1 (*Bam*HI/*Hin*dIII)	This work
pX-Flag-His/ Sub 2	Putative MIA substrate 2 (*Bam*HI/*Hin*dIII)	This work
pX-Flag-His/ Sub 2/ C105S	Putative MIA substrate 2 (*Bam*HI/*Hin*dIII), point mutation C105S	This work

Name	***Characteristics/Application***	***Reference***
pX-Flag-His/ Sub 2/ C117S	Putative MIA substrate 2 (*Bam*HI/*Hin*dIII), point mutation C117S	This work
pX-Flag-His/ Sub 3	Putative MIA substrate 3 (*Bam*HI/*Hin*dIII)	This work
pX-Flag-His/ Sub 4	Putative MIA substrate 4 (*Xma*I/*Hin*dIII)	This work
pX-Flag/ *MIA40s*	*MIA40* residues 1-70 and 284-403 (*Xma*I/*Hin*dIII)	This work
pX-Flag/ *MIA40s*/ SPS	*MIA40* residues 1-70 and 284-403 (*Xma*I/*Hin*dIII), point mutation C85S and C87S	This work
pX-Flag/ Sub 1	Putative MIA substrate 1 (*Bam*HI/*Hin*dIII)	This work
pX-Flag/ Sub 2	Putative MIA substrate 2 (*Bam*HI/*Hin*dIII)	This work
pX-Flag/ Sub 2/ C105S	Putative MIA substrate 2 (*Bam*HI/*Hin*dIII), point mutation C105S	This work
pX-Flag/ Sub 2/ C117S	Putative MIA substrate 2 (*Bam*HI/*Hin*dIII), point mutation C117S	This work
pX-Flag/ Sub 3	Putative MIA substrate 3 (*Bam*HI/*Hin*dIII)	This work
pX-Flag/ Sub 4	Putative MIA substrate 4 (*Xma*I/*Hin*dIII)	This work
P. falciparum knock out and rescue constructs		
pL7/ gRNA/ 3'/ 5'/ *PFERV*	*PFERV* guide RNA, 3' (*Eco*RI/*Nco*I) and 5' (*Sac*II/*Xba*I) homologous region	This work
pL7/ gRNA/ 3'/ 5'/ *PFTIM13*	*PFTIM13* guide RNA, 3' (*Eco*RI/*Nco*I) and 5' (*Sac*II/*Xba*I) homologous region	This work
pHBIRH/ *PFERV*/ 3mismatch	*RLUC* was replaced with *PFERV* (*Not*I/*Sac*I), silent point mutations T249C, T252C and T255C	This work
Yeast plasmid shuffling constructs		
pRS314/ *MIA40s*	*MIA40* residues 1-70 and 284-403	Peleh *et al.* 2016
pRS314/ *MIA40s*/ SPS	*MIA40* residues 1-70 and 284-403, point mutation C85S and C87S	Peleh *et al.* 2016
pYX232/ Chimera 1	*SCERV1* residues 1-82 and *LTERV* residues 17-312 (*Eco*RI/*Xho*I)	Specht *et al.* 2018 Maike Eberhardt*
pYX232/ Chimera 1/ Mia40MTS	*SCMIA40* residues 1-70, *SCERV1* residues 1-82 and *LTERV* residues 17-312 (*Eco*RI/*Xho*I)	Specht *et al.* 2018

Name	***Characteristics/Application***	***Reference***
pYX232/ Chimera 2	*SCERV1* residues 1-82 and *LTERV* residues 17-299 (*Eco*RI/*Xho*I)	Specht *et al.* 2018 Maike Eberhardt*
pYX232/ Chimera 2/ Mia40MTS	*SCMIA40* residues 1-70, *SCERV1* residues 1-82 and *LTERV* residues 17-299 (*Eco*RI/*Xho*I)	Specht *et al.* 2018
pYX232/ Chimera 3	*SCERV1* residues 1-82 and *LTERV* residues 17-133 (*Eco*RI/*Xho*I)	Specht *et al.* 2018 Maike Eberhardt*
pYX232/ Chimera 3/ Mia40MTS	*SCMIA40* residues 1-70, *SCERV1* residues 1-82 and *LTERV* residues 17-133 (*Eco*RI/*Xho*I)	Specht *et al.* 2018
pYX232/ Chimera 4	*SCERV1* residues 1-181 and *LTERV* residues 117-312 (*Eco*RI/*Xho*I)	Specht *et al.* 2018 Maike Eberhardt*
pYX232/ Chimera 4/ Mia40MTS	*SCMIA40* residues 1-70, *SCERV1* residues 1-181 and *LTERV* residues 117-312 (*Eco*RI/*Xho*I)	Specht *et al.* 2018
pYX232/ Chimera 5	*SCERV1* residues 1-181 and *LTERV* residues 117-299 (*Eco*RI/*Xho*I)	Specht *et al.* 2018 Maike Eberhardt*
pYX232/ Chimera 5/ Mia40MTS	*SCMIA40* residues 1-70, *SCERV1* residues 1-181 and *LTERV* residues 117-299 (*Eco*RI/*Xho*I)	Specht *et al.* 2018
pYX232/ Chimera 6	*SCERV1* residues 1-29, *LTERV* residues 300-304 and *SCERV1* residues 34-189 (*Eco*RI/*Xho*I)	Specht *et al.* 2018 Maike Eberhardt*
pYX232/ Chimera 6/ Mia40MTS	*SCMIA40* residues 1-70, *SCERV1* residues 1-29, *LTERV* residues 300-304 and *SCERV1* residues 34-189 (*Eco*RI/*Xho*I)	Specht *et al.* 2018
pYX232/ *LTERV*	*LTERV* (*Bam*HI/*Xho*I)	Eckers *et al.* 2013
pYX232/ *LTERV*/ Mia40MTS	*SCMIA40* residues 1-70 and *LTERV* (*Bam*HI/*Xho*I)	Specht *et al.* 2018
pYX232/ #1 *LTERV*/ C-term	*LTERV* residues 123-314 (*Eco*RI/*Xho*I)	Specht *et al.* 2018
pYX232/ #1 *LTERV*/ C-term/ Mia40MTS	*SCMIA40* residues 1-70 and *LTERV* residues 123-314 (*Eco*RI/*Xho*I)	Specht *et al.* 2018
pYX232/ #2 *LTERV*/ N-term	*LTERV* residues 1-119 *Eco*RI/*Xho*I)	Specht *et al.* 2018
pYX232/ #2 *LTERV*/ N-term/C17S	*LTERV* residues 1-119 (*Eco*RI/*Xho*I), point mutation C17S	Specht *et al.* 2018
pYX232/ #2 *LTERV*/ N-term/ Mia40MTS	*SCMIA40* residues 1-70 and *LTERV* residues 1-119 (*Eco*RI/*Xho*I)	Specht *et al.* 2018

Name	*Characteristics/Application*	*Reference*
pYX232/ #3 *LTERV*/ C300S/ C304S	*LTERV* (*Eco*RI/*Xho*I, point mutation C300S and C304S	Specht *et al.* 2018
pYX232/ #3 *LTERV*/ C17S/ C300S/ C304S	*LTERV* (*Eco*RI/*Xho*I), point mutation C17S, C300S and C304S	Specht *et al.* 2018
pYX232/ #4 *LTERV*/ C63S	*LTERV* (*Eco*RI/*Xho*I), point mutation C63S	Specht *et al.* 2018
pYX232/ #4 *LTERV*/ C17S/ C63S	*LTERV* (*Eco*RI/*Xho*I), point mutation C17S and C63S	Specht *et al.* 2018
pYX232/ #5 *LTERV*/ C300S	*LTERV* (*Eco*RI/*Xho*I), point mutation C300S	Specht *et al.* 2018
pYX232/ #5 *LTERV*/ C17S/ C300S	*LTERV* (*Eco*RI/*Xho*I), point mutation C17S and C300S	Specht *et al.* 2018
pYX232/ #6 *LTERV*/ C17S	*LTERV* (*Eco*RI/*Xho*I), point mutation C17S	Specht *et al.* 2018
pYX232/ #6 *LTERV*/ C17S/ Mia40MTS	*SCMIA40* residues 1-70 and *LTERV* (*Eco*RI/*Xho*I), point mutation C17S	Specht *et al.* 2018
pYX232/ #7 *LTERV*/ C92S/ C109S	*LTERV* (*Eco*RI/*Xho*I), point mutation C92S and C109S	Specht *et al.* 2018
pYX232/ #7 *LTERV*/ C17S/ C92S/ C109S	*LTERV* (*Eco*RI/*Xho*I), point mutation C17S, C92S and C109S	Specht *et al.* 2018
pYX232/ *PFERV*	*PFERV* (*Nco*I/*Xho*I)	Eckers *et al.* 2013
pYX232/ *PFERV*/ Mia40MTS	*SCMIA40* residues 1-70 and *PFERV* (*Nco*I/*Xho*I)	Specht *et al.* 2018
pYX232/ *SCERV1*	*SCERV1* (*Eco*RI/*Xho*I)	Eckers *et al.* 2013

*Centre for Infectious Diseases, Parasitology, University Hospital Heidelberg
**Laboratoire de Parasitologie - Mycologie, Montpellier, France
***Biochemistry, University of Kaiserslautern, Kaiserslautern, Germany

2.1.8 Bacterial strains

Table 2.8 | List of *E. coli* strains

Strain	*Genotype*	*Application*	*Source*
XL-1 blue	recA1 endA1 gyrA96 thi-1 hsdR17 supE44 relA1 lac [F´ proAB $lacI^qZ\Delta M15$ Tn10 (Tetr)].	Cloning	Qiagen
NovaBlue Singles™ competent cells	endA1 hsdR17 (r_{K12}^- m_{K12}^+) supE44 thi-1 recA1 gyrA96 relA1 lac F'[$proA^+B^+$ $lacI^qZ\Delta M15$::Tn10] (Tet^R)	Cloning	Merck

2.1.9 *Leishmania* strains

The *L. tarentolae* WT strain listed below was genetically manipulated by introducing episomal DNA using the *Leishmania* expression vectors pX-backbone, pX-Flag and pX-Flag-His. For a detailed listing of constructs transfected into *L. tarentolae* see Table 2.7.

Table 2.9 | List of *L. tarentolae* strains

Strain	***Source***
UC	André Schneider*

*Department of Chemistry and Biochemistry, University of Bern, Bern, Switzerland

2.1.10 *Plasmodium* strains

The listed *P. falciparum* strains were used for further genetic manipulations. A complete list of constructs that were introduced into these strains can be found in Table 2.7.

Table 2.10 | List of *P. falciparum* strains

Strain	***Characteristics***	***Source***
3D7	Origin: derived from NF54	Michael Lanzer*
3D7pUF1-Cas9	Transgene parasite line expressing Cas9	Verena Staudacher*

*Centre for Infectious Diseases, Parasitology, University Hospital Heidelberg

2.1.11 Yeast strains

The *S. cerevisiae* knock out strains listed below were further genetically modified by transfecting episomal DNA as part of the yeast expression vectors pRS314 and pYX232. For more detailed information see Table 2.7.

Table 2.11 | List of *S. cerevisiae* strains

Strain	***Genotype***	***Application***	***Source***
YPH499Δmia40	*ura3-52*, ***lys2****-801^{amber}*, ***ade2****-101^{ocre}*, ***trp1****-Δ63*, *his3-Δ200*, ***leu2****-Δ1, mia40::His5* [pRS316*SCMIA40, URA3*]	Plasmid shuffling	Johannes Herrmann*
YPH501Δerv1	*ura3-52*, ***lys2****-801^{amber}*, ***ade2****-101^{ocre}*, ***trp1****-Δ63*, *his3-Δ200*, ***leu2****-Δ1, erv1::His3* [pRS426*MET*25*SCERV1, URA3*]	Plasmid shuffling	Johannes Herrmann*

*Cell Biology, University of Kaiserslautern, Kaiserslautern, Germany

2.1.12 Selection drugs

Antimalarial drugs were prepared in DMSO and further diluted in RPMI1640. All stock solutions were stored at -20°C under light protection.

Table 2.12 | List of selection drugs

Drug	*Stock solution*	*Working concentration*	*Supplier*
E. coli			
Ampicillin	100 mg/mL in 50 % ethanol	100 µg/mL	AppliChem
Kanamycin	25 mg/mL in ddH_2O	25 µg/mL	AppliChem
L. tarentolae			
G418 disulphate	50 mg/mL in ddH_2O	0.1 mg/mL	AppliChem
P. falciparum			
Atovaquone	200 µM in RPMI 1640	100 nM	Sigma Aldrich
Blasticidin S	10 mg/mL in HEPES buffer	2 µg/mL	Invivogen
WR99210	20 µM in RPMI 1640	5 nM	Jacobus Pharmaceutical

2.1.13 Kits

Table 2.13 | List of commercial kits

Kit	***Manufacturer***
Amersham ECL Western Blotting Detection Reagents	GE Healthcare
Basic Parasite Nucleofector™ Kit 2	Lonza
In Fusion HD Cloning Kit	Clontech
Plasmid Mini/Midi/Maxi Kit	Qiagen
SuperSignal West Femto	Thermo Scientific
TOPO TA – Cloning Kit	Invitrogen
Wizard® SV Gel and PCR Clean-Up System	Promega

2.1.14 Software and databases

Table 2.14 | List of software and databases

Software/Database	***Source***
BioEdit	http://bioedit.software.informer.com/7.2/
Clustal Omega Alignment tool	https://www.ebi.ac.uk/Tools/msa/clustalo/
CorelDraw X7	Corel Corporation
EndNote X7	Thomson Reuters

Software/Database	*Source*
ExPASy	https://www.expasy.org/
JustBio	http://www.justbio.com
MS Office	Microsoft
NCBI (Database)	http://www.ncbi.nlm.nih.gov
NEBcutter	V2.0 http://nc2.neb.com/NEBcutter2/
PlasmoDB	http://plasmodb.org/plasmo/
Pro-data SX	Applied Photophysics
Protospacer	http://www.protospacer.com/
SigmaPlot 13.0	Systat Software, Inc.
Saccharomyces Genome Database (SGD)	https://www.yeastgenome.org/
Spectra manager	JASCO
TriTrypDB	http://tritrypdb.org/tritrypdb/

2.2 Sterilisation

All media, buffers and solutions were sterilised by autoclaving at 121 °C for 15 min. Glass materials, pipette tips, reaction tubes, other disposals, liquid waste and bags were autoclaved at 121 °C for 20 min. Heat instable solutions were instead filter sterilised using a pore size of 0.22 µm.

2.3 Molecular biology methods

2.3.1 Cloning constructs for genetic manipulation of *P. falciparum*

The pL7 constructs to knock out *PFERV* and *PFTIM13* were generated over numerous different cloning steps. Guide sequences were determined by the protospacer software and generated by annealing the complementary primers pL6/gRNA/s and pL6/gRNA/as. Oligonucleotides were therefore boiled at 94 °C for 2 min and slowly cooled to room temperature (RT). The resulting guide DNA was fused into the *Avr*II/*Btg*ZI restriction sites of plasmid pL6 using the In-Fusion HD Cloning Kit according to the manufacturer's protocol. Three' and 5' homologous regions were amplified by polymerase chain reaction (PCR) from genomic DNA (gDNA) of strain 3D7 using *Taq* DNA polymerase and the primer pair 3'MCS/*Eco*RI/pL6/s and 3'MCS/*Nco*I/pL6/as or 5'MCS/*Sac*II/pL6/s and 5'MCS/*Xba*I/pL6/as, respectively. The obtained PCR fragments were subcloned into TOPO-TA according to manufacturer's protocol and introduced into pL6 via the restriction sites *Eco*RI/*Nco*I (3') and *Sac*II/*Xba*I (5').

To generate the pHBIRH/*PFERV*/3mismatch rescue plasmid, *PFERV* was first mutated by site-directed mutagenesis to protect the episomal *ERV* copy from Cas9 activity. Silent point mutations were

introduced by Gino Turra at the position T249C, T252C and T255C at proximity to the protospacer adjacent motif (PAM) to decrease the likelihood of a stable sgRNA/DNA heteroduplex (Cong *et al.*, 2013; Hsu *et al.*, 2013; Sternberg *et al.*, 2014; Stemmer *et al.*, 2015). The previously cloned pQE30/*PFERV* (Eckers *et al.*, 2013) was used as template. The construct was finally introduced into vector pHBIRH via the *Not*I/*Sac*I restriction sites.

2.3.2 Cloning constructs for genetic manipulation of *L. tarentolae*

For protein production in *Leishmania* and purification purposes, two pX vectors were designed (Linda Liedgens and Mirko Höhn) having either a C-terminal $FLAG_3$-tag or a C-terminal $FLAG_3$-His_8-tag. Tags were amplified from vector pLPC (provided by Gino Turra) using *Pfu* DNA polymerase and the primers pX-backbone/*FLAG*/s and pX-backbone/*FLAG*/as or pX-backbone/*FLAG*+His_8/as, respectively. Both tags were introduced separately in vector pX-backbone using the restriction sites *Hin*dIII/*Not*I to produce the new plasmids pX-Flag and pX-Flag-His (Mirko Höhn).

The putative substrates 1-4 of the oxidative protein folding pathway were amplified from gDNA by the primer pair *Lt*SubstrateX/s and *Lt*SubstrateX/as, and *Taq* DNA polymerase. Constructs were subsequently subcloned into pDRIVE (Mirko Höhn). Cysteine point mutations of the substrates 2 and 4 were introduced by site-directed mutagenesis using primers listed in Table 2.6 (section "Mutagenesis primer", by Mirko Höhn and myself). All the pDRIVE constructs served as templates in a following PCR reaction using *Pfu* DNA polymerase and the primer pairs *Lt*SubstrateX/*Bam*HI/s and *Lt*SubstrateX/*Hin*dIII/as or *Lt*Substrate4/*Xma*I/s and *Lt*Substrate4/*Hin*dIII/as, respectively. Substrates were introduced into the *Bam*HI/*Hin*dIII or in case of substrate 4 into the *Xma*I/*Hin*dIII restriction sites of the *Leishmania* expression vectors pX-Flag and pX-Flag-His. For recombinant expression in *E. coli*, the substrates were amplified from pDRIVE by the primer pair *Lt*SubstrateX/*Nco*I/s and *Lt*SubX/*Hin*dIII/*/as and cloned into pET28 using the *Nco*I/*Hin*dIII restriction sites (Mirko Höhn).

MIA40s and *MIA40s-SPS* were obtained from PCR using the primers pX/*SCMIA40*/*Xma*I/s and pX/*SCMIA40*/*Hin*dIII*/as, the plasmids pRS314/*MIA40s* or pRS314/*MIA40s*/SPS as templates, and *Pfu* DNA polymerase. Both constructs were subsequently cloned into the vectors pX-Flag and pX-Flag-His as exemplified above.

LTERV truncations and cysteine mutants were previously cloned in plasmids pQE30 and pYX232 by Elisabeth Eckers and Maike Eberhardt (Eckers *et al.*, 2013; Specht *et al.*, 2018) and were *Taq*-amplified with the primers pairs pX/KISS/*Bam*HI/tN/s and pX/*LTERV*/*Xba*I/rC/as ($LTERV^{C\text{-}term}$), and pX/*LTERV*/*Bam*HI/rN/s and pX/*LTERV*/*Xba*I/tC/as ($LTERV^{N\text{-}term}$), or pX/*LTERV*/*Bam*HI/rN/s and pX/*LTERV*/*Xba*I/rC/as ($LTERV^{C300S/C304S}$, $LTERV^{C63S}$, $LTERV^{C300S}$, $LTERV^{C17S}$, $LTERV^{C92S/C17S}$). All PCR products were finally cloned into the *Bam*HI/*Xba*I restriction sites of vector pX-backbone.

2.3.3 Polymerase chain reaction (PCR)

PCR was used to amplify DNA fragments or to introduce mutations by site-directed mutagenesis. Reactions were performed in a total volume of 50 µL with gDNA or plasmid DNA as templates and primers listed in Table 2.1. *Pfu* DNA polymerase was favoured over *Taq* for fragments larger than 500 bp. Overlap extension PCR was performed with Phusion DNA polymerase. A standard cloning PCR reaction was pipetted on ice as described in Table 2.15.

Table 2.15 | Pipetting scheme of a standard cloning PCR reaction

Volume	Component
5 µL	10× Taq buffer
2 µL	dNTPs
0.5 µL	DNA template
1 µL	sense primer (100 µM)
1 µL	antisense primer (100 µM)
0.5 µL	*Taq* DNA polymerase
ad 50 µL	ddH_2O

PCR cycling conditions (Table 2.16) were chosen according to fragment size, operating polymerase (see Table 2.4) and melting temperature of the primers. The latter was calculated using the formula:

$$T_m = 4 \times N\,(G + C) + 2 \times M\,(A + T) - 5\ °C$$

Table 2.16 | Standard PCR program using *Taq* DNA polymerase

Step	Cycles	Temperature	Time
Initial denaturation	1	94 °C	120 sec
Denaturation	30	94 °C	45 sec
Annealing	30	52 °C	45 sec
Elongation	30	68 °C	60 sec
Final elongation	1	68 °C	120 sec
	hold	4 °C	

2.3.4 Site-directed mutagenesis

Point mutations were generated by site-directed mutagenesis. Mutated oligonucleotides were between 25 and 45 bases in length, which should result in a melting temperature of T_m > 78 °C. They were further designed to terminate at either the bases G or C and the mismatch was ideally introduced in the middle of the primer. Mutagenesis PCR was carried out in four different batches (A-D) in a total reaction volume of 50 µL each, adopting *Pfu* polymerase (Table 2.17).

Table 2.17 | Pipetting scheme for a standard mutagenesis PCR

A	B	C	D	Component
-	-	2 µL	2 µL	DMSO
5 µL	5 µL	5 µL	5 µL	*Pfu* buffer with $MgSO_4$
4 µL	4 µL	4 µL	4 µL	dNTPs
1 µL	1 µL	1 µL	1 µL	DNA template
1 µL [100 µM]	1 µL [1 µM]	1 µL [100 µM]	1 µL [1 µM]	sense primer
1 µL [100 µM]	1 µL [1 µM]	1 µL [100 µM]	1 µL [1 µM]	antisense primer
1 µL	1 µL	1 µL	1 µL	*Pfu* DNA polymerase
ad 50 µL	ad 50 µL	ad 50 µL	ad 50 µL	ddH_2O

Typically, a mismatch reaction was cycled as follows in Table 2.18.

Table 2.18 | Standard PCR program for mutagenesis PCR

Step	Cycles	Temperature	Time
Initial denaturation	1	94 °C	60 sec
Denaturation	18	94 °C	30 sec
Annealing	18	65 °C	60 sec
Elongation	18	72 °C	9 min
Final elongation	1	72 °C	9 min
	hold	4 °C	

Following PCR reaction, the pooled 200 µL of methylated template DNA was digested by adding 22.5 µL buffer CutSmart (NEB) and 2 µL *Dpn*I. The mixture was incubated overnight at 37 °C.

2.3.5 Purification of DNA

DNA fragments obtained from PCR or preparative restriction digestion were purified directly or after agarose gel electrophoresis and extraction from the gel by using the Wizard® SV Gel and PCR Clean-Up System. Thereby primers, salts, enzymes and agarose were removed. Clean-up was performed according to the manufacturer's protocol and DNA was finally eluted in 30 µL of the supplied water.

2.3.6 Restriction digest of DNA

DNA fragments obtained from PCR or plasmid DNA were subsequently cleaved with restriction endonucleases for subcloning or analytical purposes, respectively. Restriction enzymes were handled

according to manufacturer's recommendations. For subcloning, 30 µL of the purified PCR product or 5 µL of a plasmid preparation were digested in a total volume of 50 µL, containing 5 µL of the appropriate 10× buffer (NEB) and 0.5 µL of each restriction enzyme. The mixture was typically incubated at 37 °C for 3 h or overnight. Analytical digestions were set in a total volume of 20 µL. Therefore 5 µL plasmid DNA were incubated with 2 µL 10× buffer and 0.1 µL of each restriction enzyme at 37 °C for at least 1 h. Restriction digestions were subsequently evaluated by agarose gel electrophoresis.

2.3.7 Agarose gel electrophoresis

DNA fragments and plasmids were examined for their size, quantity and purity by agarose gel electrophoresis. Samples were supplemented with 6× loading dye purple (NEB) and loaded to a 1-2 % agarose gel in 1× TAE buffer. For detection, 1 µL/mL Midori Green was added to the loading dye as well as the DNA ladder. Gels were run at 100-150 V for 15-40 min, visualised by an UV transilluminator and documented with a camera.

1× TAE buffer 40 mM Tris/HAc, 1 mM EDTA, pH 7.6

2.3.8 Ligation of DNA fragments

Recombinant plasmids were generated by joining DNA fragments into the vector using cohesive ends. Typically inserts were mixed in a ratio of 5:1 with the digested vector reaching a total volume of 20 µL. Additionally 2 µL buffer and 1 µL T4 ligase were added before incubating the mixture at 16 °C overnight.

2.3.9 Transformation of chemically competent *E. coli* cells

Chemically competent *E. coli* XL1-blue cells (stored at -80°C, 50 µL) were thawed on ice, homogenised and complemented with 0.5-10 µL of plasmid DNA or ligation mixture. Cells were hold on ice for at least 20 min, heat shocked at 42 °C for 90 sec and rested on ice for another 5 min. Afterwards 500 µL of pre-warmed SOC or LB medium was added, and the cells were incubated in a thermomixer at 500 rpm and 37 °C for 1 h. Finally, 20-200 µL of the cell mixture were plated on agar plates containing 100 µg/ml ampicillin or kanamycin, depending on the resistance cassette of the vector. For delicate ligations, cells were centrifuged at 3000× g for 30 sec and all cells were spread in a total volume of 200 µL. Plates were incubated at 37 °C overnight, sealed by parafilm, and stored at 4 °C for up to three weeks.

NovaBlue Singles™ Competent Cells were handled and transformed according to manufacturer´s protocol.

SOC-medium 2 % (w/v) tryptone, 0.5 % (w/v) yeast extract, 10 mM NaCl, 2.5 mM KCl, 10 mM $MgCl_2$, 20 mM glucose

2.3.10 Analytical PCR

E. coli colonies obtained from transformation were screened for the desired insert by analytical PCR. A single *E. coli* colony was picked from the transformation plate and transferred to a new agar plate, which was sectioned and labelled clone by clone, as well as into a PCR reaction tube containing 5 µL ddH_2O. The plate was incubated at 37 °C overnight and the cell-water-mixture was used as template for the following PCR reaction. Ideally, primer pairs were chosen to bind to the vector on one side and to the insert on the other side. Colony PCR reactions were performed according to the conditions stated in Table 2.16 after blending the components mentioned below.

Table 2.19 | Pipetting scheme for a colony PCR

Volume	Component
5 µL	DNA template (colony resuspended in water)
1 µL	10× Taq buffer
0.4 µL	dNTPs
0.2 µL	sense primer (100 µM)
0.2 µL	antisense primer (100 µM)
0.1 µL	*Taq* DNA polymerase
Ad 10 µL	ddH_2O

2.3.11 Culture of *E. coli*

E. coli cells were cultured in LB, SOC or YT medium supplemented either with ampicillin or kanamycin, depending on the resistance cassette of the vector.

For plasmid DNA Mini, Midi and Maxi preparations, a single *E. coli* colony was picked from a LB agar plate and cultured in a total volume of 3 mL, 200 mL or 500 mL of liquid LB medium at 37 °C and 160 rpm overnight. Midi and Maxi cultures were inoculated with a pre-culture of 3 mL that was grown for at least 4 h.

Small-scale cultures of *E. coli* were grown in 10 mL YT medium overnight under standard conditions to produce recombinant DNA sufficient for a single *L. tarentolae* transfection.

LB-medium 25 g LB- medium (Roth), ad 1 L ddH_2O, autoclaved

LB-agar	40 g LB-agar (Roth), ad 1 L ddH_2O, autoclaved
SOC-medium	2 % (w/v) tryptone, 0.5 % (w/v) yeast extract, 10 mM NaCl, 2.5 mM KCl, 10 mM MgCl2, 20 mM glucose, sterile filtered
2× YT-medium	2.5 % (w/v) tryptone, 2 % (w/v) yeast extract, 0.5 % (w/v) NaCl, pH 7, autoclaved

2.3.12 Isolation of plasmid DNA from *E. coli* cells

Plasmid DNA was isolated from *E. coli* cells following the alkaline lysis protocol from Birnboim and Doly (1979). In a small-scale isolation, 2 mL of an overnight culture were centrifuged (>13000× g, 1 min, 4 °C) and the harvested cells were subsequently resuspended in 100 µL ice-cold buffer P1. Cell lysis was initiated upon addition of 200 µL buffer P2, maintained for up to 5 min on RT and finally terminated by 150 µL buffer P3. Cell waste and gDNA was pelleted (>13000× g, 10 min, 4 °C) and the supernatant was precipitated with 600 µL isopropanol. The isolated plasmid DNA was washed in 600 µL ice-cold 70 % ethanol (>13000× g, 5 min, 4 °C), dried under red light for 15-30 min and dissolved in 30 µL ddH_2O. Alternatively, 2-8 mL of *E. coli* cultures were harvested, and plasmid DNA was isolated using the QIAprep™ Spin Miniprep Kit according to manufacturer´s protocol. DNA was eluted in 30-60 µL ddH_2O. Plasmid DNA Midi and Maxi preparations were performed employing the respective Qiagen kit according to the manufacturer´s protocol. Midi preparations were eluted in 200 µL ddH_2O whereas Maxiprep's were dissolved in 800 µL TE buffer.

Buffer P1	50 mM Tris, 10 mM EDTA, pH 8, 0.1 mg/mL RNase A, stored at 4 °C
Buffer P2	0.2 M NaOH, 1 % (w/v) SDS, stored RT
Buffer P3	1.8 M KAc/HAc, pH 5.2, stored at 4 °C
TE buffer	10 mM Tris/HCl, 1 mM EDTA, pH 7.5

2.3.13 Sequencing

DNA sequences were verified by Sanger sequencing executed by GATC Biotech (Konstanz, Germany) or Seq-it (Kaiserslautern, Germany). Primers were provided by the companies or are described in Table 2.6. To meet the requirements of the companies, DNA obtained from Mini plasmid preparations were diluted 1:5 or 1:10 and primers were sent in a concentration of 10 pmol/µL. The results were analysed with the program BioEdit and the online tools JustBio, ClustalOmega and ExPASy.

2.3.14 Determination of DNA concentration

For *L. tarentolae* and *P. falciparum* transfections, it was necessary to determine the concentration and purity of the prepared plasmid DNA. Therefore, the absorption at 280 and 260 nm was measured with a NanoDrop™ spectrophotometer and the concentration was calculated from that. Purity was checked by evaluation of the quotient A260nm/A280nm. Pure DNA showed values between 1.8 and 2.0 while lower or higher values were indicating contaminations with proteins or RNA.

2.3.15 Precipitation of plasmid DNA

Plasmid DNA was disinfected prior to transfection of *P. falciparum* and *L. tarentolae* parasites. Therefore, aliquoted DNA was acidulated with 20 µL 3 M sodium acetate at pH 5 in a total volume of 200 µL and precipitated by adding 500 µL ice-cold 100 % ethanol. The mixture was vortexed shortly and incubated at -20 °C for at least 30 min. Afterwards, the DNA was pelleted at 20800× g and 4 °C for 30 min and washed with 500 µL ice-cold 70 % ethanol. Finally, the DNA pellet was air-dried under sterile conditions and resuspended in 10-30 µL sterile ddH_2O or TE buffer. Sterile DNA aliquots were stored at -20 °C.

TE buffer 10 mM Tris/HCl, 1 mM EDTA, pH 7.5

2.4 Biochemical methods

2.4.1 Bradford-Assay for determination of protein concentration

Protein concentrations were determined based on the protocol of Bradford (1976). For this purpose, a calibration curve was generated with 0-14 µg/mL BSA, which was prepared freshly for each measurement. Single-use cuvettes were filled with 800 µL ddH_2O less the volume of the protein solution, which was previously determined as an appropriate dilution. All samples were assembled in triplicates and for at least two different protein dilutions. The reaction was initiated by adding 200 µL Bradford reagent to each sample in an interval of exactly 20 sec and mixed thoroughly. Samples were incubated for 15 min at RT and subsequently the absorbance at 595 nm was measured using the software spectra manager. The calibration curve was fitted to a hyperbolic function using Sigma Plot and the desired protein concentration was computed using the formula:

$$y = a * x / (b + x) \quad \text{(with y=absorbance and x= concentration)}$$

2.4.2 Precipitation of proteins

Proteins were precipitated from a solution by the addition of five to six volumes (for one volume solution) of ice-cold 100 % acetone (Fic *et al.*, 2010). The mixture was vortexed shortly and incubated at -20 °C overnight. After centrifugation (15 000× g, 15 min, 4 °C), the protein pellet was air-dried for 15 min at RT and dissolved in the appropriate amount of 2-5× Laemmli buffer (+15 % β-mercaptoethanol [β-ME]). This was vortexed at least twice for 30 sec or until the pellet had completely dissolved and boiled at 95 °C for 5 min unless otherwise stated.

2× Laemmli buffer 125 mM Tris/HCl pH 6.8, 20 % glycerol, 4 % (w/v) SDS, 0.04 % bromophenol blue

5× Laemmli buffer 50 mM Tris/HCl pH 6.8, 25 % glycerol, 10 % (w/v) SDS, 0.1 % bromophenol blue

2.4.3 SDS-Polyacrylamide gel electrophoresis (SDS-PAGE)

Recombinant and native proteins were separated by sodium dodecyl sulphate polyacrylamide gel electrophoresis (SDS-PAGE) according to their molecular mass. Correspondingly, the pore size of the gel was matched using 10-18 % acrylamide in the separating gel.

Small polyacrylamide gels were cast with the Mini-PROTEAN system (BioRad), while large gels (approx. 16 × 14 cm) were prepared using a lab own technique. In any case, ethanol-cleaned glass plates were separated by a spacer and placed in the supplied casting stand (BioRad) or in a liquid agar-sealed stand. Separating and stacking gels were prepared as indicated below. The cast separating gel (approx. 5 mL for a small and approx. 15 mL for a large gel) was covered with 100 % isopropanol until complete polymerisation. Thereafter, isopropanol was discarded and the stacking gel (approx. 2 mL for a small and approx. 5 mL for a large gel) was poured and completed with a comb (10-15 wells for a small and 14-21 wells for a large gel).

Proteins were resolved under denaturing conditions (95 °C for 5-10 min) or after heating (37 °C for 30 min) using a discontinuous buffer system (Laemmli, 1970). The samples were boiled or heated in 2-5× Laemmli buffer under non-reducing or reducing (with 15-30 % β-ME) conditions. Polyacrylamide gels were set in an electrophoresis tank filled with SDS running buffer, loaded with 5-20 µL sample along with 5 µL protein marker and run at 25 mA per small or 70 mA per large gel for at least 1 h. After electrophoresis had ended, the gel was either stained in Coomassie Brilliant Blue or processed via western blot analysis.

Separating gel buffer 1.5 M Tris/HCl, pH 8.8

Stacking gel buffer 1 M Tris/HCl, pH 6.8

Table 2.20 | Pipetting scheme for separating and stacking gels sufficient for four small or two large polyacrylamide gels

Separating gel	12 %	15 %	18 %	Stacking gel
30 % acrylamide mix	12 mL	15 mL	18 mL	1.7 mL
buffer	7.5 mL	7.5 mL	7.5 mL	1.25 mL
10 % SDS	0.3 mL	0.3 mL	0.3 mL	0.1 mL
10 % APS	0.3 mL	0.3 mL	0.3 mL	0.1 mL
TEMED	0.012 mL	0.012 mL	0.012 mL	0.01 mL
ddH_2O	ad 30 mL	ad 30 mL	ad 30 mL	ad 10 mL

Sealing agar 1 % agar (w/v) in SDS running buffer

SDS running buffer 25 mM Tris, 250 mM glycine, 0.1 % (w/v) SDS, pH 8.3

2× Laemmli buffer 125 mM Tris/HCl pH 6.8, 20 % glycerol, 4 % (w/v) SDS, 0.04 % bromophenol blue

5× Laemmli buffer 50 mM Tris/HCl pH 6.8, 25 % glycerol, 10 % (w/v) SDS, 0.1 % bromophenol blue

2.4.4 Coomassie Brilliant Blue staining

Protein samples separated by SDS-PAGE were stained in Coomassie Brilliant Blue to visualise all present proteins. Separating and stacking gels were therefore disassembled and only the separating gel was carefully transferred to the staining solution, which was incubated at RT for at least 1 h or overnight on a rocking platform. Subsequently, the staining solution was replaced with destainer and washed several times. For complete clearance of background staining, the gel was additionally incubated in ddH_2O overnight without shaking.

Staining solution 25 % (v/v) isopropanol, 10 % (v/v) acetic acid, 0.05 % (w/v) Coomassie Blue G250

Destaining solution 25 % (v/v) isopropanol, 10 % (v/v) acetic acid

2.4.5 Western blot analysis

SDS-PAGE-separated proteins that were not stained with Coomassie Blue were transferred by semi-dry or wet electro transfer systems to nitrocellulose or PVDF membranes for immunodetection. All membranes, acrylamide gels, Whatman papers and sponges were pre-incubated in transfer buffer before usage.

For wet blotting, the gel was placed onto a nitrocellulose membrane or alternatively onto a PVDF membrane, that was previously activated in methanol. Membrane and gel were sandwiched between

three Whatman papers and a sponge on each side. The blotting sandwich was assembled to the Mini-PROTEAN blotting module (BioRad) according to manufacturer's instructions. Transfer buffer and a cooling unit were filled into the blotting chamber before protein transfer was initiated at 100 V for 1 h.

In a semi-dry transfer procedure, the membrane was placed onto five Whatman papers and was covered with the gel. The blotting pile was completed by another five sheets of Whatman paper and arranged at the anode of the PerfectBlue Semi-Dry Electro Blotter. One small gel was blotted at 100 mA and a large gel at 250 mA for 1 h.

Transfer buffer 20 mM Tris, 150 mM glycine, 20 % (v/v) methanol, 0.02% (w/v) SDS

2.4.6 Membrane staining with Ponceau S

Loading controls for immunoblotting were obtained by reversible visualisation using PonceauS. Above that, the transfer efficiency could be monitored, and the membrane could be cut more precisely. PVDF membranes were rinsed in methanol for 30 sec before they were transferred to the PonceauS solution whereas nitrocellulose membranes were directly incubated in the dye. Membranes were rotated on a rocking platform for up to 10 min and rinsed with ddH_2O until the background became clear. Protein staining was documented before the membrane was completely destained in TBS.

Ponceau S solution 3 % (w/v) Ponceau S, 3 % (w/v) trichloroacetic acid

TBS 10 mM Tris/HCl, 0.9 % (w/v) NaCl, pH 7.4

2.4.7 Immunodetection of proteins

Individual proteins on the blotted membrane were identified by immunodecoration employing a variety of self-made or commercial antibodies (Table 2.5).

Following PonceauS staining, the completely destained membrane was treated with blocking buffer to prevent nonspecific binding of antibodies. The blocking step was carried out at RT for 1 h on a rocking platform. Afterwards the membrane was incubated shaking with the primary antibody at 4 °C overnight. The next day, the primary antibody was removed, and the membrane was washed at least three times for 10 min each in TBS. To meet the requirements of a specific antibody, this washing step might be expanded and/or enhanced to TBS-T or TBS-TT buffer. A horseradish peroxidase-conjugated secondary antibody was supplied for 1-2 h with shaking at RT. The membrane was subsequently washed for at least three times à 10 min in TBS, TBS-T or TBS-TT.

For protein detection, freshly mixed detection reagent (Amersham ECL Western Blotting Detection Reagents or SuperSignal West Femto) was applied equally onto the membrane and incubated shortly.

Chemiluminescence was exposed to a radiographic film or alternatively captured by a Lumi-Imager (Roche).

TBS	10 mM Tris/HCl, 0.9 % (w/v) NaCl, pH 7.4
TBS-T	TBS, 0.1 % (v/v) Tween 20
TBS-TT	TBS, 0.1 % (v/v) Tween 20, 0.2 % (v/v) Triton X-100
Blocking buffer	5 % (w/v) low-fat milk powder in TBS
Antibody solutions	antibodies were diluted in blocking buffer as indicated in Table 2.5

2.4.8 Membrane stripping

Membranes may be used several times to detect various proteins of a similar molecular weight. To avoid a confused signal due to a previously applied primary antibody, this procedure should only be used for primary antibodies that respond to unequal secondary antibodies (rabbit vs. mouse).

After one protein of interest was detected via chemiluminescence activity, the remaining detection reagent was removed by washing the membrane in TBS for 10 min. The previously applied antibodies were detached from the membrane while shaking in stripping buffer. The stripping buffer was replaced three times every 10 min. Finally, the membrane was washed twice in TBS for 10 min each and twice in TBS-T for 5 min each. After this, the standard protocol for immunodecoration was followed starting with the blocking step.

Stripping buffer	15 g glycine, 1 g SDS, 10 mL Tween 20, *ad* 1 l ddH_2O pH 2.2

2.5 Cell biological procedures and genetic manipulation of *L. tarentolae*

L. tarentolae UC wildtype parasites were cultivated and genetically manipulated in a sterile environment by using a laminar flow hood. Therefore, all buffers, solutions and disposals were autoclaved or sterile filtrated (section 2.2) and additionally disinfected with 70 % ethanol before being transferred to the sterile bench.

2.5.1 Cryoconservation of *L. tarentolae*

For long-term storage, *Leishmania* strains were cryopreserved in liquid nitrogen. Healthy moving parasites in the mid-logarithmic phase (5-9× 10^7cells/mL) were diluted 1:2 in 700 µL freshly prepared

brain heart infusion (BHI) freezing solution and translocated to a cryovial. This was wrapped in paper tissue and incubated at -80 °C for at least 24 h before the vial was frozen in liquid nitrogen.

BHI freezing solution 370 mg BHI, 30 % (v/v) glycerol, 10 µg/mL hemin solution, ad 10 mL

2.5.2 Thawing of *L. tarentolae* cryocultures

Cryotubes of frozen *L. tarentolae* cells were removed from the liquid nitrogen and thawed quickly in a 27 °C water bath. Thawed parasites were inoculated in 10 mL pre-warmed BHI medium and carefully stirred before the remaining glycerol was removed by centrifugation (1500x g, 10 min, RT). The parasite pellet was dissolved in 1 mL of fresh BHI medium and incubated for the first 24 h at 27 °C without shaking or antibiotics, before cells were finally transferred to continuous culture.

2.5.3 Continuous culture of *L. tarentolae*

L. tarentolae promastigotes were cultivated in BHI liquid medium at 27 °C and 50 rpm. Under standard conditions, parasites were grown in a 25 cm^2 culture flasks (standing upright) in a total culture volume of 10 mL. In case larger numbers of parasites were needed, culture volume was increased up to 1 L, with the culture claiming max. 33 % of the Erlenmeyer flask. The culture was maintained in the mid-log phase (approx. 5× 10^7 cells/mL) by splitting the cells 1:10 or according to their condition every day or at every other day. To select for transgenic parasite lines, G418 was added to the medium at a concentration of 0.1 mg/mL.

BHI medium 37 g BHI powder, ad 1 L ddH_2O, 10 µg/mL hemin solution

Hemin solution 2 mg/mL hemin chloride in 0.05 M NaOH

G418 50 mg/mL G418 sulphate in ddH_2O

2.5.4 Determination of cell density

To determine the specific number of cells in a culture, 100 µL of the suspended cells were mixed with 1× SSC fixation solution and incubated at RT for 5 min. The suspension was injected into a Neubauer counting chamber and analysed under a microscope by counting at least four of the 16 squares. The overall cell density was calculated by multiplying the average number of the cells counted by the dilution factor (in 1× SSC) and dividing this by the volume of the square (4 nL). The calculated number corresponded to × 10^6 cells/mL of cell culture.

20× SSC 3 M NaCl, 0.3 M Na_3citrate, pH 7.4

1× SSC fixation solution 10 % (w/v) paraformaldehyde in 1× SSC

2.5.5 Transfection of *L. tarentolae*

L. tarentolae parasites in the mid-log phase, were stable transfected (Beverley and Clayton, 1993) using the Basic Parasite Nucleofector Kit 2 (Lonza) based on the manufacturer's protocol.
For each trial, 5×10^7 cells were harvested by centrifugation (1500× g, 3 min, RT), washed in 1 mL transfection buffer and finally dissolved in 100 µL Nucleofector solution. The suspension was supplemented with 7-20 µg sterile plasmid DNA and transferred into the provided electroporation cuvette. Cells were electroporated using the program U-033 and afterwards immediately inoculated in 9.5 mL pre-warmed BHI by rinsing the cuvette with 500 µL medium. For recreation, the electroporated cells were first incubated in liquid medium overnight without shaking or antibiotics before the culture was centrifuged (1500× g, 10 min, RT) and reduced to 1 mL, which was spread onto a selection BHI agar plate. The plate was sealed with two layers of parafilm and incubated at 27 °C with the agar at the bottom. First colonies of transgenic parasites were expected ten days post transfection.

For each transfected parasite line, up to four single clones were picked from the agar plate and inoculated in 30 µL BHI medium, which was cultivated without shaking. The motion and density of the young cells were checked daily by examining a drop of culture on a glass slide under the microscope. Healthy cultures were gradually up-scaled to standard culture volumes.

BHI agar 3.7 % BHI, 0.08 % (w/v) folic acid, 0.8 % (w/v) agar, 10 % (v/v) heat-inactivated FCS, 20 µg/mL hemin, 40 µg/mL G418

Transfection buffer 21 mM HEPES, 137 mM NaCl, 5 mM KCl, 0.7 mM NaH_2PO_4, 6 mM Glucose in ddH_2O, pH 7.4

2.5.6 Analysis of growth characteristics of *L. tarentolae* cells

The impact of genetic modifications on the *Leishmania* organism was analysed by observing parasite growth. Wildtype and transgenic parasite lines from a continuous culture were counted (section 2.5.4) and 5×10^6 cells/mL were transferred into a new culture flask comprising 10 mL of culture volume. Cell growth was studied under standard conditions including shaking and selection pressure. Every 24 h and for a period of six days, the cells were counted and the optical density (OD) was measured at 600 nm (cells were previously diluted to $OD_{600} < 1$). The SigmaPlot software graphically evaluated the collected data set and was used to fit a regression line.

2.5.7 Preparation of *L. tarentolae* cell lysates

Whole cell lysates of *L. tarentolae* were prepared for western blot analysis and contained 5× 10^7 parasites for a single sample. The cells were collected by centrifugation (1500× g, 10 min, RT) and directly lysed in the presence of 5× Laemmli buffer. For reducing conditions, the buffer was supplemented with 15-30 % β-ME. Parasites were resuspended, and gDNA was disrupted by shearing the samples eight times over a reaction tube rack. Before storage or application onto an SDS-PAGE gel, the samples were heated at 37 °C for 30 min or boiled at 95 °C for 10 min.

5× Laemmli buffer 50 mM Tris/HCl pH 6.8, 25 % glycerol, 10 % (w/v) SDS, 0.1 % bromophenol blue

2.5.8 Preparation of *L. tarentolae* cell lysates treated with NEM

Parasites were previously treated with NEM to alkylate free thiols and thereby enrich a potentially mixed disulphide intermediate. Parasites were harvested, dissolved in 2 mL PBS and separated into two 1 mL samples of 5× 10^7 cells each. A freshly prepared NEM solution was added to both samples to a final concentration of 100 mM and was incubated for 5 min in the dark. After the NEM was removed (10 000× g, 3 min), one sample was lysed under reducing and the other under non-reducing conditions in a 5× Laemmli buffer containing 10 mM NEM as described earlier (section 2.5.7).

PBS 1.84 mM KH_2PO_4, 10 mM Na_2HPO_4, 137 mM NaCl, 2.7 mM KCl, pH 7.4

NEM 200 mM *N*-ethylmaleimide in PBS

2.5.9 Preparation of *L. tarentolae* cell lysates treated with diamide and DTT

To stabilise potential intermolecular disulphide bonds, parasites were pre-treated with the oxidizing agent diamide or the reducing agent DTT. For each treatment 10^8 cells were harvested and resuspended in 2 mL PBS. The suspension was subsequently complemented with the same volume of a 10 mM diamide or 4 mM DTT solution and was incubated at RT for 5 min. After centrifugation (1500× g, 10 min, RT), the parasites were treated with NEM and lysed as described above.

Diamide 10 mM diamide in PBS

DTT 4 mM dithiothreitol in PBS

2.5.10 Redox mobility shift assay

Proteins were examined for their redox state by adding the alkylating substance mm(PEG)$_{24}$ to *L. tarentolae* cell lysates in Laemmli buffer to alter the migration behaviour of reduced proteins in SDS-PAGE.

For each sample 5× 10^7 cells were collected and resuspended in 20 µL 5× Laemmli buffer (without β-ME) as mentioned above (section 2.5.7). The lysates for reducing controls were supplemented with a freshly prepared 3.75 mM TCEP solution and incubated at 27 °C for 30 min (mild reduction) or at 95 °C for 10 min (strong reduction). Afterwards, all samples were supplemented with 15 mM mm(PEG)$_{24}$ or DMSO as control and incubated in the dark for 1 h. Samples were finally boiled at 95 °C for 10 min.

TCEP	50 mM Tris(2-carboxyethyl)phosphine in ddH_2O, pH 7.4
mm(PEG)$_{24}$	250 mM methyl-PEG-maleimide in DMSO

2.5.11 Differential fractionation of *L. tarentolae*

The membrane association of mitochondrial proteins was studied with a combination of hypotonic cell swelling followed by mild and selective lysis by digitonin (Vercesi *et al.*, 1991; Castro *et al.*, 2008; Hide *et al.*, 2008; Peleh *et al.*, 2014).

Cells were harvested in the mid-log phase by spinning 10^9 cells at 1500× g and 4 °C for 10 min and resuspended in 10 mL ice-cold PBS, of which 1 mL was removed as untreated control (sample A). After another centrifugation step, the sample A pellet was dissolved in 300 µL SH buffer and stored on ice. The remaining PBS suspension (9 mL) was centrifuged, resuspended in 245 µL of ice-cold swelling buffer per 10^8 cells (2205 mL), and incubated on ice for 20 min. Sucrose stock solution was added to a final concentration of 7.5 % (w/v) to stop cell lysis and the mixture was aliquoted into eight 280 µL samples. Each of the eight samples containing 10^8 cells were supplemented with 20 µL SH buffer containing varying amounts of digitonin (0, 1.25 mg/mL, 2.5 mg/mL, 5 mg/mL, 10 mg/mL, 25 mg/mL, 50 mg/mL) or 2 % (v/v) Triton X-100. The solubilisation was performed for 30 min on ice while occasionally vortexing. Finally, all samples, including sample A, were centrifuged (20 000× g, 30 min, 4 °C) to separate the mitoplast pellet from the soluble protein content in the supernatant. The supernatant was precipitated (2.4.2) before both fractions were resuspended in 50 µL 5× Laemmli (+ 6 M Urea + 15 % β-ME) as explained earlier (2.5.7) and heated at 37 °C for 30 min.

PBS	1.84 mM KH_2PO_4, 10 mM Na_2HPO_4, 137 mM NaCl, 2.7 mM KCl, pH 7.4
SH buffer	0.6 M sorbitol, 20 mM HEPES, pH 7.4, 1× protease inhibitor was added freshly
Swelling buffer	20 mM HEPES, pH 7.2, 1× protease inhibitor was added freshly
Sucrose stock	60 % (w/v) sucrose in ddH_2O

2.6 Cell biological procedures and genetic manipulation of *P. falciparum*

P. falciparum parasites were cultivated and treated sterile using a laminar flow hood. All media, solutions and disposals were sterilised as described in section 2.2 and stored at 4 °C or -20 °C. Materials were further disinfected with 70 % ethanol before entering the laminar flow hood.

2.6.1 Cryoconservation of *P. falciparum* parasites

P. falciparum infected red blood cells (iRBCs) were stored for long-term in liquid nitrogen. Therefore, a 3-5 % ring stage parasite culture was centrifuged (300× g, 5 min) and the pellet was resuspended dropwise in the same amount of pre-warmed freezing solution. The mixture was transferred to a cryovial and frozen immediately.

Freezing solution 28 % (v/v) glycerol, 0.65 % (w/v) NaCl, 3 % (w/v) sorbitol

2.6.2 Thawing of *P. falciparum* cryocultures

Cryovials containing frozen iRBCs were removed from the liquid nitrogen and thawed quickly at 37 °C in a water bath. The cells were transferred to a 15 mL tube and taken up dropwise in 0.2 volumes of thawing solution I, which was incubated for 2 min. Afterwards, ten volumes of thawing solution II were added stepwise before the cell suspension was centrifuged at 300× g for 5 min. The cell pellet was resuspended slowly in ten volumes thawing solution III and centrifuged again. Cells were finally washed in 10 mL pre-warmed complete medium, supplemented with an equal amount of fresh human erythrocytes and continuously cultured.

Thawing solution I 12 % (w/v) NaCl

Thawing solution II 1.6 % (w/v) NaCl

Thawing solution III 0.9 % (w/v) NaCl, 0.2 % (w/v) glucose

Complete medium RPMI 1640 (25 mM HEPES, L-Glutamine), 4.5 % AlbuMax II, 200 µM hypoxanthine, 2.7 µg/mL gentamicin

2.6.3 Continuous culture of *P. falciparum* blood stage parasites

Blood stage parasites of the *P. falciparum* 3D7 strain were cultured based on standard procedures (Trager and Jensen, 1976) in an atmosphere of 5 % CO_2, 5 % O_2 and 90 % N_2 at 37 °C and a humidity of 90 %. The parasites were grown with 3.6 % human A^+ erythrocytes in cell culture flasks or petri dishes reaching a total volume of 14 mL. Depending on the parasitaemia or the condition of the cells, the

culture medium was renewed daily, every other day or three times a week, with a parasitaemia ranging between 0.5 and 10 %. A >9 % ring stage or >5 % trophozoite/schizont stage culture was split to maintain optimal growth conditions. For genetic manipulations, the medium was supplemented with 100 nM Atovaquone to maintain the pUF1-Cas9 transfected cell line, with 5 nM WR99210 for pL7 or with 2 µg/mL Blasticidin for positive selection of pHBIRH.

Complete medium RPMI 1640 (25 mM HEPES, L-Glutamine), 4.5 % AlbuMax II, 200 µM hypoxanthine, 2.7 µg/mL gentamicin

2.6.4 Giemsa staining

Giemsa-stained blood smears were evaluated to estimate the parasitaemia and parasite stages as well as the viability and morphology of a parasite culture. A blood sample was taken from the bottom of the cell culture and spread onto a glass slide, which was air-dried, fixed in 100 % methanol for 30 sec and subsequently stained in a freshly prepared 10 % (v/v) Giemsa solution for at least 20 min. The stained slides were rinsed with deionised water to remove the surplus Giemsa solution and analysed under a light microscope at 100× magnification. To calculate the parasitaemia of a culture, a serious number of RBCs were counted and parasitaemia was expressed as the percentage of iRBCs relative to the total number of RBCs.

2.6.5 Synchronisation of a *P. falciparum* culture

In order to obtain a tightly synchronised parasite culture, trophozoite and schizont stage parasites were eliminated by osmotic lysis sparing only parasites in the early ring stage (Lambros and Vanderberg, 1979). This procedure was applied in preparation for parasite transfection.

Cells were harvested by centrifugation (300× g, 5 min) and resuspended in ten volumes of a pre-warmed 5 % sorbitol solution, which was incubated for 5 min at RT. The remaining ring stage parasites were washed in 10 mL of medium and transferred to a new culture dish for cultivation.

Sorbitol solution 5 % (w/v) sorbitol in ddH_2O

2.6.6 Transfection of *P. falciparum* schizont stage parasites

P. falciparum parasites were genetically manipulated by the spontaneous uptake of DNA from pre-loaded non-infected RBCs (Deitsch *et al.*, 2001).

A tightly synchronised parasite culture (36 h after the synchronisation) was diluted to a parasitaemia of 1 % schizonts and prepared in a culture dish with 100 µL iRBCs and 8 mL medium. The loading of

RBCs was initiated by washing 2 mL of freshly donated erythrocytes twice in 6 mL ice-cold incomplete cytomix (centrifugation at 800× g for 2 min). The washed cells (400 µL) were mixed with 400 µL cytomix and 100 µg plasmid DNA and transferred into two chilled electroporation cuvettes in which the mixture was incubated on ice for 5 min. Electroporation was carried out at 0.3 kV voltage and 950 µF capacitance with a time constant ranging between 12 ms and 18 ms using Gene Pulser (BioRad). Alternatively, blood cells were prepared as described above and electroporated using Nucleofector 2b (Lonza) with one of the programs X-001 or U-033. Thereafter, the cuvettes were incubated on ice for another 5 min and rinsed twice with 2 mL medium to relocate all loaded RBCs into a 15 mL tube. Lysed cells were discarded with the supernatant after centrifugation (800× g, 2 min) and the loaded RBC pellet was taken up in 5 mL medium and added to the previous prepared schizont culture.

The culture was inspected after 24 h with an expected parasitaemia of 1-2 % rings and the medium was exchanged. To increase parasite's chances of invading a loaded RBC, the procedure was repeated 48 h after the first transfection. The appropriate selection marker (Table 2.12) was first added to the medium, the day after the second transfection (day 3). The culture was fed with fresh medium at each day of the first week after transfection, and three times a week afterwards. Fresh erythrocytes were added once a week in a volume of 50-100 µL. A first appearance of transfectants was expected three weeks post transfection and a culture was discontinued after 60 days without visible parasites.

The plasmids pL7/*PFERV* and pL7/*PFTIM13* were transfected into the transgenic parasite line 3D7pUF1-Cas9 (Table 2.10).

Cytomix (incomplete) 120 mM KCl, 0.15 mM $CaCl_2$, 2 mM EGTA, 5 mM $MgCl_2$, 10 mM K_2HPO_4, 10 mM KH_2PO_4, 25 mM HEPES, pH 7.6

2.6.7 Limiting dilution assay

Clonal lines of transfected parasites were produced by limiting dilution. The transgene culture was synchronised 24 h in advance and parasitaemia was determined shortly before the procedure. Furthermore, the concentration of RBCs was estimated by a haemocytometer and used to calculate the concentration of parasites per millilitre of resuspended culture. The starting culture was set to 2 parasites/mL, 2 % haematocrit plus the appropriate selection marker and distributed to the first two rows of a 48-well-plate by adding 500 µL per well. Cells were further diluted 1:10 and 1:100 in the next two rows to increase the chances of a clonal line. The medium was replaced three times a week and 10 µL fresh erythrocytes were added once a week to each well. Clonal lines were expected after two weeks and were then transferred into continuous culture.

2.7 Cell biological procedures and genetic manipulation of *S. cerevisiae*

S. cerevisiae was cultivated and genetically modified under sterile conditions. Cells were handled under a laminar flow hood and all media, solutions and disposals were autoclaved (chapter 2.2) or sterile filtrated using a pore size of 0.2 µm. Sterile media and solutions were stored at 4 °C or -20 °C.

2.7.1 Continuous culture and storage of *S. cerevisiae*

S. cerevisiae cells were grown at 30 °C in synthetic minimal medium (S) or in YP medium in liquid and on agar plates. Liquid cultures were shaken at 130-160 rpm. Culture medium was supplemented with either of the carbon sources glucose (D), galactose (Gal), or glycerol (G) and auxotrophic mutant strains were additionally supplied with the amino acids tryptophan, lysine, leucine, and histidine as well as the bases adenine and uracil depending on their genetic background.

For long-term storage, 800 µL of a liquid culture were mixed 1:2 with freezing solution and cryopreserved at -80 °C. Cells were thawed by scraping off tiny amounts of the glycerol culture and streaking the material onto an agar plate. Plates were incubated at 30 °C for three days before cells could be transferred into liquid culture. Agar plates were sealed with parafilm and stored at 4 °C for up to a month.

YP medium	10 g Bacto yeast extract, 20 g peptone, 2 % glucose (YPD) or 2 % galactose (YPGal) or 3 % Glycerol (YPG), ad 1 L ddH_2O
YP agar	10 g Bacto yeast extract, 20 g peptone, 20 g agar, 2 % glucose (YPD) or 2 % galactose (YPGal) or 3 % Glycerol (YPG), ad 1 L ddH_2O
S medium	6.7 g Difco YNB w/o AS, 2 % glucose (SD) or 2 % galactose (SGal) or 3 % Glycerol (SG), if required: 20 mg adenine sulphate, 20 mg uracil, 20 mg tryptophan, 20 mg histidine, 30 mg leucine, 30 mg lysine, ad 1 L ddH_2O
S agar	6.7 g Difco YNB w/o AS, 20 g agar, 2 % glucose (SD) or 2 % galactose (SGal) or 3 % Glycerol (SG), if required: 20 mg adenine sulphate, 20 mg uracil, 20 mg tryptophan, 20 mg histidine, 30 mg leucine, 30 mg lysine, ad 1 L ddH_2O
Freezing solution	30 % (v/v) glycerol in ddH_2O, sterile filtrate

2.7.2 Transformation of *S. cerevisiae*

Yeast strains were genetically manipulated based on standard protocols (Gietz and Schiestl, 2007a;b). Therefore, a single colony of the host strain was cultured in 10 mL SD medium (including auxotrophic nutrients) until mid-logarithmic (mid-log) phase. The approximate number of cells in the culture was

determined by measuring the optical density (OD) at 600 nm, with cultures diluted to a reading of OD_{600} <1. Within that range, a value of 0.1 was considered to be roughly proportional to a cell density of 3× 10^6 cells/mL (Bergman, 2001). For a single transformation, 5× 10^8 cells were harvested by centrifugation (1750× g, 5 min, 4 °C), washed once in 10 mL ddH_2O and resuspended in 50 µL ddH_2O.

Salmon sperm carrier DNA was denatured at 95 °C for 10 min and chilled immediately on ice. The transformation buffer was composed of 50 µL resuspended cell pellet, 240 µL PEG solution, 36 µL LiOAc solution, 10 µL denatured carrier DNA, 21 µL ddH_2O and 3 µL plasmid DNA. The mixture was vortexed at high speed for 1 min and incubated at 42 °C and 500 rpm for 50 min in a thermomixer. Afterwards the cells were centrifuged at 13 000× g for 30 sec and the cell pellet was resuspended in 500 µL ddH_2O of which 200 µL were spread onto selection agar plates without tryptophan. These were incubated at 30 °C for up to four days before single colonies were picked and cultured independently.

LiOAc solution	1 M lithium acetate dihydrate in ddH_2O, sterile filtrate
PEG solution	50 % (w/v) PEG 3350 in ddH_2O
Carrier DNA	10 µg/µL salmon sperm DNA solution
SD agar (-Trp)	6.7 g Difco YNB w/o AS, 20 g agar, 2 % glucose, 20 mg adenine sulphate, 30 mg leucine, 30 mg lysine, if required: 20 mg histidine, ad 1 L ddH_2O

2.7.3 Plasmid shuffling/ complementation assays

Proteins were tested for their ability to functionally replace essential yeast proteins by plasmid shuffling assays (Eckers *et al.*, 2013; Specht *et al.*, 2018). The constructs to test were introduced (on pYX232) into a knock out cell line, in which the essential yeast gene was deleted from the chromosome (*Δerv1, Δmia40*) but which possessed an episomal copy on the *URA3*-expressing plasmid pRS426 (*SCERV1*) or pRS316 (*SCMIA40*). Up to six single clones of the transfected cell line were grown in highly uracil-containing medium SD+2.5xUra (without tryptophan to preserve the pYX232 plasmid) at 30 °C and 130 rpm overnight.

The cultures of individual clones were diluted 1:50 in ddH_2O and spotted in 10 µL drops onto SD agar and FOA plates for control and selection, respectively. Plates were sealed with parafilm and incubated for three to four days at 30 °C, 37 °C or RT.

For drop dilution assays, a single clone was cultured as described above and first diluted to OD_{600} = 0.1. This was passed through a serial dilution to obtain a blend of 1:10, 1:100 and 1:1000. Drops of the undiluted culture and of each dilution were spotted on SD agar plates and on FOA plates, sealed and incubated for up to four days at 30 °C, 37 °C or RT. For documentation purposes, the plates were photographed on each day.

Cell material obtained from FOA plates was examined for the presence of viable cells by cultivating single colonies or, in absence of such, smears of background material in liquid FOA medium under standard conditions. If cell accumulation was detected within three days, cultures were subsequently diluted and spotted onto FOA and SD agar plates (-Ura) as described above. Colonies, expressing proteins that could complement for the essential yeast protein, were expected to only grow on FOA but not on the control plates (-Ura), since they lack the *URA3*-plasmid.

SD+2.5×Ura	6.7 g Difco YNB w/o AS, 2 % glucose, 50 mg uracil, 20 mg adenine sulphate, 30 mg leucine, 30 mg lysine, if required: 20 mg histidine, ad 1 L ddH_2O
SD agar (-Trp-Ura)	6.7 g Difco YNB w/o AS, 20 g agar, 2 % glucose, 20 mg adenine sulphate, 30 mg leucine, 30 mg lysine, if required: 20 mg histidine, ad 1 L ddH_2O
SD agar (-Trp+Ura+FOA)	6.7 g Difco YNB w/o AS, 20 g agar, 2 % glucose, 50 mg uracil, 20 mg adenine sulphate, 30 mg leucine, 30 mg lysine, 1 g FOA, if required: 20 mg histidine, ad 1 L ddH_2O
SD (-Trp+Ura+FOA)	6.7 g Difco YNB w/o AS, 2 % glucose, 50 mg uracil, 20 mg adenine sulphate, 30 mg leucine, 30 mg lysine, 1 g FOA, if required: 20 mg histidine, ad 1 L ddH_2O

2.7.4 Cell fractionation/quick mitochondria isolation

Clones which were studied after FOA selection and found to only grow in the presence of uracil were subsequently fractionated into mitochondria-containing pellet and cytosol-containing supernatant and examined for their protein content by western blot analysis. Alternatively, mitochondria were roughly isolated from yeast cells to use in other experiments as mentioned below.

Each of the clonal cell lines were cultured in 50 mL SD+Ura medium under standard conditions in the late-log phase (OD_{600} = 0.8-1.8). Cell amounts equivalent to ten OD volumes were harvested (1750× g, 10 min, 4 °C) and taken up in 300 µL ice-cold SMK^{80} buffer. For cell disruption, 200 µL glass beads were added and the suspension was vortexed six times for 30 sec each (stored on ice in between) before cell debris were removed together with the glass beads by centrifugation (1000× g, 3 min, 4 °C). The supernatant was transferred to a fresh reaction tube and mitochondria were pelleted at 20 000× g for 15 min at 4 °C. The pellet was directly boiled at 95 °C for 5 min in 20 µL 2× Laemmli buffer (+15 % β-ME). The supernatant was precipitated (section 2.4.2) and dissolved as described for the pellet.

To isolate mitochondria, yeast strains were grown in complete YP medium complemented with either glucose or glycerol as carbon sources and cultured until the late exponential phase (OD_{600} = 2-4). Ten OD volumes of culture were used to gain approximately 25 µg mitochondria. Cells

corresponding to 10 OD volumes were harvested (1750× g, 10 min, 4 °C) and dissolved in 150 µL ice-cold SMK^{80} buffer. Afterwards 200 µL glass beads were added to vortex the cells for 2 min at highest speed. After glass beads and cell debris were pelleted (1000× g, 3 min, 4 °C), mitochondria were collected by centrifugation (20 000× g, 30 min, 4 °C) and resuspended in 20 µL SH buffer. Of the supernatant, 75 µL were precipitated as defined earlier (section 2.4.2).

SD (-Trp+Ura)	6.7 g Difco YNB w/o AS, 2 % glucose, 20 mg uracil, 20 mg adenine sulphate, 30 mg leucine, 30 mg lysine, if required: 20 mg histidine, ad 1 L ddH_2O
SMK^{80} buffer	0.6 M sorbitol, 20 mM MOPS, 80 mM KCL, pH 7.4, 1 mM PMSF was added freshly
PMSF	100 mM phenylmethylsulphonyl fluoride in 100 % ethanol
2× Laemmli buffer	125 mM Tris/HCl pH 6.8, 20 % glycerol, 4 % (w/v) SDS, 0.04 % bromophenol blue

2.7.5 DNA extraction from *S. cerevisiae*

To verify the genotype of a yeast strain, genetic material was extracted from the cells (Looke *et al.*, 2011) and subjected to analytical PCR (2.3.2).

The yeast cells of a liquid culture (100-200 µL) measuring an OD_{600} of 0.4 were centrifuged (1750× g, 5 min, 4 °C) and incubated in 100 µL extraction buffer at 70 °C for 5 min. Subsequently, 300 µL of 100 % ice-cold ethanol were added and the mixture was vortexed briefly. The DNA was obtained by centrifugation (15 000× g, 3 min) and rinsed with 300 µL of ice-cold 70 % ethanol before being dissolved in 100 µL ddH_2O. The DNA solution was spun at 15 000× g for 15 sec to pellet cell debris before 1 µL was used in PCR.

Extraction buffer	200 mM lithium acetate dihydrate, 1 % (w/v) SDS in ddH_2O

2.7.6 Analysis of growth characteristics of *S. cerevisiae*

In order to study the influence of genetic modifications on the organism, particular strains were monitored in liquid medium and on agar plates while metabolising a variety of carbon sources. For growth assays on agar plates, cells were cultured in SD medium in the logarithmic growth phase under standard conditions. Cultures were diluted to an absorbance of 0.1 in sterile ddH_2O and drop dilution assays were performed as described in section 2.7.3. Cells in each dilution were applied in 10 µL drops onto SD, SGal and SG agar plates without tryptophan and incubated at 30 °C for up to 12 days. Pictures were taken for documentation at day three, five, eight and twelve.

Growth assays in liquid medium were carried out in a Tecan plate reader, which recorded the OD at 600 nm every hour after shaking the cultures for 550 sec at 183 rpm. Cells were previously cultured in liquid SD, SG or SGal medium for at least 5 days before the growth curve started. The cultures were diluted to OD_{600} = 0.1 in the corresponding medium and 200 µL were transferred in triplicates to a flat transparent 96-well-plate (Greiner). The growth was monitored over a period of 48 h at 30 °C.

S medium (-Trp) 6.7 g Difco YNB w/o AS, 2 % glucose (SD) or 2 % galactose (SGal) or 3 % Glycerol (SG), 20 mg adenine sulphate, 20 mg uracil, 30 mg leucine, 30 mg lysine, if required: 20 mg histidine, ad 1 L ddH_2O

S agar (-Trp) 6.7 g Difco YNB w/o AS, 20 g agar, 2 % glucose (SD) or 2 % galactose (SGal) or 3 % Glycerol (SG), 20 mg adenine sulphate, 20 mg uracil, 30 mg leucine, 30 mg lysine, if required: 20 mg histidine, ad 1 L ddH_2O

2.7.7 Proteolytic susceptibility assay

The localisation of proteins within mitochondria was approached in more detail by solubilising isolated mitochondria in steps and assaying the protein accessibility for proteinase K. Please keep in mind that the protocol below did not reach satisfaction with mitochondria isolated by quick preparation.

Forty OD volumes of yeast culture were prepared according to standard protocol (section 2.7.4) and finally dissolved in 80 µL SH buffer (containing ~100 µg mitochondria). To gradually open the mitochondria, the suspension was aliquoted into four 20 µL samples and replenished with either 180 µL SH, swelling, or lysis buffer to reach a final concentration of 100 µg/mL. All buffers were incubated on ice for 20 min before proteinase K (or water as control) was added at a concentration of 0.1 mg/ml. Proteolysis was carried out on ice for 30 min and was terminated by the addition of 4 mM PMSF which was incubated on ice for 10 min. The suspension was finally centrifuged (20 000× g, 30 min, 4 °C) and boiled for 5 min in 80 µL 2× Laemmli buffer (+ 15 % β-ME).

SH buffer 0.6 M sorbitol, 20 mM HEPES, pH 7.4

Swelling buffer 20 mM HEPES, pH 7.2

Lysis buffer 20 mM HEPES, 1 % (v/v) Triton X-100, pH 7.4

Proteinase K 10 mg/mL in ddH_2O

PMSF 100 mM phenylmethylsulphonyl fluoride in 100 % ethanol

2× Laemmli buffer 125 mM Tris/HCl pH 6.8, 20 % glycerol, 4 % (w/v) SDS, 0.04 % bromophenol blue

2.7.8 Carbonate extraction assay

Membrane association of mitochondrial proteins was studied, among others, by carbonate extraction assays that were modified from a previously described protocol (Eckers *et al.*, 2013). Please note that the following approach has not yet matured to full satisfaction when using mitochondria isolated by quick preparations.

Yeast strains were cultured in complete YPG medium in the late-log phase (OD_{600} = 2-4) before 10 OD volumes (~25 µg mitochondria) were harvested twice and disrupted (chapter 2.7.4). One of the mitochondrial pellets was directly boiled in 25 µL 2× Laemmli buffer (+ 15 % β-ME). The other pellet was resuspended in 100 µL swelling buffer supplemented with freshly prepared 100 µL Na_2CO_3, mixed for 15 sec and incubated on ice for 1 h. The suspension was ultracentrifuged (125 000× g, 1 h, 4 °C) and the pellet was dissolved in 25 µL Laemmli buffer (+ 15 % β-ME) while the supernatant was precipitated first (chapter 2.4.2).

Swelling buffer 20 mM TRIS, pH 7.2

Na_2CO_4 200 mM sodium dihydrogen carbonate, pH 11

2.7.9 Differential fractionation of yeast mitochondria by digitonin

Another method to investigate the membrane association of proteins in yeast mitochondria comprised a stepwise solubilisation process using hypotonic swelling and a digitonin concentration gradient (Cordeiro and Freire, 1995).

Yeast cells were cultured in complete YPD medium under standard conditions until 40 OD volumes were collected (2500× g, 5 min, 4 °C) in the late-log phase (OD_{600} = 2-5). Cells were generally treated as shown for *Leishmania* (section 2.5.11) with minor modifications. Briefly, hypotonic swelling was carried out in 2205 µL ice-cold swelling buffer that was incubated for 30 min on ice and terminated upon the addition of 315 µL sucrose stock solution. The cells were aliquoted into eight 280 µL samples and replenished with different dosages of digitonin (0, 0.2 mg/mL, 1 mg/mL, 2 mg/mL, 4 mg/mL, 10 mg/mL, 20 mg/mL) or 2 % (v/v) Triton X-100 in 20 µL SH buffer. The digitonin was incubated for 30 min at 30 °C before it was removed by centrifugation (20 000× g, 20 min, 4 °C) and replaced by 45 µL 2× Laemmli buffer (+ 15 % β-ME; 95 °C for 5 min).

SH buffer 0.6 M sorbitol, 20 mM HEPES, pH 7.4, 1× protease inhibitor was added freshly

Swelling buffer 20 mM HEPES, pH 7.2, 1× protease inhibitor was added freshly

3 Results

3.1 Yeast *SCERV1* complementation assays

*Lt*Erv appears to operate in *Leishmania* without a Mia40 homologue, resulting in the inability to interact with *Sc*Mia40 and to replace *Sc*Erv1 (Eckers *et al.*, 2013). Clearly, the leishmania oxidative protein folding system has evolved structural features that make it incompatible with the yeast system. To define structure-function-relationships that might be relevant to the lack of communication between both systems, a set of chimeras as well as mutant *Lt*Erv variants were generated (by Maike Eberhardt, Elisabeth Eckers, and myself) and analysed in a yeast Δ*erv1* background (Specht *et al.*, 2018).

3.1.1 Chimeric *Lt*Erv can functionally replace *Sc*Erv1

The two most prominent structural variations between the Erv homologues of *Leishmania* and yeast are (I) the C-terminal addition of a KISS-domain to *Lt*Erv and (II) the position and composition of the redox-active "shuttle" cysteine pair (Figure 3.1A). The relevance of the latter was approached as the first 16 amino acids of the *Lt*Erv N-terminus were replaced by the yeast shuttle arm (chimera 1-3) or as the complete *Sc*Erv1 N-terminus and flavodomain were fused to the C-terminal part of *Lt*Erv (chimera 4 and 5). Concurrently, the C-terminal arm and the KISS-domain were systematically removed from the constructs (chimera 1-3 and 4-5) to demonstrate the influence of these protist structures. In chimera 6, the yeast shuttle arm's CRSC-motif was exchanged with the *Leishmania* CQVYC-motif to address the activity of the protist shuttle cysteine pair independently of its position in the protein (Figure 3.1A).

Chimeric constructs were introduced into a haploid yeast Δ*erv1* strain that additionally expressed wildtype *SCERV1* on a *URA3* plasmid (Figure 3.1B). For negative selection and plasmid shuffling, transfected cells were grown on 5-fluoroorotic acid (FOA), which is converted to toxic 5-fluorouracil in the presence of *URA3.* Since the only available full-length copy of the essential *SCERV1* must be dismissed in the presence of FOA, yeast cell survival depends on a functional chimeric Erv as illustrated in Figure 3.2.

In contrast to the negative control that expressed *Lt*Erv, viable cells could be isolated from FOA agar plates for all the chimera (Figure 3.1B, Supplementary figure 1A). To ensure complete plasmid shuffling, the absence of *Sc*Erv1 and presence of the chimeric protein in yeast mitochondria were confirmed for at least three different clones of each strain by subcellular fractionation and western blot analysis (Figure 3.1C, Supplementary figure 2A). For chimera 3 and 6, I additionally confirmed the genotype by analytic PCR (Supplementary figure 2B).

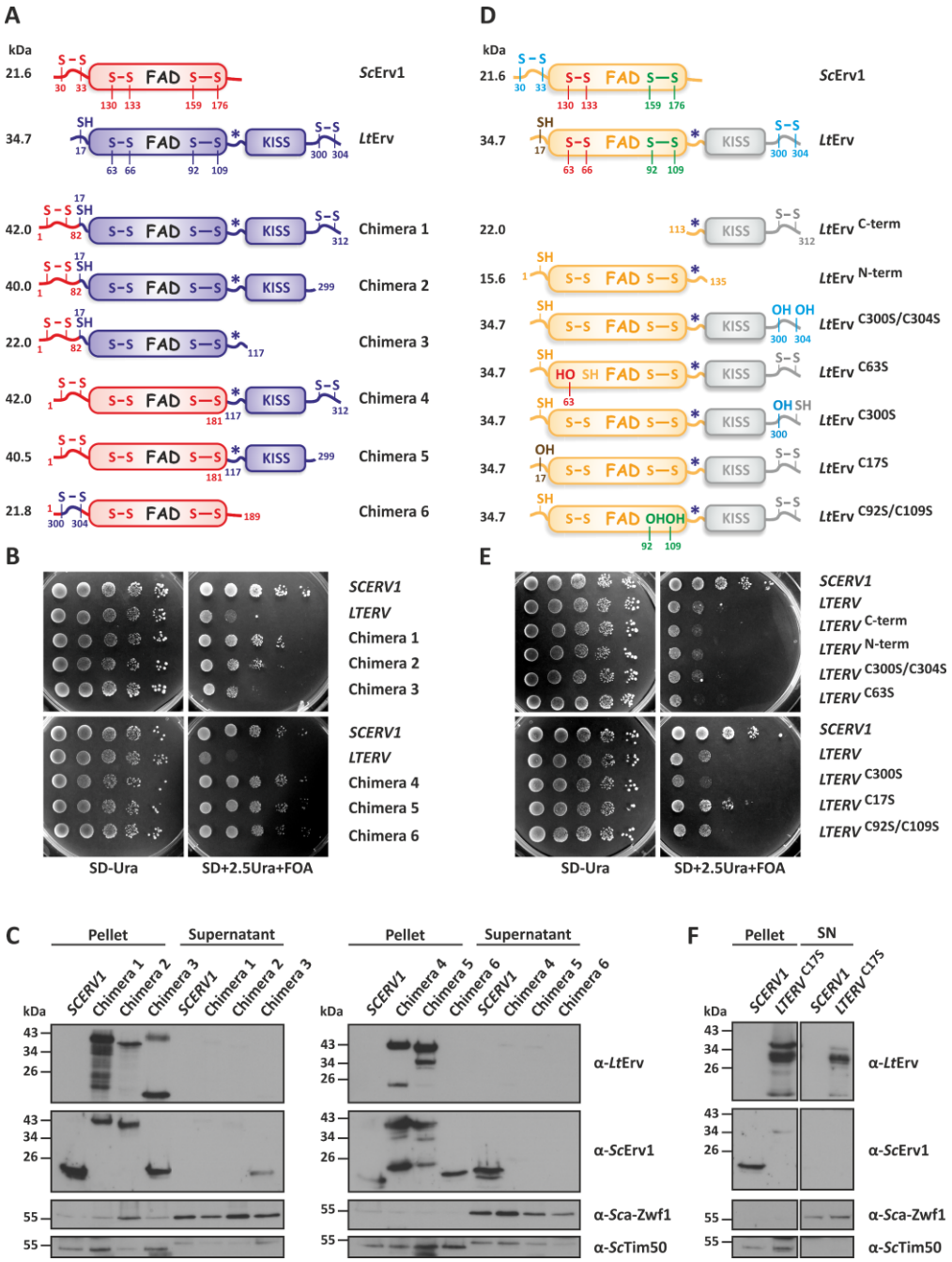

Figure 3.1 | Yeast *SCERV1* complementation assays with chimeric and mutant *LTERV*. **(A)** Schematic summary of the constructs encoding *Sc*Erv1 (red), *Lt*Erv (blue) and the indicated chimera 1-6. The peptide antibody binding site for α-*Lt*Erv is marked with an asterisk. **(B, E)** Δ*erv1* cells containing *SCERV1* on a *URA3* plasmid and the indicated chimera or mutant (or WT yeast or WT parasite Erv) on plasmid pYX232 were subjected to plasmid shuffling using 5-fluoroorotic acid (FOA). Shown are representative drop dilution assays on agar plates with and without FOA for one of four independent biological replicates. All chimera, mutant *Lt*Erv^{C17S} and WT *Sc*Erv1 rescued the loss of endogenous yeast Erv1. Strains expressing any of the other mutant or truncated *Lt*Erv variants as well as the negative control (WT *Lt*Erv) died in the presence of FOA. **(C, F)** Western blot analysis of subfractionated yeast cells expressing the indicated constructs. Chimera and *Lt*Erv^{C17S} were imported into mitochondria (pellet fraction) while WT *Sc*Erv1 was lost in all strains. Cytosolic glucose-6-phosphate dehydrogenase (*Sc*Zwf1) and mitochondrial *Sc*Tim50 were used as controls. **(D)** Schematic summary of truncated and mutant *Lt*Erv variants. Cysteine point mutations are highlighted in separate colours for the "distal" or "shuttle" cysteine pair (blue), the clamp forming residue (brown), the "proximal" or active site pair (red), and the structural disulphide bond (green). For additional information see Supplementary figure 1-3. Adapted from Specht *et al.* (2018).

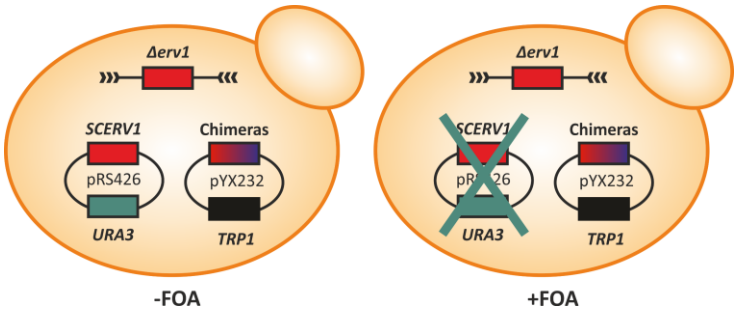

Figure 3.2 | Schematic representation of plasmid shuffling assays. A Δ*erv1* strain with an episomal *SCERV1* copy on the *URA3* plasmid pRS426 was transfected with plasmid pYX232 expressing either of the chimeras (left). Strains were negatively selected in the presence of 5-fluoroorotic acid (FOA) to exclude the *URA3* plasmid, which would otherwise turn FOA into a toxic substance. Once the only source of yeast Erv1 has been eliminated, the cell depends on a functional chimeric Erv to complement the loss (right). Modified from Specht *et al.* (2018).

3.1.2 Mutant *Lt*Erv^{C17S} can functionally complement the loss of *Sc*Erv1

Complementation assays with chimeric *Lt*Erv suggested that this protist Erv homologue can, at least in principle, adopt the function of *Sc*Erv1. To further investigate the structural requirements for a successful *Sc*Erv1 complementation, I analysed additional *Lt*Erv variants, that were either N- or C-terminally truncated (*Lt*Erv$^{C\text{-term}}$ and *Lt*Erv$^{N\text{-term}}$) versions of the full-length protein or in which the distal, proximal, structural, and clamp cysteine residues were replaced (Figure 3.1D).

Although the different *Lt*Erv mutants grew normally in the absence of FOA, neither *Lt*Erv$^{C\text{-term}}$ nor *Lt*Erv$^{N\text{-term}}$ were able to rescue the loss of *Sc*Erv1 (Figure 3.1E, Supplementary figure 1A). However, the systematic replacement approach yielded the functional mutant *Lt*Erv^{C17S}, in which the clamp residue was replaced. Single clones of the *Lt*Erv^{C17S} strain were subcellular fractionated and the replacement of *Sc*Erv1 by the mutant *Leishmania* protein was verified by western blot analysis (Figure 3.1F). Cells from the other mutant strains that were isolated from FOA agar plates, were either dead or still contained *Sc*Erv1 (Supplementary figure 3).

It might be worth mentioning that the mutation in *Lt*Erv^{C17S} had an additional effect on the localisation, since the protein was found to a certain degree in the cytosolic fraction. In contrast, mutations of the distal cysteine residues in *Lt*Erv$^{C300S/C304S}$ or of one of the proximal cysteines in *Lt*Erv^{C63S} did not interfere with the mitochondrial localisation of the protein (Supplementary figure 3).

3.1.3 Cys17 does not interfere with the complementation ability of other mutants

Mutations of the distal, proximal, and structural cysteines did not alter the ability of *Lt*Erv to rescue a *scerv1* knock out strain but only the replacement of the clamp residue C17 resulted in successful complementation. This result indicates a dominant negative effect of this cysteine residue that may

have overshadowed the actual complementation ability of the remaining cysteine mutants. To exclude this possibility, I exchanged the clamp residue Cys17 by a serine in all the cysteine mutants and repeated the complementation experiments (Figure 3.3A). Nevertheless, none of the new constructs showed any gain of *Sc*Erv1 function (Figure 3.3B).

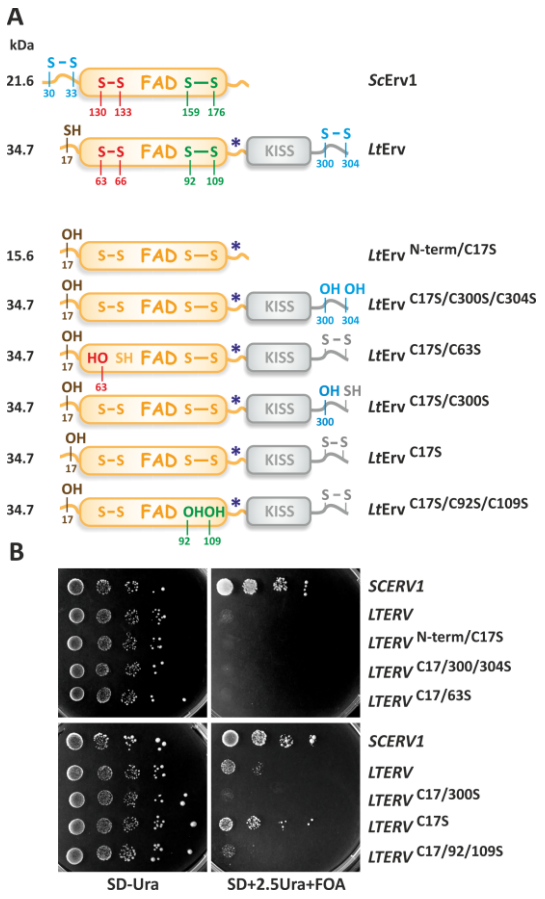

Figure 3.3 | Yeast *SCERV1* complementation assays with mutant *Lt*Erv^{C17S} constructs. **(A)** Schematic representation of *Lt*Erv^{C17S} constructs. **(B)** Drop dilution assay on agar plates as described in Figure 3.1. Shown are representative drop dilutions for one of three independent biological replicates. Adapted from Specht *et al.* (2018).

3.1.4 *Lt*Erv^{C17S} and chimera 1, 2 and 6 have specific growth phenotypes

Yeast strains that were previously able to complemented for *Sc*Erv1 were further characterised in liquid medium and on agar plates by their growth in minimal medium with glucose (SD), galactose (SGal), or glycerol (SG) as the provided carbon source (Figure 3.4, Supplementary figure 4). Chimera 1 displayed a prominent phenotype in metabolising each of the three carbon sources, which could be observed in liquid as well as on agar medium. Chimera 2 grew normally in glucose and galactose medium, but the growth in glycerol liquid medium was impaired. This phenotype was not present on SG agar plates. Chimera 3 showed no abnormalities in growth compared to WT *Sc*Erv1. In contrast, chimeras 4 and 5 exceeded the growth of the control strain on SGal and SG agar plates but not in liquid

medium. The growth of chimera 6 was affected on glycerol agar plates and marginally in liquid SD medium. Cells expressing *Lt*Erv^{C17S} revealed no deviation from the control when grown on agar plates and in liquid glucose medium. However, the growth of these cells in liquid SGal and SG was increased in the initial 12 h but was saturated earlier at a lower overall final cell density.

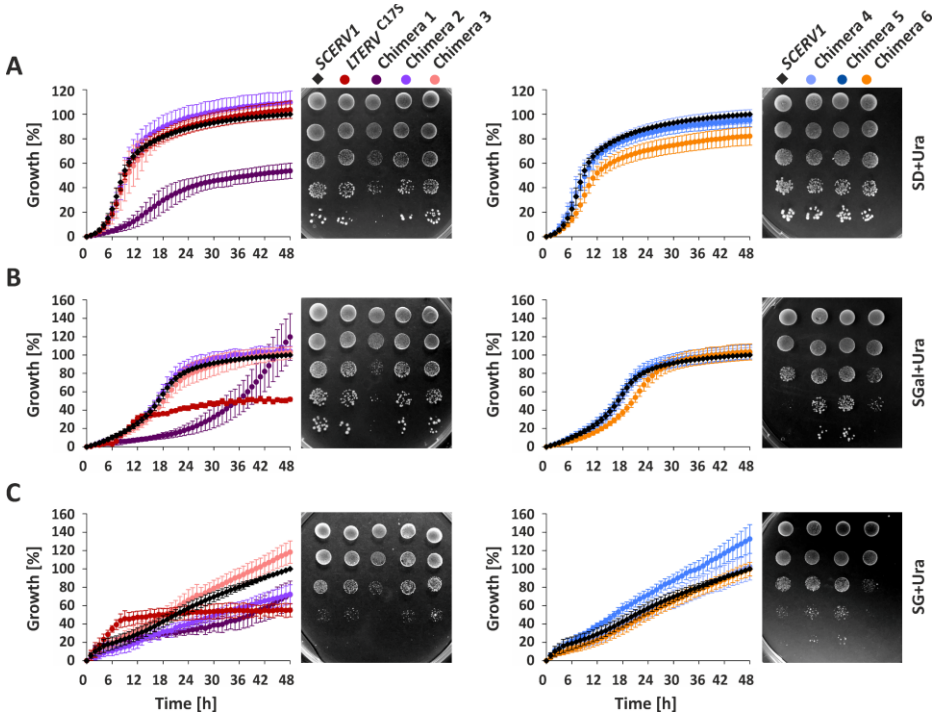

Figure 3.4 | Growth assays of complemented Δ*erv1* strains. Yeast strains expressing chimera 1-6 or *Lt*Erv^{C17S} were analysed in liquid and on agar minimal medium containing **(A)** 2 % glucose (SD) or **(B)** 3 % galactose (SGal) or **(C)** 3 % glycerol (SG) as carbon source. Individual values of growth curves in liquid medium represent the mean ± standard deviation of three to five independent biological replicates. Values were normalised to the growth of the Δ*erv1* strain complemented with WT *SCERV1* (black diamonds). Representative drop dilution assays for one of three to four independent biological replicates were pictured at day 3 (SD), day 5 (SGal) or day 8 (SG). For more detailed information see Supplementary figure 4. Adapted from Specht *et al.* (2018).

3.2 Yeast *SCMIA40 c*omplementation assays

The absence of a Mia40 homologue in parasitic protists may be due to the fact that *Lt*Erv is a single player who fulfils both the functions of Erv1 and Mia40 (Haindrich *et al.*, 2017). Since the above results suggest that the KISS domain, which is by name specific for kinetoplastid protists, does not inhibit *Lt*Erv in yeast and no obvious function for this domain is known so far, there is plenty of room to hypothesise. In one of these, the KISS domain acts as a receptor that binds the hydrophobic patch of imported proteins before they interact with the shuttle disulphide (Sideris and Tokatlidis, 2007; Banci *et al.*, 2009; Kawano *et al.*, 2009; Sideris *et al.*, 2009; Koch and Schmid, 2014b; Peleh *et al.*, 2016). In short, the hitherto unknown function of the KISS domain, in combination with the shuttle arm, might be the replacement of the missing Mia40. Another potential replacement candidate is residue C17, which is

absent in yeast Erv1 and might also exert a receptor function (Deponte and Hell, 2009; Guo *et al.*, 2012; Eckers *et al.*, 2013).

In order to test the hypothesis, weather protist Erv and in particular the mentioned structures actually possess Mia40 functions in yeast, I followed another plasmid-shuffling approach in Δ*mia40* yeast cells.

3.2.1 Protist Erv homologues cannot complement the loss of *Sc*Mia40

Expression plasmids with full-length *PFERV*, *LTERV* and the mutants *LTERV*$^{C\text{-term}}$, *LTERV*$^{N\text{-term}}$, and *LTERV*^{C17} were transfected into a haploid Δ*mia40* yeast strain and tested for their ability to functionally replace a wildtype *SCMIA40*-expressing *URA3* plasmid upon negative selection with FOA (Figure 3.5B, C; Supplementary figure 1B). The absence of viable cells on selection plates indicated that none of the protist Erv variants could complement the loss of *Sc*Mia40. Endogenous Mia40 could only be replaced by the truncated functional version *Sc*Mia40s. The results were reproduced in drop dilution assays using alternative temperatures (Figure 3.5D).

To exclude the possibility that the tested Erv constructs were not complementary due to mislocalisation within the yeast mitochondria, I adapted them to yeast standards. Fusing the N-terminal mitochondrial targeting signal and transmembrane segment of *Sc*Mia40 (Mia40N) to the constructs, should target them to the same location in the IM as the endogenous protein (Figure 3.5E). Yet, all the constructs failed to complement the loss of yeast Mia40 (Figure 3.5F, G).

3.2.2 Chimeric Erv cannot perform Mia40 operations

Chimeric Erv was previously shown to complement the loss of *Sc*Erv1 (Figure 3.1). Furthermore, some of the chimeras showed defects in oxidizing *Sc*Mia40, suggesting that these chimeras might have a Mia40-like activity that would obviate oxidation of the yeast protein (Specht *et al.*, 2018). I tested this hypothesis for chimera 1-6 as well as for their Mia40N-fusion constructs in *SCMIA40* complementation assays (Figure 3.6). Again, none of these constructs were able to rescue the Δ*mia40* strain.

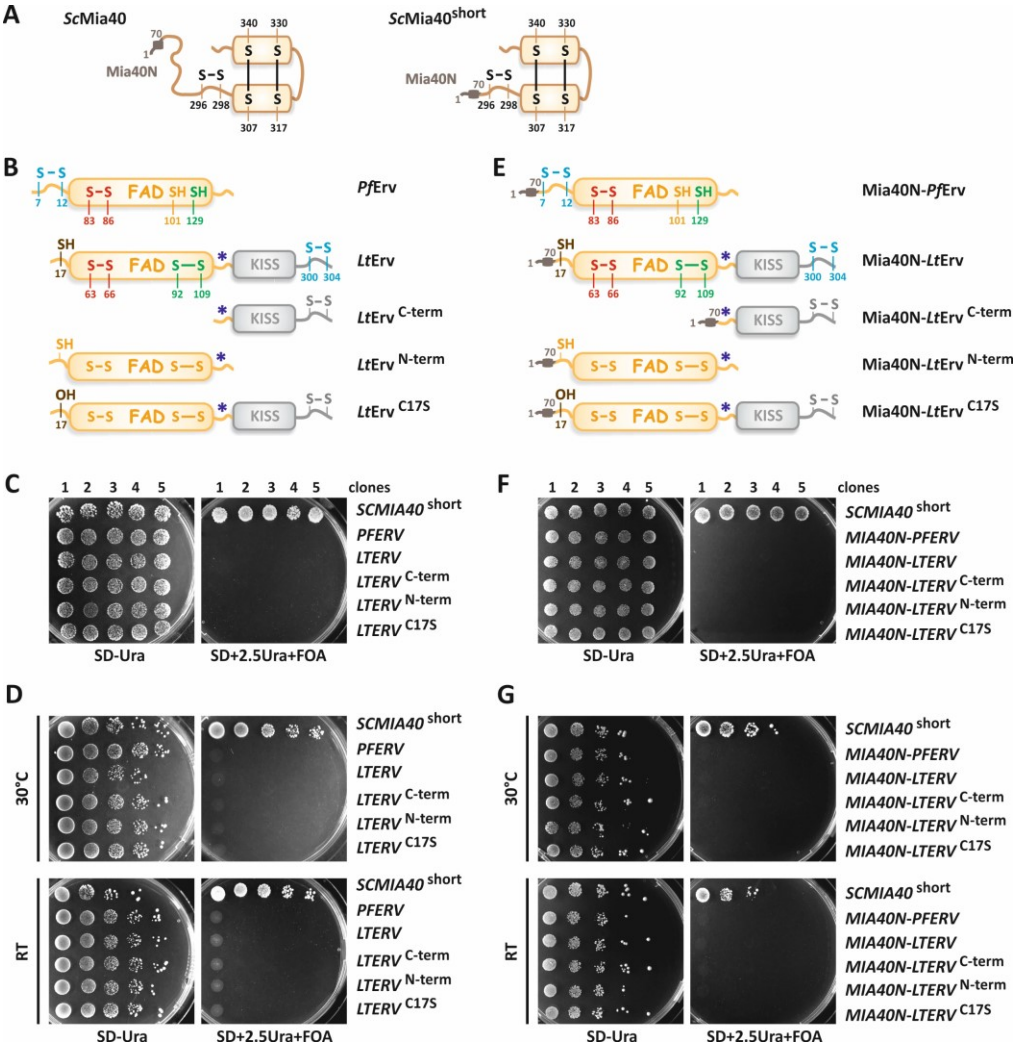

Figure 3.5 | Yeast *SCMIA40* complementation assays with full-length, truncated and mutant protist Erv. (A) Schematic representation of wildtype *Sc*Mia40 (left) and its N-terminally truncated version (right). N-terminal mitochondrial targeting signal and transmembrane segment (Mia40N) are highlighted. **(B)** Schematic summary of constructs encoding wildtype *Pf*Erv, *Lt*Erv and its truncated and mutated variants. Disulphides are highlighted in colours. **(C)** A Δ*mia40* strain harbouring an episomal copy of *SCMIA40* on a *URA3* plasmid was transfected with the indicated constructs on plasmid pYX232 and subjected to plasmid shuffling. *SCMIA40*^{short} on plasmid pRS314 served as positive control. **(D)** Drop dilution assays were performed in parallel and incubated at the indicated temperatures. Shown are representative experiments for one of three independent biological replicates. **(E)** Schematic summary of Mia40N-fusion-constructs **(F)** and **(G)** Plasmid shuffling approaches with Mia40N-fusion-constructs. RT= room temperature. Adapted from Specht *et al.* (2018).

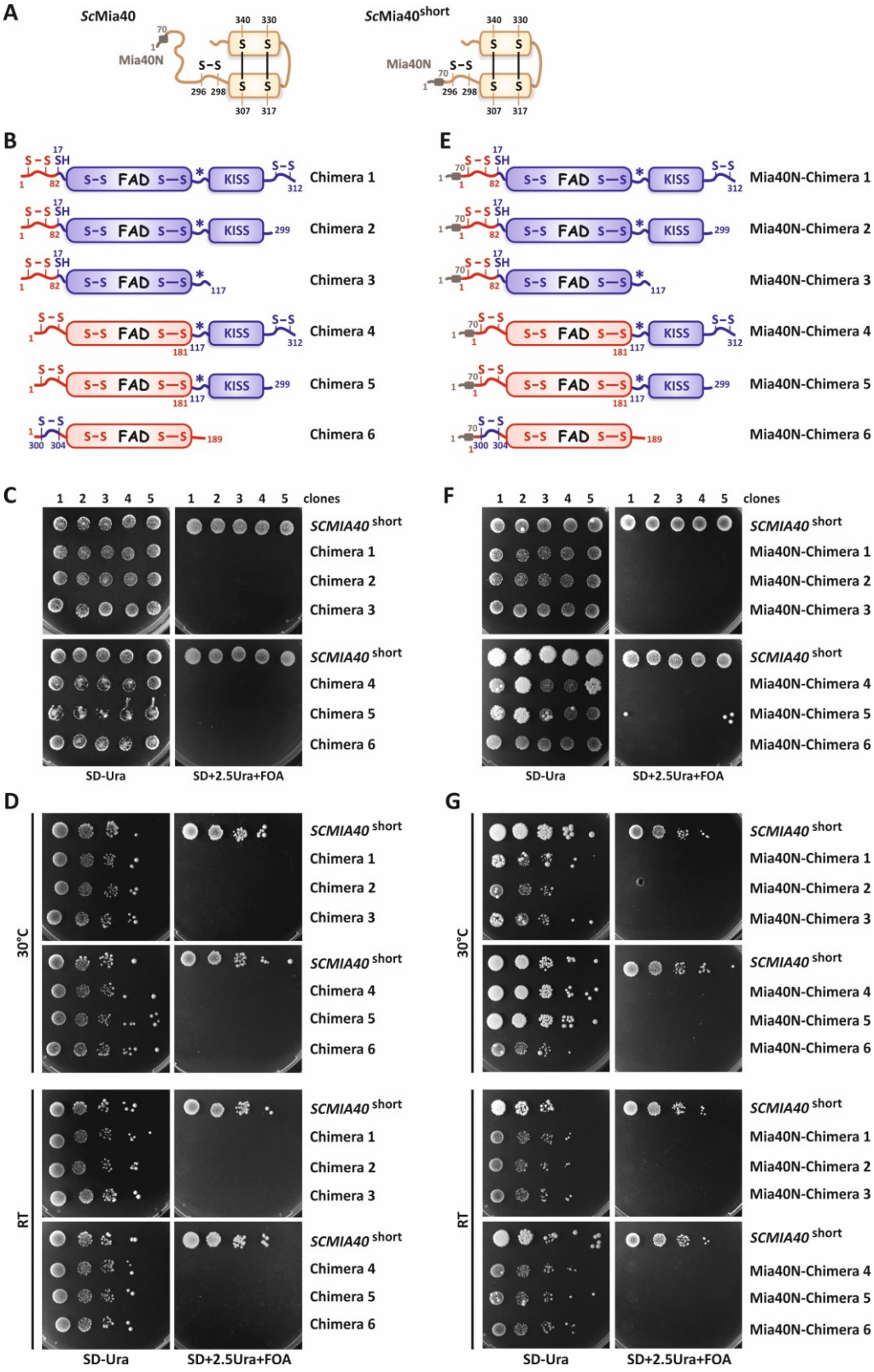

Figure 3.6 | Yeast *SCMIA40* complementation assays with chimeric *LTERV* constructs. (A) Schematic summary of full length *Sc*Mia40 and truncated *Sc*Mia40^{short}. N-terminal mitochondrial targeting signal and transmembrane domain (Mia40N) are highlighted. **(B)** and **(E)** Schematic representation of chimeric *Lt*Erv 1-6 with and without Mia40N. **(C)** and **(F)** Complementation assays with indicated constructs as described earlier. **(D)** and **(G)** Plasmid shuffling experiments were repeated as drop dilution assays at the indicated temperatures. RT= room temperature. Adapted from Specht *et al.* (2018).

3.3 Membrane association studies with *Lt*Erv

In contrast to soluble *Sc*Erv1, *Lt*Erv receives a tight membrane association in the IMS of both *Leishmania* and yeast (Eckers *et al.*, 2012; Eckers *et al.*, 2013). This property might also include the mechanism used to import *Lt*Erv into mitochondria in a Mia40-independent manner. Nevertheless, one of the main goals of this study was to identify the membrane that *Lt*Erv is associated with by establishing a differential fractionation protocol to solubilise the intact cells down to the IMS (Figure 3.7).

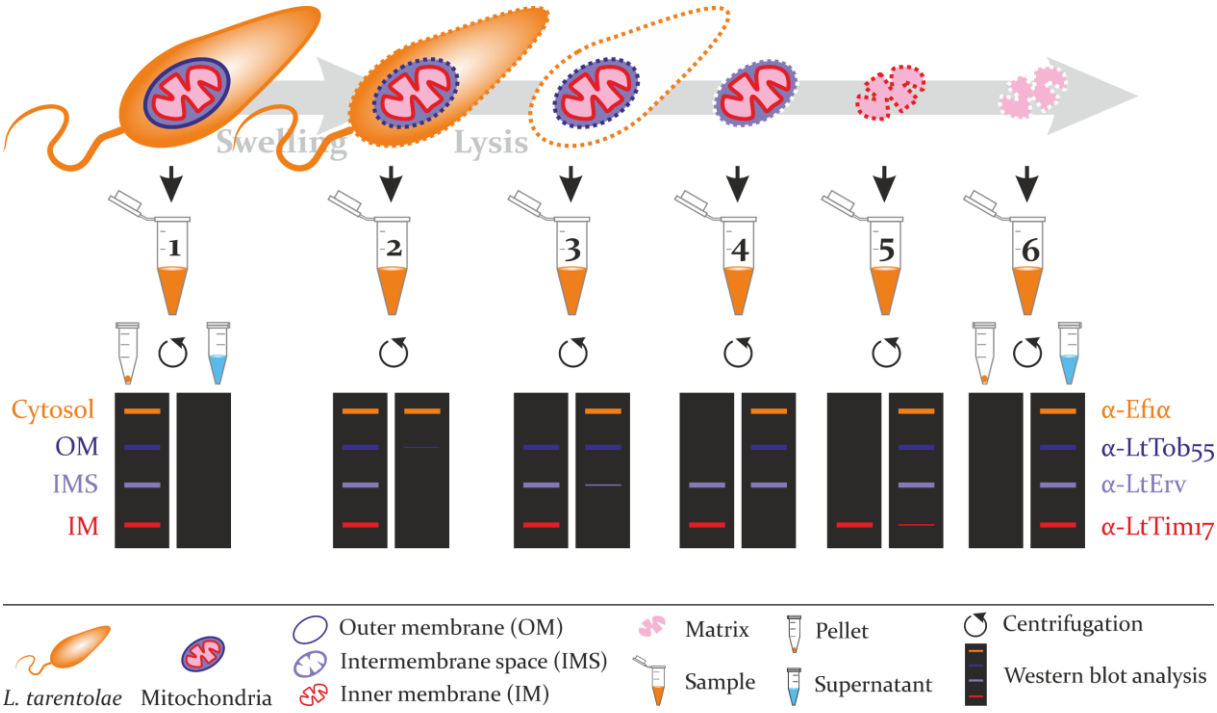

Figure 3.7 | Schematic summary of the differential fractionation protocol for *L. tarentolae*. **(1)** Intact parasites were harvested and subjected to a solubilisation procedure consisting of **(2)** hypotonic swelling and **(3-6)** a digitonin concentration gradient to progressively lyse the membranes of the parasite and its mitochondrion. Samples were taken from each step, separated into pellet and supernatant fraction and analysed by immunoblotting. The solubilisation process was followed by decoration with specific marker antibodies against the mitochondrial compartments and the cytosol.

3.3.1 Establishing a protocol for differential fractionation in *L. tarentolae*

In order to establish a reliable procedure for differential fractionation of *Leishmania* parasites, I tested and combined many protocols provided for yeast (Cordeiro and Freire, 1995) and *Kinetoplastida* (Vercesi *et al.*, 1991; Castro *et al.*, 2008; Hide *et al.*, 2008; Basu *et al.*, 2013; Peleh *et al.*, 2014; Mani *et al.*, 2017) to optimise each step along the experiment. Major attention was paid to buffer composition and final volume, incubation temperature and duration, proper amount of physical and chemical stress, supernatant precipitation, and western blot conditions. Samples were taken after each step,

centrifuged and analysed by western blotting using specific marker antibodies against each mitochondrial compartment and the cytosol.

In a first set of experiments, parasites were **directly subjected to a digitonin** concentration gradient to make sure, mitochondria are intact, and the lysis effects are due to a defined amount of digitonin (Figure 3.8A). As a result, Erv became soluble from the pellet at the addition of 200 µg of digitonin per 10^8 cells (indicated by red arrow) while the marker proteins for the OM (Tob55) and IM (Tim17) were still attached to the mitochondria. This indicates a porous OM, unable to preserve the IMS content (similar to scenario 3 in Figure 3.7). Although, acetone precipitation significantly improved the yield of the supernatant proteins as compared to trichloroacetic acid (TCA), bands were still faint und unsteady in appearance.

To overcome these problems, I applied an **additional shear stress** to the lysed cells to proper detach the OM from the mitochondria (see scenario 4 in Figure 3.7). I tested the influence of increasing shear stress on parasites under two different digitonin pressures (Figure 3.8B). At 100 µg digitonin/10^8 cells, the OM was usually destroyed to such an extent that Erv protein levels reached 50 % in the pellet and supernatant. In contrast, at 250 µg digitonin/10^8 cells, all of the IMS protein was soluble in the supernatant. Shear stress had no effect on Tob55 protein levels in the pellet. Acetone precipitation was prolonged to an overnight incubation at -20 °C and resulted in reliable strong protein bands. The shear stress procedure was finally extended by a hypotonic swelling step in advance of the physical pressure (Figure 3.8C). Consequently, Tob55 gradually accumulated in the supernatant fraction, while the IMS content became soluble exclusively upon lysis with Triton X-100. This approach was promising but never reproducible which is why strategies were changed.

Another barrier on the way to an evaluable outcome involved the α-*Lt*Tim17 antibody activity. To define **western blot conditions** suitable for both, the intermembrane proteins *Lt*Tob55 and *Lt*Tim17, as well as membrane-associated *Lt*Erv, I screened several SDS-PAGE and western blot alterations. This included Laemmli buffers supplemented with different amounts of urea (0, 4 M, 6 M) and incubation temperatures (5-10 min at 95 °C, 10-20 min at 65 °C, 10 min at 70°C, 30 min at 37 °C) as well as blotting membranes (nitrocellulose vs. PVDF), techniques (semidry vs. wet) and buffers (incl. 20 % [v/v] methanol, w/o SDS). The most important conditions are summarised in Figure 3.8D. Best results were obtained with samples incubated for 30 min at 37 °C in a 6 M urea-5× Laemmli buffer prior to separation by SDS-PAGE and subsequently wet-blotted on PVDF membrane (Figure 3.8E).

Since shear stress did not provide the intended effect, I tried to weaken the attachment of the OM with a gentle **hypotonic buffer system** that would allow to restrain mitochondrial leakage until the intended digitonin lysis (see scenario 2 in Figure 3.7). I first analysed the effect of the standard DT or

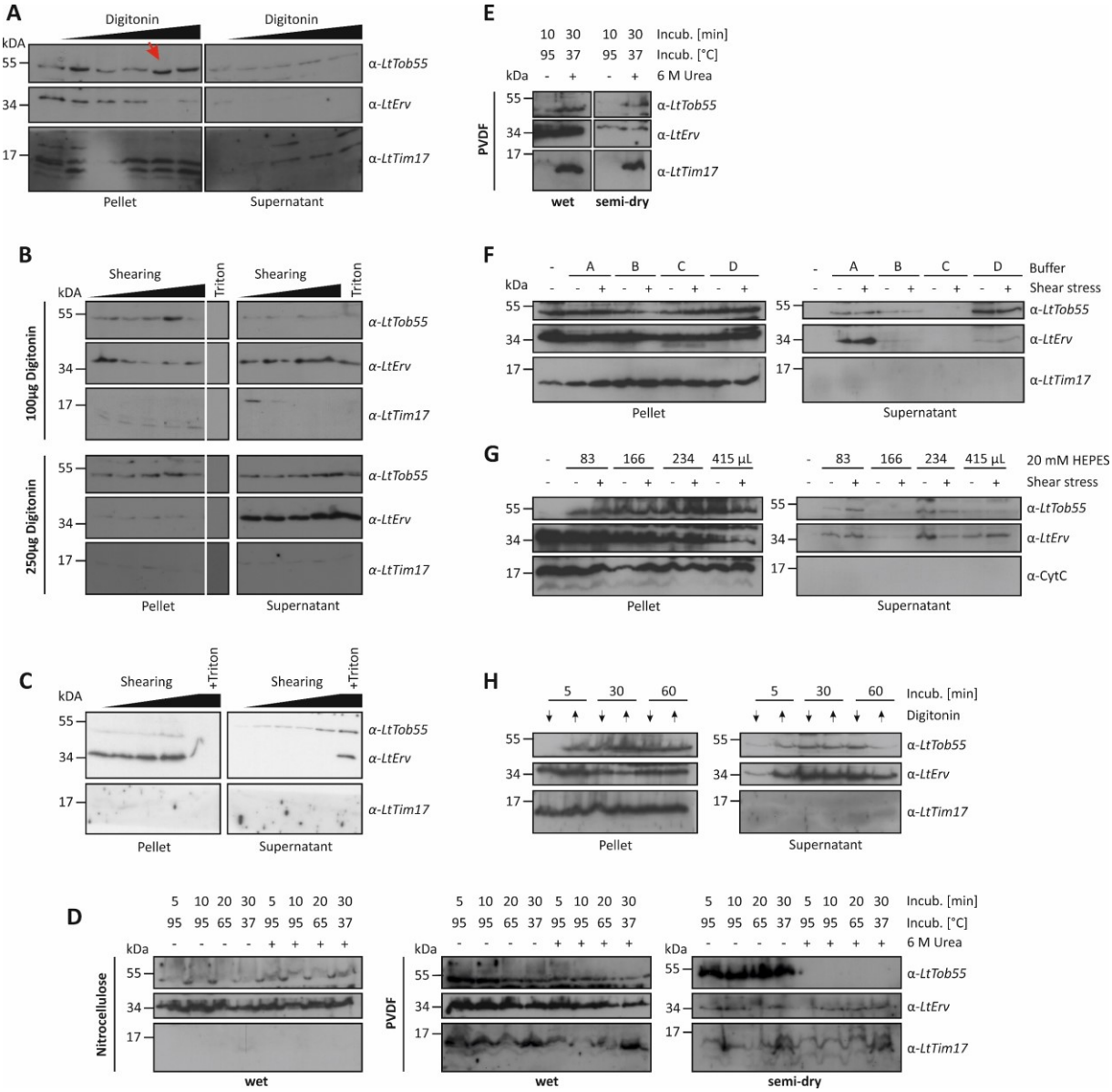

Figure 3.8 | Preliminary experiments for a differential fractionation protocol. *L. tarentolae* WT cells (5× 10^7 per lane) were harvested and treated as indicated before fractionation into pellet and supernatant. Samples were analysed by immunoblotting using marker antibodies against the outer (α-*Lt*Tob55, OM) and the inner mitochondrial membrane (α-*Lt*Tim17, IM), and the intermembrane space (α-*Lt*Erv, IMS) **(A)** Preliminary treatment with an increasing digitonin concentration gradient (0, 50, 100, 150, 200, 250 µg digitonin/10^8 cells). Erv was lost in the pellet upon 200 µg digitonin while Tob55 and Tim17 were unaffected (red arrow). Supernatant was precipitated in acetone at -20 °C for 1 h (and overnight in the following approaches) and all samples were boiled at 95 °C in 5× Laemmli buffer (+ 15 % β-ME) and blotted semidry on nitrocellulose membrane. **(B)** Influence of increasing shear stress (0, 2, 4, 6, 8×) onto parasites after digitonin treatment. Erv was equally distributed in pellet and supernatant at 100 µg digitonin/10^8 cells and almost completely soluble upon 250 µg digitonin. Shearing had no effect. **(C)** Influence of increasing shear stress after parasite swelling in hypotonic buffer (1 mM Tris). Tob55 was gradually accumulating in the supernatant. Tim17 detection failed. Samples were dissolved in Laemmli as described in A. **(D)** and **(E)** Troubleshooting for western blot conditions. Cells were harvested, and the pellet resuspended in 5× Laemmli with or without urea and incubated as indicated. Samples were blotted wet or semidry on nitrocellulose or PVDF membrane. **(E)** Best signals were obtained by blotting wet on PVDF with samples in 6 M urea buffer and incubation at 37 °C for 30 min. These conditions were used for the following experiments. **(F)** Troubleshooting for hypotonic swelling conditions. Cells were resuspended in the indicated buffers following different protocols. Tested were [A] 1 mM EDTA, 1mM Tris, pH 7.9 for 10 min at RT, [B] 5 mM $K_xH_xPO_4$, pH 7.9, 5 mM EDTA, 1 mM PMSF for 25 min on ice, [C] 1 mM MOPS-KOH pH 7.2, 0.25 mM EDTA, 25 mM sucrose for 30 min on ice, and [D] 20 mM HEPES-KOH pH 7.2 for 20 min on ice. Buffer D induced the intended gentle detachment of the OM (seen in supernatant). **(G)** Different volumes of HEPES buffer were tested to resuspend the cell pellet. Most promising results were obtained with 234 µL buffer without shear stress. **(H)** Parasites were resuspended in PBS supplemented with either 100 µg (↓) or 250 µg (↑) digitonin/10^8 cells and incubated on ice as indicated. Major differences between both concentrations were captured in the pellet at 30 min and in the supernatant at 5 min incubation. Both were tested further.

DTE buffer at various concentrations (1-20 mM) and incubation procedures (5-10 min at RT or 5-20 min on ice). None of the conditions achieved the desired result (data not shown). Therefore, I compared four different buffer systems with and without the application of additional shear stress. The outcome was quite diverse, ranging from no (buffer C) and reverse-intended (buffer A) effects to the actual intended effect of slowly dissolving the OM without damaging the IMS (see supernatant fraction, Figure 3.8F). This effect was still weak in buffer B but striking in buffer D, consisting of 20 mM HEPES. The gentleness of this treatment became clear as neither the pellet fraction showed any differences compared to the negative control nor the IM was affected in any way. Again, shear stress did not influence the outcome. In follow-up approaches, I determined a final volume of 234 µL 20 mM HEPES buffer to resuspend the cell pellet and incubation for 20 min on ice (data not shown) for optimal swelling conditions (Figure 3.8G).

Finally, the **incubation time of the digitonin** concentration gradient was reviewed on ice for 5 min, 30 min and 60 min. Despite auspicious preliminary results with the 5 min-approach (Figure 3.8H), incubation at 30 min was later found to provide more conclusive and reproducible data. That is because after 5 min, sufficient to accumulate proteins in the supernatant, the majority of mitochondrial proteins remained in the pellet fraction and this protein overload affected the running behaviour of the samples and thus the reproducibility of the experiment (data not shown).

In summary, an extensive evaluation of different conditions was carried out to establish a protocol for the differential fractionation of leishmania mitochondria. The complete final protocol provided reproducible results and is explained in detail in section 2.5.11.

3.3.2 *Lt*Erv is associated to either the inner or outer mitochondrial membrane

The strategy to identify the mitochondrial membrane in question involved a stepwise solubilisation procedure of the entire parasite by hypotonic cell swelling in combination with a mild detergent to lyse the parasite and the OM (Figure 3.9).

The OM was attacked and became slightly permeable upon parasite swelling in hypotonic 20 mM HEPES buffer, as suggested by the *Lt*Tob55 signal in the supernatant (line 11). *Lt*Erv remained inside mitochondria until the addition of 50 µg digitonin/10^8 cells (lines 10-13) that released significant amounts of the IMS protein into the soluble fraction (line 14). At 100-200 µg digitonin/10^8 cells, the OM was completely detached from the mitochondria, as indicated by the loss of *Lt*Tob55 signal in the pellet (lines 6-7), and major proportions of *Lt*Erv accumulated in the supernatant (lines 15-16). In contrast, the signals for the IM proteins *Lt*Tim17 and Cyt*c* were present in the pellet fraction up to a concentration of >500 µg digitonin/10^8 cells (lines 1-8). Both of these signals appeared in the

supernatant fraction in the presence of 2 % Triton X-100 (line 18) while only the *Lt*Tim17 was lost in the pellet (line 9).

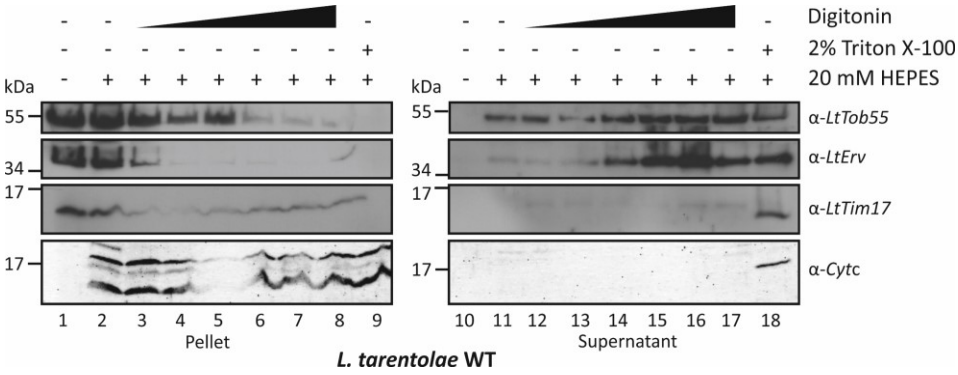

Figure 3.9 | Western blot analysis of differential fractionation of *L. tarentolae* wildtype cells. Cells (5× 10^7 per lane) were harvested, washed in PBS and treated as indicated before fractionation by centrifugation. Pellet samples were dissolved in 5× Laemmli + 6 M Urea and heated at 37 °C for 30 min. The supernatant was first precipitated in acetone overnight at -20 °C. Western blot was carried out in a wet blot process using PVDF membrane. Specific antibodies were used to label the outer mitochondrial membrane (*Lt*Tob55), the inner membrane space (*Lt*Erv), and the inner mitochondrial membrane using both the integral protein *Lt*Tim17 and the associated Cyt*c*. Digitonin concentration gradient: 0, 10, 25, 50, 100, 200, 500 µg/10^8 cells. Figure represents preliminary results in a representative western blot analysis of at least two biological replicates.

3.3.3 Characteristics of the Mia40-independent protein import of *Lt*Erv

Erv is a central component of the redox-relay system importing cysteine-rich proteins into the IMS but also substrate to this machinery (Terziyska *et al.*, 2007). Although, *Lt*Erv does not cooperate with *Sc*Mia40 it was shown to accumulate inside the IMS when imported into yeast mitochondria (Eckers *et al.*, 2013). Taking *Lt*Erv mutant constructs (Figure 3.1D) I intended to investigate the underlying property for its import and correct localisation in yeast mitochondria.

Preliminary experiments with a Δ*scerv1* strain expressing *Lt*Erv on plasmid pYX232 and *Sc*Erv1 on pRS426 were performed to re-establish a protocol for submitochondrial localisation (Figure 3.10). Mitochondria were isolated in a quick procedure and subjected to proteolysis. The cytosolic fraction could be successfully separated from the mitochondria-containing pellet fractions (SN vs. P1). The largest part of the IMS marker proteins were protected from proteolytic degradation as long as the OM was intact (P2). Under hypoosmotic conditions, the OM was expected to rupture surrendering IMS proteins to protease activity. Unexpectedly, *Lt*Erv was still not affected from protease activity, such as the matrix marker Tim44, while the IMS marker proteins *Sc*Erv1 and Tim50 were degraded. However, the slight degradation of the IMS content in P2 suggest that the mitochondria are already slightly damaged before hypotonic treatment.

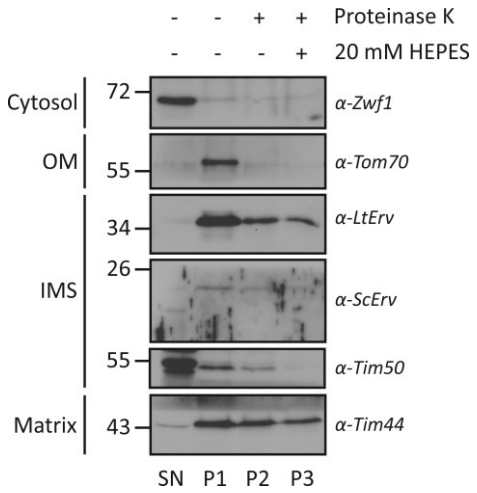

Figure 3.10 | Submitochondrial localisation studies in yeast. Yeast mitochondria were obtained by quick mitochondria preparation and incubated with or without proteinase K at isosmotic or hypoosmotic conditions. Immunodecoration was carried out using marker antibodies against the cytosol, outer mitochondrial membrane (OM), intermembrane space (IMS) and matrix. The figure shows a representative western blot of at least two independent biological replicates.

3.4 Knock out studies of *PFERV* and *PFTIM13*

While Erv1 was discovered decades ago as an essential protein in yeast (Lisowsky, 1992) and more recently in *T. brucei* (Basu *et al.*, 2013) and *L. infantum* (Specht *et al.*, 2018), *Pf*Erv was still unexplored. I generated a CRISPR/Cas9 strategy to knock out *PFERV* and the small *PFTIM13* by double crossover (Figure 3.11). Viable clonal lines were obtained for a potential Δ*pftim13* strain by limiting dilution and are yet to be analysed. In contrast, the attempt to knock out *PFERV* was unsuccessful, suggesting another essential Erv homologue. However, only one guide RNA was tested in a single experiment.

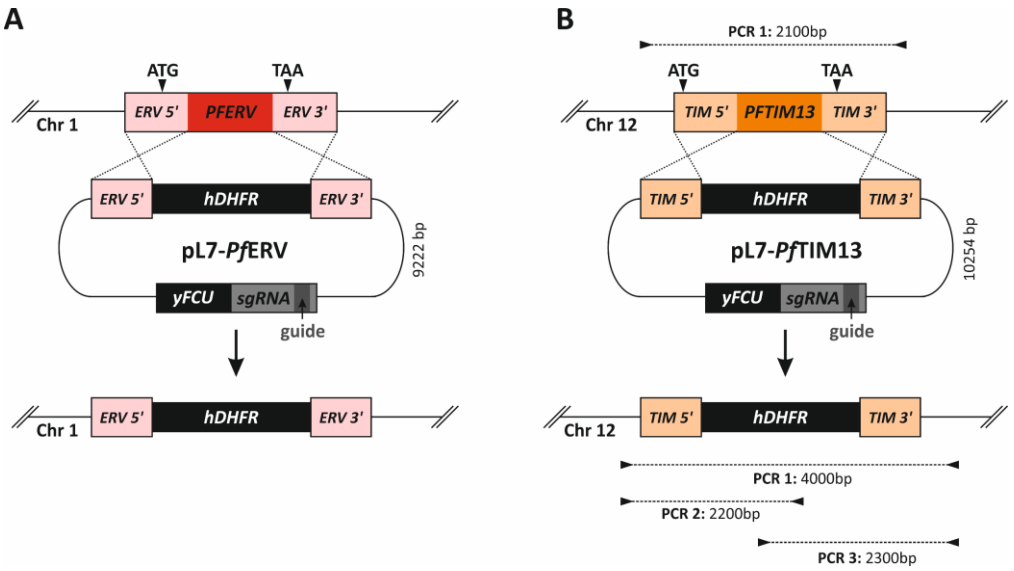

Figure 3.11 | Generation of *P. falciparum* 3D7 Δ*pferv* and Δ*pftim13* knockout strains. Schematic summary of the **(A)** Δ*pferv* and **(B)** Δ*pftim13* knockout strategy by double crossover with the plasmids pL7-*Pf*Erv or pL7-*Pf*Tim13, respectively. Annealing sites of primers for Δ*pftim13* and the size of the expected PCR products are indicated.

3.5 Examination of the oxidative folding machinery in *L. tarentolae*

In a previous study, we aimed to identify a potential Mia40-replacement candidate by using overexpressed *Lt*Erv and *Lt*sTim1 as bait proteins in pull-down experiments. Since both proteins proved to be inappropriate for that purpose, due to technical reasons (Liedgens, 2018), we switched to newly discovered substrates of the oxidative protein folding pathway (Peikert *et al.*, 2017). Four candidates were cloned into a *Leishmania* expression vector (Mirko Höhn) encoding either a C-terminal Flag- or Flag-His-tag and analysed in a wildtype background. Simultaneously, I introduced *Sc*Mia40s into *L. tarentolae* to study the behaviour of the parasites in presence of this otherwise missing redox enzyme.

3.5.1 Trapping of mixed disulphide intermediates with putative MIA substrates

Peikert *et al.* (2017) have recently published a list of putative substrates of the oxidative folding pathway obtained from knockdown studies in *T. brucei*. Out of 25 proteins, four were chosen according to several characteristics, including molecular mass, sequence coverage, existence of cysteine motifs and total number of cysteines, and finally phylogenetic conservation in *Kinetoplastida*, *Apicomplexa* and *Opisthokonts* (Liedgens, 2018). Homologues were cloned from *L. tarentolae* gDNA (Mirko Höhn) and were consequently overexpressed in a wildtype strain.

The substrates have two to four cysteines. Substrate 1 (Tb927.9.7980/LtaP04.0660) and substrate 3 (Tb927.10.15790/LtaP19.1110) contain classical twin Cx_9C motifs (Figure 3.12A). All substrates were 24 kDa or smaller in size to separate them from *Lt*Erv in western blot analysis and either soluble in the IMS or equipped with one or two putative transmembrane domains. Cysteine point mutations were introduced in substrate 2 (Tb927.10.4280/LtaP35.0210) and substrate 4 (Tb927.11.13510/ LtaP09.1390) to further stabilise mixed disulphide intermediates (Mirko Höhn).

Substrates 1-4, including two cysteine mutants of substrate 2 (C105S or C117S), were successfully expressed in *L. tarentolae* and one of four clones for each line was selected for the following experiments (data not shown). In order to chemically trap a mixed disulphide intermediate, formed between a potential Mia40 adapter replacement and the substrate, free cysteines were blocked with *N*-ethylmaleimide (NEM). If such a short-lived intermediate was formed, the NEM should stabilise this structure since an intramolecular disulphide bond cannot be restored with an alkylated cysteine. Additionally, the living cells were previously treated with the oxidizing agent diamide or the reducing component DTT to alter the redox state and potentially generate a more fortunate redox equilibrium. In the end, the cells were boiled in Laemmli buffer under non-reducing and reducing (+ β-ME) conditions and analysed by immunoblotting.

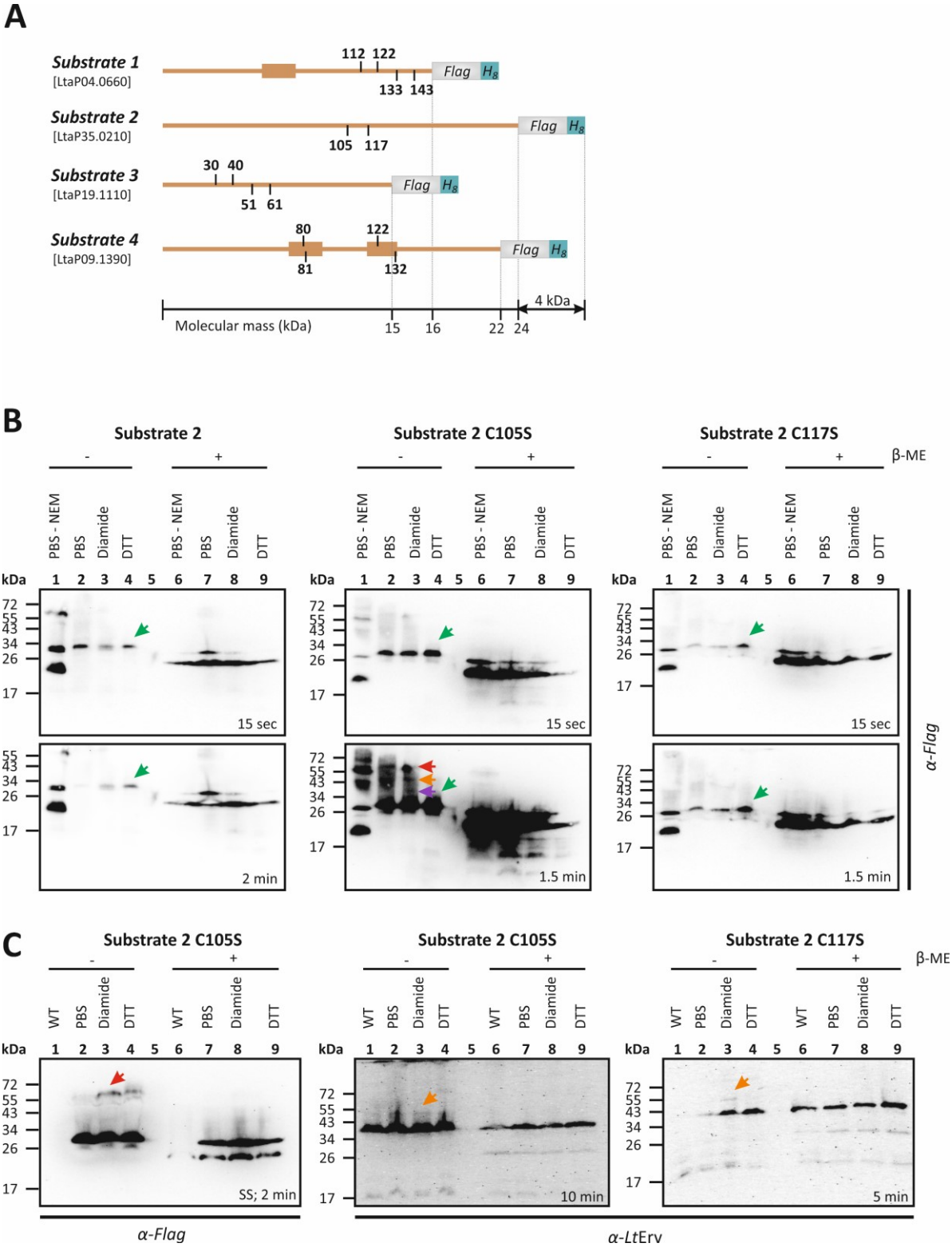

Figure 3.12 | Chemically trapping a Mia40 adapter replacement. (A) Schematic summary of the selected new substrates of the oxidative protein folding pathway of the IMS that were selected by Linda Liedgens based on the identified homologues in *T. brucei* by Peikert *et al.* (2017). Boxes symbolise putative transmembrane elements and the position of cysteine residues are highlighted with black numbers. Flag- and His-tags are displayed disproportionally. Substrate size with and without tags are indicated below. **(B)** Parasites expressing Flag-His-tagged substrate 2 or the cysteine point mutants C105S or C117S were harvested and treated as indicated. Free thiols were modified by NEM and subsequently analysed by western blotting under non-reducing and reducing (+β-ME) conditions. Immunodecoration with α-Flag showed higher molecular bands at ~30 kDa (green arrow), ~34 kDa (purple arrow), ~50 kDa (orange arrow), ~60 kDa (red arrow). Exposure times are highlighted. **(C)** Comparison of western blot membranes decorated with α-Flag or α-*Lt*Erv. Higher molecular bands are highlighted with arrows as described above. Figure represents preliminary data of up to two biological replicates with 5×10^7 cells per lane.

A representative blot for this procedure using parasite strains that express Flag-His-tagged substrate 2 or the cysteine mutants C105S or C117S is shown in Figure 3.12B. The Flag antibody visualised the substrate under reducing conditions with a double band at around 26 kDa. Under non-reducing conditions, the conspicuous double band was lost, and the size shifted to a molecular mass of about 30 kDa in the presence of NEM (green arrow). A sample without NEM was loaded as a control and displayed a band corresponding to the calculated molecular substrate mass of 28 kDa as well as several unspecific higher molecular bands and one lower molecular band at ~20 kDa. Only the cysteine point mutant C105S revealed potential interaction candidates at a mass of ~60 kDa (red arrow), ~50 kDa (orange arrow), and ~34 kDa (purple arrow).

In another approach, both cysteine mutants were treated as described above and the western blot membrane was probed with either α-Flag or α-*Lt*Erv to check whether they disclose a common higher molecular weight band (Figure 3.12C). This would suggest *Lt*Erv interacting directly with the substrates. Decoration with α-Flag presented again a band in the higher molecular range at about ~60 kDa for substrate 2 C105S-Flag-His (red arrow). After diamide treatment, α-*Lt*Erv exposed an additional protein of about ~50 kDa (orange arrow) for both the Flag-His-tagged C105S and C117S mutant substrates.

In summary, preliminary results with the cysteine point mutants of substrate 2, propose potential mixed disulphide intermediates of a molecular mass of ~60 kDa (red arrow), ~50 kDa (orange arrow), or ~34 kDa (purple arrow). The ~50 kDa band might reflect a direct interaction of *Lt*Erv with the substrate.

3.5.2 Redox inactive *Sc*Mia40^{SPS} triggers a hyperactive phenotype in *L. tarentolae*

Mia40 is an essential redox enzyme in yeast and other *Opisthokonts* importing cysteine-rich proteins into the IMS of mitochondria. *L. tarentolae* as a member of the parasitic protists is missing this homologue and, so far, no replacement was discovered. We were therefore curious to know how parasites would handle the sudden presence of Mia40 and expressed a redox-active (Mia40s^{Flag}) and inactive (Mia40s-SPS^{Flag}) version of the protein in a *Leishmania* wildtype background (Figure 3.13).

Mia40-SPSs^{Flag} grew slightly faster than the wildtype strain (no plasmid) during the initial two days and reached earlier the stationary phase with a lower overall cell density (Figure 3.13A). In contrast, wildtype cells grew hardly better than the strain expressing Mia40s^{Flag}. The most prominent feature concerned the increased motility of Mia40s-SPS^{Flag} cells. While all the three strains showed classic cell morphology (Figure 3.13B), parasites harbouring Mia40s-SPS^{Flag} appeared to move hyperactively when observed on a glass slide (data not shown). This phenotype has not yet been further investigated but seemed to be absent in cells expressing redox-active Mia40s^{Flag}. Finally,

western blot analysis with a α-Flag antibody verified the presence of the Mia40 variants in the indicated lines while *Lt*Erv and *Lt*Tob55 served as loading controls (Figure 3.13C).

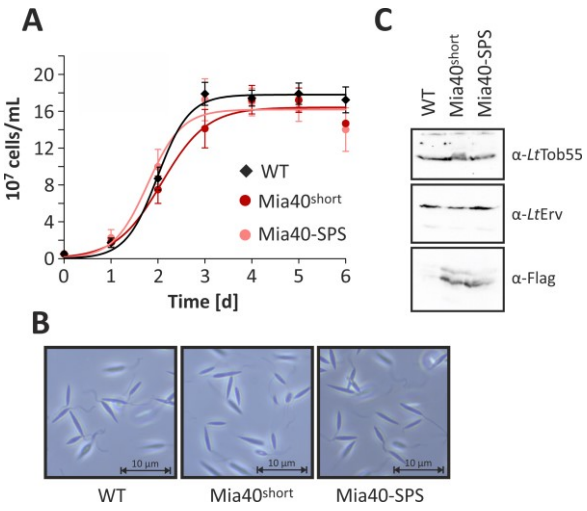

Figure 3.13 | Heterologous expression and characterisation of *Sc*Mia40 in *L. tarentolae*. (A) Growth curve analysis of wildtype (WT) parasites or cells expressing Flag-tagged *Sc*Mia40^{short} or *Sc*Mia40s-SPS. Cell density was determined by counting every 24 h over a period of six days. Values represent the mean ± standard deviation of three independent biological replicates. Transgenic parasite lines grew under G418 selection pressure. **(B)** Light microscopy images of *L. tarentolae* promastigotes harbouring the indicated constructs. **(C)** Western blot analysis with 5× 10^7 cells per line. Immunodecoration was performed with α-Flag to visualise the substrates and α-*Lt*Erv and α-*Lt*Tob55 as loading controls.

3.5.3 Redox state of *Sc*Mia40 in *L. tarentolae*

After heterologous expression and characterisation of *Sc*Mia40 in *L. tarentolae,* I was interested in the redox-state that this protein has in the host organism. In yeast, *Sc*Mia40 contains six cysteine residues. Four of which form intramolecular structural disulphide bonds in a Cx_9C motif and two are present in the redox active CPC motif (Figure 3.14A). At steady-state level, the CPC motif was shown to be 70-80 % oxidized to maintain oxidative protein folding (Kojer *et al.*, 2012). If *Sc*Mia40 is functional in *L. tarentolae,* one would expect a similar redox-state as shown for yeast, with a stable, hardly reduceable disulphide bond in the Cx_9C motif and a simple-to-reduce CPC motif.

In a redox mobility shift assay, free cysteines were modified with the alkylating compound methyl-PEG-24-maleimide ($mmPEG_{24}$), which slowed migration of the affected protein on SDS-PAGE by 1.2 kDa per accessible thiol (Figure 3.14B). Without the thiol modifying compound, the mildly reduced *Sc*Mia40 showed a band at the calculated molecular mass of about 24 kDa (line 1). A similar band was produced for the untreated and unmodified sample, which reflects the physiological redox state (line 2). The addition of $mmPEG_{24}$ led to a migration change of about 2 kDa (line 3+10) compared to the unmodified protein (line 2+9), indicating the presence of two accessible cysteine residues. In addition, cells were treated with the reductant tris(2-carboxyethyl)phosphine (TCEP) at 27 °C or 95 °C for mild or harsh reduction, respectively and were subsequently modified with $mmPEG_{24}$. Reduction at 27 °C

shifted the molecular mass of *Sc*Mia40 to about 26 kDa, which likely corresponds to modification of the reduced CPC motif (line 4). In contrast, *Sc*Mia40 gained an additional mass of ~7 kDa under harsh reducing conditions, signalling modification of all cysteines in the protein (line 5). Both the diamide and DTT control presented very faint bands at a molecular mass of 26 kDa, indicating a partially reduced redox state (line 6+7).

In conclusion, preliminary results suggest a partially reduced redox state of *Sc*Mia40 in *L. tarentolae*, indicating that the yeast protein is not functional in the protist host.

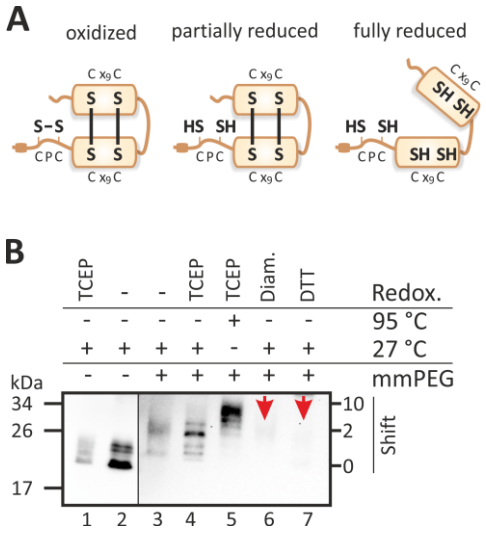

Figure 3.14 | Redox state of *Sc*Mia40 in *L. tarentolae*. (A) Schematic representation of *Sc*Mia40 in its oxidized, partially reduced and fully reduced redox state. C= cysteine, P= proline, x= any amino acid, S= sulphide, SH= thiol **(B)** Redox mobility shift assay. Parasites expressing Flag-tagged *Sc*Mia40s were treated with diamide, DTT, or PBS as control and lysed in Laemmli buffer with or without the reductant TCEP at 27 °C or 95 °C. Free thiols were subsequently modified with mmPEG$_{24}$ resulting in a mass shift of 1.2 kDa per accessible cysteine residue. Samples containing 1.25× 10^7 cells per lane were analysed by western blotting using α-Flag. Shown is one blot at two different exposure times. Redox. = redox agent.

4 Discussion

The mitochondrial protein import is a central component of life and has been in the focus of research for decades, studying model organisms mainly belonging to the group of opisthokonts (Neupert and Herrmann, 2007; Chacinska *et al.*, 2009; Endo and Yamano, 2009; Schmidt *et al.*, 2010; Dimmer and Rapaport, 2012; Dudek *et al.*, 2013; Peleh *et al.*, 2016). Although this group contains many important representatives, such as mammals and yeast, it only speaks for one of five major eukaryotic lineages (Adl *et al.*, 2012) and therefore cannot reflect a general picture. In the present study, protocols and procedures for the standard model organism *S. cerevisiae* were used and combined with organisms from two other eukaryotic branches, *P. falciparum* from the group of *SAR* and *L. tarentolae* as a member of the *Excavates* (Figure 1.1). With these comparative studies it should be possible to better understand the evolution of eukaryotes.

4.1 Structure-function analyses of *Lt*Erv

The main objective of this thesis was to unravel structure-function relationships of the protist protein *Lt*Erv and its unusual C-terminal KISS domain. *Lt*Erv accumulates inside the IMS of yeast mitochondria but is unable to adopt the function of its yeast homologue *Sc*Erv1 (Eckers *et al.*, 2012). The underlying hypothesis claimed a structure within the parasite protein to prevent *Lt*Erv to be functional with *Sc*Mia40 in the redox-relay system of yeast. A set of chimeric constructs were generated, in which certain *Leishmania* properties were exchanged by critical yeast protein structures to narrow a potential inhibiting or incompatible arrangement (Figure 3.1). Fusing the N-terminal “shuttle” arm of *Sc*Erv1 to the truncated *Leishmania* amino terminus allowed the protist protein to properly function in a Δ*scerv1* knock-out strain (chimera 1-3). This behaviour was slightly negatively influenced by truncation of the parasite’s C-terminal “shuttle” arm (chimera 2) and even more by removal of the entire carboxyl terminus including the KISS domain (chimera 3). Nevertheless, cells harbouring chimera 3 were viable and showed a normal growth behaviour in the following experiments (Figure 3.4). This proposes that the Erv domain is in principle functional in yeast when extended by the yeast shuttle arm to communicate between *Sc*Mia40 and the *Lt*Erv domain.

The Erv shuttle arm is required for the oxidase activity of the protein and consists of an conserved cysteine pair in a highly variable motif (Figure 1.7) and is either located at the N-terminus, as in yeast, mammals and apicomplexans, or at the C-terminus (Hofhaus *et al.*, 2003; Levitan *et al.*, 2004; Vitu *et al.*, 2006; Ang and Lu, 2009; Bien *et al.*, 2010; Banci *et al.*, 2011; Basu *et al.*, 2013; Eckers *et al.*, 2013; Ang *et al.*, 2014). Similar to *Lt*Erv, *At*Erv1 was not functional in yeast having a CEQKSC motif in the C-terminal shuttle arm (Levitan *et al.*, 2004). On the other hand, the N-terminal shuttle cysteine motif of

apicomplexan parasites (Cx_4C) or mammals (Cx_2C) also failed to complement for *Sc*Erv1 (Lange *et al.*, 2001; Eckers *et al.*, 2013). Yet, *Leishmania*'s CQVYC motif replaced the yeast CRSC motif in the yeast shuttle arm (chimera 6), proposing that not exclusively the composition of the motif is crucial for the interaction with *Sc*Mia40. Modifications of the shuttle cysteine pair (C300S/C304S, C300S), the active site (C63S), or the structural bond (C92S/C109S) in *Lt*Erv did not change the proteins dysfunction (Figure 3.1). Yet, upon mutation of the clamp residue (C17S), the parasite Erv was able to functionally replace its yeast homologue. The N-terminal clamp residue is therefore most likely the reason why *Lt*Erv is incompatible with *Sc*Mia40 in the oxidative folding system in yeast mitochondria.

Residue C17 is partially conserved and forms a clamp disulphide bond in the mammalian ALR to stabilise the homodimer conformation but is absent in many other eukaryotes, including yeast and apicomplexan parasites (Wu *et al.*, 2003; Farrell and Thorpe, 2005; Deponte and Hell, 2009; Banci *et al.*, 2011; Eckers *et al.*, 2013). In accordance with the present results, it was reported that heterologous human ALR remains in the cytosol and does not complement for *Sc*Erv1 when imported synthetically into yeast mitochondria. However, when the amino terminus of ALR was extended by a bipartite pre-sequence or replaced by the first 92 amino acids of the yeast protein, it was imported and functional in yeast mitochondria (Lange *et al.*, 2001; Sztolsztener *et al.*, 2013). How C17 exactly causes incompatibility of *Lt*Erv in yeast and which may be its physiological relevance in *Leishmania* remains to be investigated. Likewise, the effectiveness of the interaction between *Lt*Erv^{C17S} and *Sc*Mia40 needs to be explored in more detail, since yeast cells expressing the mutant Erv grew fine on glucose but were facing trouble on non-fermentable carbon sources (Figure 3.4). This behaviour reflects an impaired mitochondrial respiration potentially caused by a defective protein import machinery. A similar phenotype was observed for the chimera 1, 2, and 6, which grew normally on FOA media, but revealed certain growth defects on non-fermentable carbon sources (Figure 3.4). The same chimeras interacted with but only ineffectively oxidized *Sc*Mia40, which in turn had a negative impact on the import of cysteine-rich proteins into the IMS (Specht *et al.*, 2018). In contrast, yeast cells containing the chimeras 4 or 5 were free of any growth defect and the interplay between the yeast shuttle arm and the yeast flavodomain coordinated an optimal oxidation of Mia40 regardless of the KISS domain (Specht *et al.*, 2018). Previously, a *Sc*Erv1-defective strain was reported with reduced vegetative growth on glucose and the immediate deprivation of respiratory functions on non-fermentable carbon sources that was associated with the loss of the mitochondrial genome (Lisowsky, 1994). However, viability and consistent growth of yeast also on non-fermentable carbon sources confirmed that mitochondria containing *Lt*Erv^{C17S} or the chimeras 1, 2, and 6 were able to respire. The respective mutant/chimera must therefore be at least partially functional in yeast.

Truncation constructs showed that neither the Erv nor the KISS domain alone are sufficient to complement for *Sc*Erv1. In addition, no negative effect of the KISS domain was observed; instead, its

presence even improved survival of chimeras 1 and 2 compared to chimera 3 (Figure 3.1) and did not affect normal growth by extending the *Sc*Erv1 domain (chimera 4 and 5; Figure 3.4). Apart from the redox-active cysteine pairs (shuttle and active site pair), the partially conserved structural disulphide bond also proved to be essential after the removal of the interfering C17 (Figure 3.3).

In summary, the protist *Lt*Erv in its wildtype form is insufficient to cooperate with Mia40 in yeast but functional when the clamp residue is exchanged by a serine or when the yeast shuttle arm is attached to the N-terminus of the protein. Nevertheless, due to phylogenetic distances, the opisthokont and kinetoplastid flavodomains are not interchangeable without complications. It is not surprising that in the course of evolution the interaction between electron donor (e.g. *Sc*Mia40) and shuttle arm as well as shuttle arm and flavodomain have been optimised. Yet, it is interesting that certain variations are still accepted.

4.2 The unusual protein import and membrane association of *Lt*Erv

There are three common sorting pathways that import proteins from their site of synthesis in the cytosol to their site of action in the IMS (Figure 1.5). Erv is a major key player of one of them, trapping small and cysteine-rich proteins via the MIA pathway (Herrmann and Hell, 2005). Likewise, *Sc*Erv1 uses this very same pathway for its own translocation and accumulation inside the IMS (Gabriel *et al.*, 2007; Terziyska *et al.*, 2007). The C-terminal part of the flavodomain (residues 134-176) is sufficient to drive import of the yeast protein, with the structural cysteine pair binding to *Sc*Mia40 for an electron exchange reaction (Kallergi *et al.*, 2012). In the present study, I aimed to identify a special structure or redox property that drives the translocation of *Lt*Erv into *Leishmania* and yeast mitochondria. In a first set of experiments, I systematically replaced all the disulphide bond forming cysteine pairs of *Lt*Erv and in combination with a mutation of the clamp residue, I tried to rescue a yeast Δ*scerv1* strain with them (Figure 3.3). In contrast to the wildtype protein, the clamp mutant *Lt*Erv^{C17S} was able to adopt *Sc*Erv1 function. Meaning, it likely interacted with *Sc*Mia40 to oxidize the partner protein and potentially also to initiate its own import. Further disruption of the redox-sensitive cysteine pairs at the shuttle arm or the active site interrupted the oxidoreductase activity of the protein, which unavoidable led to cell death. In addition, also the structural disulphide bond (C92 and C109) claimed its right to exist. Mutation of this cysteine pair may have disturbed the protein's import in a Mia40-dependent manner, as described previously by Kallergi *et al.* (2012) in experiments with *Sc*Erv1. As a result, the expressing strain was not viable. Also, subcellular fractionation of yeast cells expressing *Lt*Erv^{C17S} revealed a dual localisation of the mutant protein in the cytosol and yeast mitochondria (Supplementary figure 3). This suggests an important role for residue C17 as a signal for mitochondrial localisation. Nonetheless, specific import assays with the mutants have to test this first lead. A rather simple procedure might

include an extension of the submitochondrial localisation studies that have been performed by Eckers *et al.* (2013) and have shown that *Lt*Erv accumulates in the IMS of yeast mitochondria. Similar studies may be carried out with yeast strains expressing either of the mutant *Lt*Erv variants listed in Figure 3.1D to confirm the structure that abolishes protein import. Therefore, first experiments have been done in the framework of this thesis (Figure 3.10). Even though a quick procedure effectively separated the cytosolic fraction from the protein content of the mitochondria, the overload of protist Erv and the rather small proportions of endogenous IMS proteins (e.g. *Sc*Tim50) made it difficult to evaluate. For future attempts, it might be worth switching to a gentler procedure, which isolates mitochondria to a purer extent and makes sure they are intact upon treatment.

The absence of a Mia40 homologue in certain protist mitochondria, however, proposes an alternative, Mia40-independent explanation for the Erv import in these eukaryotes. Class I proteins, such as cytochrome b_2, Mgm1, cytochrome *c* peroxidase or even *Sc*Mia40 possess mitochondrial pre-sequences followed by hydrophobic sorting domains that direct them to the TIM23 complex and via the stop-transfer model into the inner membrane (Figure 1.5A). Afterwards, matrix targeting pre-sequences are removed from the matrix side and soluble IMS proteins can be released after a second cleavage inside the IMS (Herrmann and Hell, 2005). Sztolsztener *et al.* (2013) demonstrated that the human ALR is imported into yeast mitochondria when supplemented by the bipartite pre-sequence of cytochrome b_2, suggesting that this import route is possible but probably not exploited *in vivo*. Additionally, *Lt*Erv did not present "striking hydrophobic patches" in the analyses by Eckers and co-workers (2012; 2013), which likely excludes the TIM23 pathway. On the other hand, the same studies also uncovered a tight membrane association of endogenous and heterologous *Lt*Erv (Eckers *et al.*, 2012; Eckers *et al.*, 2013). This characteristic might out *Lt*Erv as a classical class III protein that are permanently associated to binding sites at the mitochondrial membranes (Herrmann and Hell, 2005). Class III proteins are imported independently of membrane potentials and ATP levels and fold rapidly after translocation through the TOM complex (Steiner *et al.*, 1995). To substantiate this suspicion, I established a differential fractionation protocol for *Leishmania* parasites to separate the OM from the IM and define to which membrane endogenous *Lt*Erv is associated. If the binding site contains a *trans* side receptor, it will be of advantage to know its localisation for identification and characterisation purposes. Considering the role that Erv is playing in the IMS and its final interaction with cytochrome *c* of the respiratory chain, the IM seemed to be more likely. However, preliminary results were inconclusive but rather suggested *Lt*Erv to reside close the OM. In at least two biological replicates the protist protein became free from the IMS shortly after the OM started to rupture while the marker proteins for the IM remained inside the mitochondria (Figure 3.9). This result was rather surprising and has to be substantiated by further experiments. Nevertheless, an association to the OM may be explained by the presence of the unusual ATOM complex of trypanosomatids, which takes the place

of the common OM pore Tom40 (Pusnik *et al.*, 2011). Our understanding of this noncanonical complex is still limited and novel components of the complex and the entire protist OM are constantly being discovered (Pusnik *et al.*, 2012; Niemann *et al.*, 2013; Mani *et al.*, 2015; Mani *et al.*, 2017). Therefore, it may be not unlikely that the wanted binding site for *Lt*Erv coincides with the ATOM complex, importing and trapping the protein inside the IMS. If not linked to ATOM, a potential import receptor may represent at least one of the 82 proteins that make up the proteome of the OM in trypanosomatids (Niemann *et al.*, 2013). Being located close to the OM would also have the advantage for *Lt*Erv to be in close proximity to substrates after their translocation, which have to be folded to remain in the IMS.

Additionally, one have to keep in mind that the IMS is a tiny compartment measuring only a few nanometres (Frey and Mannella, 2000) that makes harsh procedures like hypotonic swelling and detergent lysis vulnerable to errors. Further experiments have to be done to support or correct these findings. Peleh *et al.* (2014) have applied a similar approach to isolated yeast mitochondria to determine the sublocalisation of the proteins Dre2 and imsDre2 but combined the swelling and the digitonin concentration gradient with an additional proteolytic lysis. This may be an intervention to define the separation between the OM and the IM more clearly. If this strategy is not sufficient, a density gradient flotation centrifugation could be tested as used previously to identify proteins of the mitochondrial contact sites or the OM (Harner *et al.*, 2011; Niemann *et al.*, 2013). Thereby, the protein content of the different compartments can be obtained from different gradients and analysed more precisely by western blot analysis. The use of additional marker antibodies, especially for the IMS and the two membranes is highly recommended to assign the localisation clear and without ambiguity. Since *Lt*Erv is membrane associated not only in *Leishmania* but also in yeast mitochondria (Eckers *et al.*, 2013), there is the opportunity to study the same subject in two evolutionary distant organisms and in the best case, to obtain two independent but explicit results. In other words, if none of the proposed procedures succeed satisfaction, one still has the chance to study the import of *Lt*Erv at a simpler model.

Understanding where *Lt*Erv is associated is an important first step to unravel the nature of the import machinery of this protein and to identify potentially involved components. Next, it is of interest to describe the property, which causes this membrane association in the trypanosomatid protein but not in the yeast homologue. The mutant *Lt*Erv constructs have to be introduced into a Δ*lterv* strain or tagged in order to differentiate the mutants from the endogenous protein by western blot analysis. So far, we have intended to avoid the tagging of proteins to bypass potential localisation artefacts, which is why Gino Turra is currently establishing a CRISPR/Cas9 strategy for *L. tarentolae* to realise a Δ*lterv* strain in our lab. Once this is done, carbonate extraction assays and differential fractionation can be applied to comprehend which structure is mandatory for membrane association and for specific

localisation. So far, preliminary attempts have been made to re-establish a carbonate extraction protocol in yeast based on Eckers *et al.* (2013), but without providing reliable data. An authentic nominee for the structure in question might be the KISS domain, which comprises almost 200 amino acids of unknown activity and is not present in any Erv homologue of other eukaryotic classes (Eckers *et al.*, 2013). The absence of a dominant negative effect of this domain in yeast (see complementation assays 3.1.1) further supports this hypothesis and would explain its membrane-association in yeast mitochondria. A second structure that should be considered is residue C17. The cysteine residue may interrupt the interaction between *Lt*Erv and *Sc*Mia40 because it instead interacts with a membrane receptor that adheres the protein within the IMS. One way or another, C17 seems to be involved in the mitochondrial localisation of the protist protein, as discusses earlier. The final clue to explain the unusual membrane association of *Lt*Erv could be provided by an investigation of the interaction between the protein and the membrane. Apart from the presence of a membrane bound import receptor, also a protein-lipid interaction might be plausible. This can be tested by protein-lipid overlay assays using commercial lipid strips as well as liposome flotation assays (Connerth *et al.*, 2012).

In conclusion, the data obtained from this study do not yet explain in detail how *Lt*Erv is imported into leishmania and yeast mitochondria but give first indications. Data in yeast suggest that residue C17 initiates a Mia40-independent import route. Thereby, the residue may cause *Lt*Erv import as a class III IMS protein that associates with a binding site, possibly at the outer mitochondrial membrane. This pathway may import the wildtype *Lt*Erv into both yeast and leishmania mitochondria. However, when the clamp residue is exchanged, the protein most likely interacts with Mia40 and might be imported into yeast mitochondria via the classical oxidative folding pathway. In this case, the structural cysteine pair in *Lt*Erv might be crucial to form a transient mixed disulphide intermediate with *Sc*Mia40 as explained for the import of the endogenous yeast homologue.

4.3 The quest of the holy Grail - or a Mia40 adapter replacement

Mia40 was reported to be widely conserved with homologues in at least three eukaryotic supergroups (Allen *et al.*, 2008). However, the nuclear genome of certain protists, such as apicomplexan parasites and trypanosomatids, appear to lack a Mia40 homologue. The conservation of only one key component of the MIA pathway gave rise to many fundamental questions: How are cysteine-rich proteins imported in these protist groups? Is the oxidative folding pathway conserved or are the proteins imported differently? Is there a Mia40 replacement or is Erv working alone? What is the function of Erv if not oxidizing Mia40?

Without Mia40, there are three apparent possibilities how cysteine-rich proteins can be transported into mitochondria. (I) The Erv homologue is directly interacting with the substrates and does not

require a partner protein. (II) An unknown component replaces Mia40 in its position or (III) the substrates are imported in a completely different pathway. If the parasite's Erv is actually working alone, as claimed by Haindrich *et al.* (2017) and others, it should be able to directly interact and oxidize substrates of the oxidative folding pathway. In other words, it should be capable to perform Mia40 activities in a yeast model (Figure 3.5), as shown before for human CHCHD4 (Chacinska *et al.*, 2008). Since this is not the case and a variety of protist constructs failed to replace *Sc*Mia40, even though import signals were found to be evolutionary conserved (Eckers *et al.*, 2012), it is highly doubtful whether the oxidative folding system in protists consists of a single protein. This recognition is further supported by the findings of Basu *et al.* (2013), who reported that *Tb*Erv1 cannot oxidize or fold small Tim9. However, when *Tb*Erv1 was downregulated, Tim9 protein levels in the IMS gradually decreased while non-substrate protein levels were unchanged (Peikert *et al.*, 2017). This means that the kinetoplastid Erv is definitely involved in the import pathway of cysteine-containing proteins but probably depends on a partner protein.

The identification and characterisation of such a Mia40 adapter replacement was the major aim of an extensive study by Linda Liedgens (2018). Unfortunately, all strategies for the pull-down and chemical trapping of a mixed disulphide intermediate between the unknown component and the model substrate small Tim1 or the partner *Lt*Erv were unsuccessful. While Erv did not reveal any interaction partner, attempts from the substrate side were more promising but the low molecular weight and the high hydrophobicity of the protein caused problems on SDS-PAGE and western blot analysis. To overcome these problems, new substrates were carefully selected from a list of proteins, which were reduced in abundance in consequence of a RNAi-induced *Tb*Erv1 knock-down (Peikert *et al.*, 2017). Among others, a protein classified as "substrate 2" was amplified from *L. tarentolae* gDNA as an orthologue of the *T. brucei* protein Tb927.10.4280. It harbored two cysteines in a non-conserved single $Cx_{11}C$ motif and with a sequence similarity of 94 % to *T. theileri* and *T. grayi,* it presented a putative subunit of the ETC complex III. The substrate was overexpressed from a vector in *L. tarentolae* and the mixed disulphide interaction with a putative Mia40 replacement was captured by the permanent blockage of free thiols with NEM (Figure 3.12). The small alkylating reagent is thought to diffuse through the intact cell and preserve the physiological redox state by preventing artificial thiol oxidation after cellular disruption. In addition, a stable mixed disulphide was potentially generated by mutating one of the cysteine residues in the substrate, as commonly done in the analysis of disulphides (Hansen and Winther, 2009; Engelhard *et al.*, 2011; Heckler *et al.*, 2013; Mermelekas *et al.*, 2013; Rudyk and Eaton, 2014; Nakao *et al.*, 2015; Wojdyla and Rogowska-Wrzesinska, 2015). Adducts of about 34 kDa, 50 kDa and 60 kDa were detected in the higher molecular range of substrate 2 C105S when analysed under non-reducing conditions. This indicated the binding of a potential interaction partner with a molecular mass of 6 kDa, 22 kDa or 32 kDa, respectively. Since the IMS typically house molecules of

low molecular mass, often between seven and 15 kDa, it is quite plausible that the Mia40 replacement ranks in this size (Herrmann and Hell, 2005). Alternatively, the 60-kDa-band might correspond to a dimeric substrate conformation as shown previously for *Sc*Erv1 and *Lt*Erv, respectively (Terziyska *et al.*, 2009; Eckers *et al.*, 2013). Visible intermediates were absent in cell lysates containing wildtype substrate 2 or the C117S mutant. This suggests a function for residue C105 interacting with the Mia40 replacement whereas residue C117 might be unable to form mixed disulphides and may act as the resolving cysteine yielding an intramolecular disulphide (Nakao *et al.*, 2015). When the mutant constructs were analysed for their interaction with *Lt*Erv, a potential mixed disulphide was also found at 50 kDa. This might imply a direct interaction between *Lt*Erv and the substrate or represent non-identical redox partners. What this means to the oxidative folding pathway in early eukaryotes and which potential mixed disulphide might actually contain the desired Mia40 replacement is hard to interpret at this stage. However, previously established protocols for the endogenous disulphide trapping in *L. tarentolae* delivered promising results that together with the thoughtful chosen substrates may be indeed powerful enough to capture a potential Mia40 replacement. In the following steps, the correct intermediate has to be enriched and *de novo* purified before analysis by mass spectrometry can specify the potential Mia40 replacement candidate. As no fully defined medium is available to proper cultivate *L. tarentolae*, a stable isotope labelling of amino acids in cell culture (SILAC) is not possible (Liedgens, 2018). Hence, His-tagged and untagged import substrates were generated to discriminate between unspecific bindings and actual interaction partners (Dabir *et al.*, 2007).

However, it is conceivable that the replacement candidate does not bind covalently to the substrates via disulphide bridges but functions more as a *trans* side import receptor. This import option has already been discussed for *Lt*Erv above and is further supported by observations of the redox-inactive Mia40-SPS mutant in yeast (Peleh *et al.*, 2016). The authors demonstrated a Mia40-depleted strain where protein levels of Mia40 substrates were partially restored by expression of a Mia40 mutant lacking the redox-active cysteines. Instead of forming a disulphide intermediate, substrates were tightly associated to the binding pocket, which delayed but allowed a CPC-independent oxidation process. If such an interaction is present also in *Kinetoplastida* and *Apicomplexa*, the receptor could easily have been missed by the applied redox trapping methods. Another interesting phenomenon that might match this hypothesis concerns the hyperactive phenotype of *Leishmania* cells expressing the redox-inactive Mia40 (Figure 3.13). In contrast to wildtype Mia40, Mia40-SPS may be functional in *Leishmania* importing proteins via the hydrophobic binding site. Since Mia40-SPS is co-expressed with the endogenous import receptor, protein import may be intensified leading to either higher protein levels, as shown for yeast cells overexpressing *Sc*Mia40 (Terziyska *et al.*, 2005; Longen *et al.*, 2014; Peleh *et al.*, 2016), or to more efficient protein processing and localisation, as claimed by Wrobel *et al.*

(2015). In yeast and mammalian systems it has been demonstrated that more proteins are synthesised in the cytosol as actually imported into mitochondria (Fischer *et al.*, 2013; Longen *et al.*, 2014). What is more, a thyroid hormone-induced upregulation of the mitochondrial import rate in the cardiac muscle was suggested to correlate with alterations of the mitochondrial volume fraction and the area of cristae (Craig *et al.*, 1998; Colavecchia *et al.*, 2003). The observed hyperactive phenotype might therefore be connected to a boost in metabolism or other cell functions in *Leishmania*, allowing certain processes to take place more quickly. However, neither the import and correct localisation of both the *Sc*Mia40 constructs into leishmania mitochondria nor the actual increased protein levels have been tested so far. Furthermore, the growth of transgenic cell lines was analysed under G418 selection pressure while the control strain did not contain a resistance cassette and was analysed in marker free medium. For that reason, it cannot be completely excluded that the selection pressure influenced the phenotype of the transgenic parasites.

Notably, *Sc*Mia40 was expressed in leishmania cells but remained in a partially reduced redox state (oxidized Cx_9C but reduced CPC motif) (Figure 3.14). I conclude from this, that the protein is not active in these cells. It was previously found that endogenous *Sc*Mia40 was oxidized to 70-80 % to be functional, which is regulated in the IMS by Erv1 and glutathione (Kojer *et al.*, 2012). A similar scenario was described for human CHCHD4 (Erdogan *et al.*, 2018), which implies a non-redox-regulated import receptor or inadequate systems for the oxidation of this yeast protein in *L. tarentolae* mitochondria. If the Mia40 replacement does not simultaneously import and oxidize substrates in a disulphide exchange reaction but rather imports and folds substrates as a *trans* side receptor without a mixed disulphide intermediate, how are the substrates oxidized (see Figure 4.1)? I have discussed earlier that protist Erv has to be involved in the protein import, since mitochondrial substrate levels were negatively affected upon *Tb*Erv1 downregulation (Peikert *et al.*, 2017). Nevertheless, *Lt*Erv could not functionally complement for *Sc*Mi40 in yeast (Figure 3.5). However, I did not test whether *Lt*Erv can oxidize Mia40 substrates when they have previously been imported by the hydrophobic binding cleft of the *Sc*Mia40-SPS mutant, as demonstrated for *At*Erv1 (Peleh *et al.*, 2017). Additionally, the recently identified thioredoxins and glutaredoxins in the IMS may be scavenge the excess of electrons after substrate oxidation (Vogtle *et al.*, 2012; Kojer *et al.*, 2015). Once it was postulated that in the course of evolution, higher eukaryotes have supplanted the thioredoxin-based oxidation system of the bacterial periplasm by the superior MIA40 machinery (Peleh *et al.*, 2016). Based on this consideration, “primitive” eukaryotes that do not have Mia40 could still be, at least in part, dependent on the ancestor’s system.

In summary, the oxidative folding system of early eukaryotes is still puzzling because important components are absent or altered in such a way that they are no longer recognizable. Nevertheless, the import pathway seems to be conserved with Erv as central component that is conditional to some

kind of Mia40 replacement. If this replacement represents a redox-active protein or a receptor has to be examined in the future. New exciting perspectives might also be gathered with an oxidation assay that analyses the relevance of an oxidative process for protein import under physiological conditions (Fischer *et al.*, 2013; Kojer *et al.*, 2015; Peleh *et al.*, 2016). Complementation assays with a Δ*scmia40* strain co-expressing protist Erv and the redox-inactive Mia40-SPS might be interesting to explain the task of Erv as a substrate oxidase in more detail. Finally, the *L. tarentolae* strains expressing wildtype and mutant *Sc*Mia40 can be observed more closely to characterise the observed putative hyperactive phenotype and to explain how Mia40-SPS functions in *Leishmania* mitochondria.

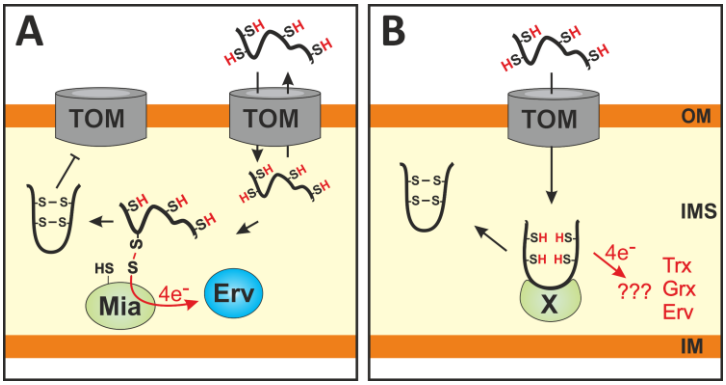

Figure 4.1 | Schematic representation of the "folding trap" and the *trans* side receptor models. (A) According to the folding trap mechanism reduced substrates are unfolded and translocated in and out of the intermembrane space (IMS) until they are oxidized and folded by Mia40. Mia40 subsequently interacts with Erv1 to transfer the electrons (e^-). **(B)** In the *trans* side receptor model, import is driven by the substrate affinity of the receptor. In case of Mia40, the substrates are subsequently oxidized and released in a folded state as shown in A. Without a redox-active cysteine, another electron receptor has to be involved. Figure was modified from Peleh *et al.* (2016).

4.4 The physiological relevance of protist Erv homologues

Chromosomal *PFERV* was impossible to delete in a primal strategy whereas the MIA substrate small Tim13 was most likely removed from the chromosome (Figure 3.11). Analytical PCRs have to be performed to verify a Δ*pftim13* strain before assessing whether *PFERV* could not be knocked out for technical or functional reasons. Either way, the protein is suspected to be essential since the Erv homologues of the parasites *L. infantum* and *T. brucei* were discovered as indispensable alongside those of fungi and mammals (Basu *et al.*, 2013; Haindrich *et al.*, 2017; Peikert *et al.*, 2017; Specht *et al.*, 2018).

In order to obtain a viable Δ*pferv* strain, I have cloned a rescue plasmid expressing a *PFERV* variant having three mismatches close to the PAM sequence to interfere with the Cas9 activity (Cong *et al.*, 2013; Hsu *et al.*, 2013; Sternberg *et al.*, 2014; Stemmer *et al.*, 2015). Chromosomal *PFERV* should be knocked-out, while the episomal copy ensures parasite's survival. In the subsequent experiments,

parasites will be either co-transfected with both the pL7 knock-out and the pHBIRH rescue plasmid or exclusively with pL7. I expect viable cells for the co-transfectants but not for the control.

Apart from its participation in the oxidative folding pathway, the protist Erv was suggested to be involved in many processes of the cell, including the maintenance of mitochondrial morphology and the export and assembly of iron sulphur clusters in the cytosol (Basu *et al.*, 2013; Basu *et al.*, 2014; Haindrich *et al.*, 2017). This might point to the physiological importance of the protein even when not oxidizing Mia40. As parasites become increasingly resistant to currently used medication, effective treatment relies on the constant exploration of new potential drug targets (WHO, 2012b, 2014). The mitochondrial import machinery comprises many essential components whose interference can have fatal consequences for the parasite (Mather *et al.*, 2007; Vaidya and Mather, 2009). In particular the essential MIA pathway exhibits particularities that differ significantly to the human system and might therefore be an excellent candidate target for drug development.

5 Conclusion

In this thesis, I analysed structure-function relationships of the protist sulfhydryl electron transferase *Lt*Erv to frame a clearer picture of the oxidative protein folding pathway in the IMS without Mia40. By understanding this "primitive" import route, valuable drug target candidates may be described, and the evolutionary development of the mitochondrial protein import system can be tracked from the roots.

*Lt*Erv consists of an amino terminal flavodomain as well as a carboxyl terminal KISS domain and encompass seven cysteine residues that form up to three intramolecular disulphide bonds (Figure 5.1). The N-terminal C17 has shown to be the main reason why the parasite Erv cannot replace the yeast homologue in its function. However, the disturbing effect can be overcome by extending the protein N-terminally by the yeast shuttle arm (Figure 5.1A) or by exchanging the cysteine residue for a serine (Figure 5.1B). Although the shuttle cysteine pair of the *Leishmania* protein differs in motif and localisation from the homologue in yeast, it can accomplish the yeast function (Figure 5.1C). Both the C-terminal shuttle cysteine pair (Figure 5.1E) and the disulphide bond in the active site (Figure 5.1H) are responsible for the oxidoreductase activity of the protein (Eckers *et al.*, 2013). By disrupting any of these redox-active cysteine motifs, the *Lt*Erv^{C17S} mutant can no longer complement for *Sc*Erv1. The structural cysteine pair is most likely responsible for intramolecular stability and might mediate a Mia40-depended import into yeast mitochondria when C17 is removed (Figure 5.1D). Even though the KISS domain is restricted to *Kinetoplastida*, it did not negatively influence the proteins' function in yeast (Figure 5.1F). On the contrary, it rather supported the parasite's flavodomain in complementation assays and did not distract the flavodomain of yeast (Figure 5.1G).

Both the KISS domain and residue C17 have assignments in the parasite protein that have not yet been fully understood. They might induce the special membrane association that imports and traps the protein in the IMS. If this import is driven by a conserved receptor or by a special protein-lipid interaction has not yet been investigated. It is however tempting to speculate that C17 interrupts the interaction with *Sc*Mia40 in yeast because it instead initiates a different import pathway via membrane association. With certainty, neither of the two structures exert full *Sc*Mia40 activity and accordingly represent no Mia40 replacement.

Since *Lt*Erv is unable to import MIA substrates on its own, there should be some kind of Mia40 replacement in parasitic protists. The most obvious scenario would be a redox-enzyme that imports and oxidizes cysteine-containing substrates in analogy to *Sc*Mia40 and subsequently interacts with *Lt*Erv to pass the received electrons to the ETC. Alternatively, an ancient Mia40 may be a simple *trans* side receptor that has no redox activity, but controls substrate import through hydrophobic binding (Figure 4.1). To do so, it requires additional assistance from redox proteins, such as thioredoxins,

glutaredoxins and maybe even Erv to oxidize and fold the substrates after their translocation. The oxidative folding pathway in protists may therefore reflect a scenario that is in between the ancient bacterial system and the superior MIA40 machinery of opisthokonts. So instead of a stepwise model, where early eukaryotes have no Mia40 at all, as it is often postulated (Allen *et al.*, 2008; Carrie and Soll, 2017; Peleh *et al.*, 2017), there may be a primitive Mia40 replacement with a receptor function.

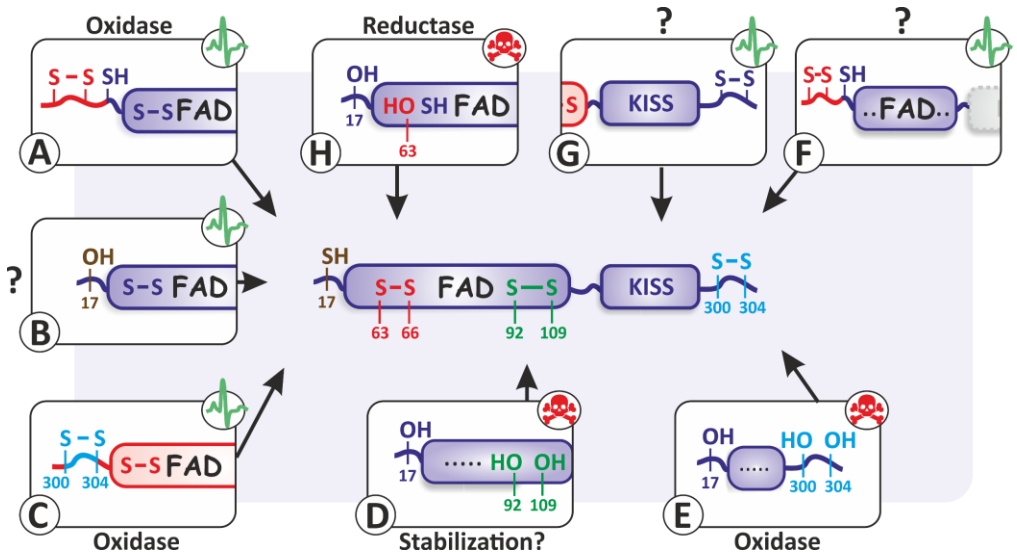

Figure 5.1 | Schematic summary of structure-function relationships of *Lt*Erv. The boxes show mutant or chimeric *Lt*Erv properties that have been tested in a yeast Δ*erv1* strain. **(A)** N-terminal extension with the yeast shuttle arm. **(B)** Mutation of C17 to serine. **(C)** Replacement of the yeast shuttle cysteine motif by the parasite motif. **(D)** Double mutation of C17 and the structural disulphide bond. **(E)** Double mutation of C17 and the shuttle cysteine pair. **(F)** Truncation of the KISS domain while the protein is extended by the yeast shuttle arm. **(G)** Influence of the KISS domain in the yeast protein. **(H)** Double mutation of C17 and the disulphide of the active site. Alterations in the protein that produced viable yeast cells are symbolised with a green pulse sign while red skulls mark the opposite. Know functions of the respective properties and indicated. Big question marks symbolise unknown function.

6 References

ABRAHAMSEN, M. S., TEMPLETON, T. J., ENOMOTO, S., ABRAHANTE, J. E., ZHU, G., LANCTO, C. A., DENG, M., LIU, C., WIDMER, G., TZIPORI, S., BUCK, G. A., XU, P., BANKIER, A. T., DEAR, P. H., KONFORTOV, B. A., SPRIGGS, H. F., IYER, L., ANANTHARAMAN, V., ARAVIND, L. & KAPUR, V. (2004): Complete genome sequence of the apicomplexan, Cryptosporidium parvum. *Science,* 304**,** 441-5.

ADEVA-ANDANY, M. M., CARNEIRO-FREIRE, N., SECO-FILGUEIRA, M., FERNANDEZ-FERNANDEZ, C. & MOURINO-BAYOLO, D. (2018): Mitochondrial beta-oxidation of saturated fatty acids in humans. *Mitochondrion*.

ADL, S. M., SIMPSON, A. G., FARMER, M. A., ANDERSEN, R. A., ANDERSON, O. R., BARTA, J. R., BOWSER, S. S., BRUGEROLLE, G., FENSOME, R. A., FREDERICQ, S., JAMES, T. Y., KARPOV, S., KUGRENS, P., KRUG, J., LANE, C. E., LEWIS, L. A., LODGE, J., LYNN, D. H., MANN, D. G., MCCOURT, R. M., MENDOZA, L., MOESTRUP, O., MOZLEY-STANDRIDGE, S. E., NERAD, T. A., SHEARER, C. A., SMIRNOV, A. V., SPIEGEL, F. W. & TAYLOR, M. F. (2005): The new higher level classification of eukaryotes with emphasis on the taxonomy of protists. *J Eukaryot Microbiol,* 52**,** 399-451.

ADL, S. M., SIMPSON, A. G., LANE, C. E., LUKES, J., BASS, D., BOWSER, S. S., BROWN, M. W., BURKI, F., DUNTHORN, M., HAMPL, V., HEISS, A., HOPPENRATH, M., LARA, E., LE GALL, L., LYNN, D. H., MCMANUS, H., MITCHELL, E. A., MOZLEY-STANRIDGE, S. E., PARFREY, L. W., PAWLOWSKI, J., RUECKERT, S., SHADWICK, L., SCHOCH, C. L., SMIRNOV, A. & SPIEGEL, F. W. (2012): The revised classification of eukaryotes. *J Eukaryot Microbiol,* 59**,** 429-93.

AKHOUNDI, M., KUHLS, K., CANNET, A., VOTYPKA, J., MARTY, P., DELAUNAY, P. & SERENO, D. (2016): A Historical Overview of the Classification, Evolution, and Dispersion of Leishmania Parasites and Sandflies. *PLoS Negl Trop Dis,* 10**,** e0004349.

ALLEN, J. W., FERGUSON, S. J. & GINGER, M. L. (2008): Distinctive biochemistry in the trypanosome mitochondrial intermembrane space suggests a model for stepwise evolution of the MIA pathway for import of cysteine-rich proteins. *FEBS Lett,* 582**,** 2817-25.

ALLEN, S., BALABANIDOU, V., SIDERIS, D. P., LISOWSKY, T. & TOKATLIDIS, K. (2005): Erv1 mediates the Mia40-dependent protein import pathway and provides a functional link to the respiratory chain by shuttling electrons to cytochrome c. *J Mol Biol,* 353**,** 937-44.

ALLEN, S., LU, H., THORNTON, D. & TOKATLIDIS, K. (2003): Juxtaposition of the two distal CX3C motifs via intrachain disulfide bonding is essential for the folding of Tim10. *J Biol Chem,* 278**,** 38505-13.

ANDREWS, K. T., FISHER, G. & SKINNER-ADAMS, T. S. (2014): Drug repurposing and human parasitic protozoan diseases. *Int J Parasitol Drugs Drug Resist,* 4**,** 95-111.

ANG, S. K. & LU, H. (2009): Deciphering structural and functional roles of individual disulfide bonds of the mitochondrial sulfhydryl oxidase Erv1p. *J Biol Chem,* 284**,** 28754-61.

ANG, S. K., ZHANG, M., LODI, T. & LU, H. (2014): Mitochondrial thiol oxidase Erv1: both shuttle cysteine residues are required for its function with distinct roles. *Biochem J,* 460**,** 199-210.

ARCHIBALD, J. M. (2015): Endosymbiosis and Eukaryotic Cell Evolution. *Curr Biol,* 25**,** R911-21.

ASHFORD, R. W. (2000): The leishmaniases as emerging and reemerging zoonoses. *Int J Parasitol,* 30**,** 1269-81.

ATAMNA, H. (2004): Heme, iron, and the mitochondrial decay of ageing. *Ageing Res Rev,* 3**,** 303-18.

BANCI, L., BERTINI, I., CALDERONE, V., CEFARO, C., CIOFI-BAFFONI, S., GALLO, A., KALLERGI, E., LIONAKI, E., POZIDIS, C. & TOKATLIDIS, K. (2011): Molecular recognition and substrate mimicry drive the electron-transfer process between MIA40 and ALR. *Proc Natl Acad Sci U S A,* 108**,** 4811-6.

BANCI, L., BERTINI, I., CEFARO, C., CIOFI-BAFFONI, S., GALLO, A., MARTINELLI, M., SIDERIS, D. P., KATRAKILI, N. & TOKATLIDIS, K. (2009): MIA40 is an oxidoreductase that catalyzes oxidative protein folding in mitochondria. *Nat Struct Mol Biol,* 16**,** 198-206.

BANNISTER, L. & MITCHELL, G. (2003): The ins, outs and roundabouts of malaria. *Trends Parasitol,* 19**,** 209-13.

BANNISTER, L. H., HOPKINS, J. M., FOWLER, R. E., KRISHNA, S. & MITCHELL, G. H. (2000): A brief illustrated guide to the ultrastructure of Plasmodium falciparum asexual blood stages. *Parasitol Today,* 16**,** 427-33.

BASU, S., LEONARD, J. C., DESAI, N., MAVRIDOU, D. A., TANG, K. H., GODDARD, A. D., GINGER, M. L., LUKES, J. & ALLEN, J. W. (2013): Divergence of Erv1-associated mitochondrial import and export pathways in trypanosomes and anaerobic protists. *Eukaryot Cell,* 12**,** 343-55.

BASU, S., NETZ, D. J., HAINDRICH, A. C., HERLERTH, N., LAGNY, T. J., PIERIK, A. J., LILL, R. & LUKES, J. (2014): Cytosolic iron-sulphur protein assembly is functionally conserved and essential in procyclic and bloodstream Trypanosoma brucei. *Mol Microbiol,* 93**,** 897-910.

BATES, P. A. (2007): Transmission of Leishmania metacyclic promastigotes by phlebotomine sand flies. *Int J Parasitol,* 37**,** 1097-106.

BATES, P. A. & ROGERS, M. E. (2004): New insights into the developmental biology and transmission mechanisms of Leishmania. *Curr Mol Med,* 4**,** 601-9.

BECHER, D., KRICKE, J., STEIN, G. & LISOWSKY, T. (1999): A mutant for the yeast scERV1 gene displays a new defect in mitochondrial morphology and distribution. *Yeast,* 15**,** 1171-81.

BERGMAN, L. W. (2001): Growth and maintenance of yeast. *Methods Mol Biol,* 177**,** 9-14.

BEVERLEY, S. M. & CLAYTON, C. E. (1993): Transfection of Leishmania and Trypanosoma brucei by electroporation. *Methods Mol Biol,* 21**,** 333-48.

BIAGINI, G. A., FISHER, N., SHONE, A. E., MUBARAKI, M. A., SRIVASTAVA, A., HILL, A., ANTOINE, T., WARMAN, A. J., DAVIES, J., PIDATHALA, C., AMEWU, R. K., LEUNG, S. C., SHARMA, R., GIBBONS, P., HONG, D. W., PACOREL, B., LAWRENSON, A. S., CHAROENSUTTHIVARAKUL, S., TAYLOR, L., BERGER, O., MBEKEANI, A., STOCKS, P. A., NIXON, G. L., CHADWICK, J., HEMINGWAY, J., DELVES, M. J., SINDEN, R. E., ZEEMAN, A. M., KOCKEN, C. H., BERRY, N. G., O'NEILL, P. M. & WARD, S. A. (2012): Generation of quinolone antimalarials targeting the Plasmodium falciparum mitochondrial respiratory chain for the treatment and prophylaxis of malaria. *Proc Natl Acad Sci U S A,* 109**,** 8298-303.

BIAGINI, G. A., VIRIYAVEJAKUL, P., O'NEILL P, M., BRAY, P. G. & WARD, S. A. (2006): Functional characterization and target validation of alternative complex I of Plasmodium falciparum mitochondria. *Antimicrob Agents Chemother,* 50**,** 1841-51.

BIEN, M., LONGEN, S., WAGENER, N., CHWALLA, I., HERRMANN, J. M. & RIEMER, J. (2010): Mitochondrial disulfide bond formation is driven by intersubunit electron transfer in Erv1 and proofread by glutathione. *Mol Cell,* 37**,** 516-28.

BIHLMAIER, K., MESECKE, N., TERZIYSKA, N., BIEN, M., HELL, K. & HERRMANN, J. M. (2007): The disulfide relay system of mitochondria is connected to the respiratory chain. *J Cell Biol,* 179**,** 389-95.

BIRNBOIM, H. C. & DOLY, J. (1979): A rapid alkaline extraction procedure for screening recombinant plasmid DNA. *Nucleic Acids Res,* 7**,** 1513-23.

BOLDOGH, I. R. & PON, L. A. (2006): Interactions of mitochondria with the actin cytoskeleton. *Biochim Biophys Acta,* 1763**,** 450-62.

BRADFORD, M. M. (1976): A rapid and sensitive method for the quantitation of microgram quantities of protein utilizing the principle of protein-dye binding. *Anal Biochem,* 72**,** 248-54.

BRIX, J., DIETMEIER, K. & PFANNER, N. (1997): Differential recognition of preproteins by the purified cytosolic domains of the mitochondrial import receptors Tom20, Tom22, and Tom70. *J Biol Chem,* 272**,** 20730-5.

BURGESS, S. L., GILCHRIST, C. A., LYNN, T. C. & PETRI, W. A., JR. (2017): Parasitic Protozoa and Interactions with the Host Intestinal Microbiota. *Infect Immun,* 85.

BUSCHER, P., CECCHI, G., JAMONNEAU, V. & PRIOTTO, G. (2017): Human African trypanosomiasis. *Lancet,* 390**,** 2397-2409.

CABIBBO, A., PAGANI, M., FABBRI, M., ROCCHI, M., FARMERY, M. R., BULLEID, N. J. & SITIA, R. (2000): ERO1-L, a human protein that favors disulfide bond formation in the endoplasmic reticulum. *J Biol Chem,* 275**,** 4827-33.

CARRIE, C., GIRAUD, E., DUNCAN, O., XU, L., WANG, Y., HUANG, S., CLIFTON, R., MURCHA, M., FILIPOVSKA, A., RACKHAM, O., VRIELINK, A. & WHELAN, J. (2010): Conserved and novel functions for Arabidopsis thaliana MIA40 in assembly of proteins in mitochondria and peroxisomes. *J Biol Chem,* 285**,** 36138-48.

CARRIE, C. & SOLL, J. (2017): To Mia or not to Mia: stepwise evolution of the mitochondrial intermembrane space disulfide relay. *BMC Biol,* 15**,** 119.

CASTRO, H., ROMAO, S., GADELHA, F. R. & TOMAS, A. M. (2008): Leishmania infantum: provision of reducing equivalents to the mitochondrial tryparedoxin/tryparedoxin peroxidase system. *Exp Parasitol,* 120**,** 421-3.

CDC. 2015. *Malaria* [Online]. Centers for Disease Control and Prevention. Available: https://www.cdc.gov/malaria/about/disease.html [Accessed August 28, 2018].

CHACINSKA, A., GUIARD, B., MULLER, J. M., SCHULZE-SPECKING, A., GABRIEL, K., KUTIK, S. & PFANNER, N. (2008): Mitochondrial biogenesis, switching the sorting pathway of the intermembrane space receptor Mia40. *J Biol Chem,* 283**,** 29723-9.

CHACINSKA, A., KOEHLER, C. M., MILENKOVIC, D., LITHGOW, T. & PFANNER, N. (2009): Importing mitochondrial proteins: machineries and mechanisms. *Cell,* 138**,** 628-44.

CHACINSKA, A., LIND, M., FRAZIER, A. E., DUDEK, J., MEISINGER, C., GEISSLER, A., SICKMANN, A., MEYER, H. E., TRUSCOTT, K. N., GUIARD, B., PFANNER, N. & REHLING, P. (2005): Mitochondrial presequence translocase: switching between TOM tethering and motor recruitment involves Tim21 and Tim17. *Cell,* 120**,** 817-29.

CHACINSKA, A., PFANNSCHMIDT, S., WIEDEMANN, N., KOZJAK, V., SANJUAN SZKLARZ, L. K., SCHULZE-SPECKING, A., TRUSCOTT, K. N., GUIARD, B., MEISINGER, C. & PFANNER, N. (2004): Essential role of Mia40 in import and assembly of mitochondrial intermembrane space proteins. *Embo j,* 23**,** 3735-46.

CHAN, D., FRANK, S. & ROJO, M. (2006): Mitochondrial dynamics in cell life and death. *Cell Death Differ,* 13**,** 680-4.

CHAUDHARY, K. & ROOS, D. S. (2005): Protozoan genomics for drug discovery. *Nat Biotechnol,* 23**,** 1089-91.

COLAVECCHIA, M., CHRISTIE, L. N., KANWAR, Y. S. & HOOD, D. A. (2003): Functional consequences of thyroid hormone-induced changes in the mitochondrial protein import pathway. *Am J Physiol Endocrinol Metab,* 284**,** E29-35.

CONG, L., RAN, F. A., COX, D., LIN, S., BARRETTO, R., HABIB, N., HSU, P. D., WU, X., JIANG, W., MARRAFFINI, L. A. & ZHANG, F. (2013): Multiplex genome engineering using CRISPR/Cas systems. *Science,* 339**,** 819-23.

CONNERTH, M., TATSUTA, T., HAAG, M., KLECKER, T., WESTERMANN, B. & LANGER, T. (2012): Intramitochondrial transport of phosphatidic acid in yeast by a lipid transfer protein. *Science,* 338**,** 815-8.

COPPOCK, D. L. & THORPE, C. (2006): Multidomain flavin-dependent sulfhydryl oxidases. *Antioxid Redox Signal,* 8**,** 300-11.

CORDEIRO, C. & FREIRE, A. P. (1995): Digitonin permeabilization of Saccharomyces cerevisiae cells for in situ enzyme assay. *Anal Biochem,* 229**,** 145-8.

COWMAN, A. F., HEALER, J., MARAPANA, D. & MARSH, K. (2016): Malaria: Biology and Disease. *Cell,* 167**,** 610-624.

COX, F. E. (2002): Systematics of the parasitic Protozoa. *Trends Parasitol,* 18**,** 108.

CRAIG, E. E., CHESLEY, A. & HOOD, D. A. (1998): Thyroid hormone modifies mitochondrial phenotype by increasing protein import without altering degradation. *Am J Physiol,* 275**,** C1508-15.

CROSS, G. A. (2005): Trypanosomes at the gates. *Science,* 309**,** 355.

DABIR, D. V., LEVERICH, E. P., KIM, S. K., TSAI, F. D., HIRASAWA, M., KNAFF, D. B. & KOEHLER, C. M. (2007): A role for cytochrome c and cytochrome c peroxidase in electron shuttling from Erv1. *Embo j,* 26**,** 4801-11.

DAITHANKAR, V. N., FARRELL, S. R. & THORPE, C. (2009): Augmenter of liver regeneration: substrate specificity of a flavin-dependent oxidoreductase from the mitochondrial intermembrane space. *Biochemistry,* 48**,** 4828-37.

DE SOUZA, W., ATTIAS, M. & RODRIGUES, J. C. (2009): Particularities of mitochondrial structure in parasitic protists (Apicomplexa and Kinetoplastida). *Int J Biochem Cell Biol,* 41**,** 2069-80.

DE SOUZA, W., DE CARVALHO, T. U. & BARRIAS, E. S. 2017. Ultrastructure of Trypanosoma cruzi and its interaction with host cells. *American Trypanosomiasis Chagas Disease.* Elsevier.

DE STEFANI, D., RAFFAELLO, A., TEARDO, E., SZABO, I. & RIZZUTO, R. (2011): A forty-kilodalton protein of the inner membrane is the mitochondrial calcium uniporter. *Nature,* 476**,** 336-40.

DEITSCH, K., DRISKILL, C. & WELLEMS, T. (2001): Transformation of malaria parasites by the spontaneous uptake and expression of DNA from human erythrocytes. *Nucleic Acids Res,* 29**,** 850-3.

DEPONTE, M. 2013. Mitochondrial Protein Import in Malaria Parasites. *In:* HOMMEL, M. & KREMSNER, P. G. (eds.) *Encyclopedia of Malaria.* New York, NY: Springer New York.

DEPONTE, M. & HELL, K. (2009): Disulphide bond formation in the intermembrane space of mitochondria. *J Biochem,* 146**,** 599-608.

DEPONTE, M., HOPPE, H. C., LEE, M. C., MAIER, A. G., RICHARD, D., RUG, M., SPIELMANN, T. & PRZYBORSKI, J. M. (2012): Wherever I may roam: protein and membrane trafficking in P. falciparum-infected red blood cells. *Mol Biochem Parasitol,* 186**,** 95-116.

DHANGADAMAJHI, G., KAR, S. K. & RANJIT, M. (2010): The survival strategies of malaria parasite in the red blood cell and host cell polymorphisms. *Malar Res Treat,* 2010**,** 973094.

DIMMER, K. S. & RAPAPORT, D. (2012): Unresolved mysteries in the biogenesis of mitochondrial membrane proteins. *Biochim Biophys Acta,* 1818**,** 1085-90.

DOLEZAL, P., DAGLEY, M. J., KONO, M., WOLYNEC, P., LIKIC, V. A., FOO, J. H., SEDINOVA, M., TACHEZY, J., BACHMANN, A., BRUCHHAUS, I. & LITHGOW, T. (2010): The essentials of protein import in the degenerate mitochondrion of Entamoeba histolytica. *PLoS Pathog,* 6**,** e1000812.

DUDEK, J., REHLING, P. & VAN DER LAAN, M. (2013): Mitochondrial protein import: common principles and physiological networks. *Biochim Biophys Acta,* 1833**,** 274-85.

ECKERS, E. 2012. *Mitochondrialer Proteintransport in Leishmania tarentolae und Charakterisierung der Hefeglutaredoxine 6-8.* Doctor of Natural Sciences Dissertation, Ludwig Maximilians University Munich

ECKERS, E., CYRKLAFF, M., SIMPSON, L. & DEPONTE, M. (2012): Mitochondrial protein import pathways are functionally conserved among eukaryotes despite compositional diversity of the import machineries. *Biol Chem,* 393**,** 513-24.

ECKERS, E., PETRUNGARO, C., GROSS, D., RIEMER, J., HELL, K. & DEPONTE, M. (2013): Divergent molecular evolution of the mitochondrial sulfhydryl:cytochrome C oxidoreductase Erv in opisthokonts and parasitic protists. *J Biol Chem,* 288**,** 2676-88.

ENDO, T. & YAMANO, K. (2009): Multiple pathways for mitochondrial protein traffic. *Biol Chem,* 390**,** 723-30.

ENGELHARD, J., CHRISTIAN, B. E., WEINGARTEN, L., KUNTZ, G., SPREMULLI, L. L. & DICK, T. P. (2011): In situ kinetic trapping reveals a fingerprint of reversible protein thiol oxidation in the mitochondrial matrix. *Free Radic Biol Med,* 50**,** 1234-41.

ERDOGAN, A. J., ALI, M., HABICH, M., SALSCHEIDER, S. L., SCHU, L., PETRUNGARO, C., THOMAS, L. W., ASHCROFT, M., LEICHERT, L. I., ROMA, L. P. & RIEMER, J. (2018): The mitochondrial oxidoreductase CHCHD4 is present in a semi-oxidized state in vivo. *Redox Biol,* 17**,** 200-206.

ERDOGAN, A. J. & RIEMER, J. (2017): Mitochondrial disulfide relay and its substrates: mechanisms in health and disease. *Cell Tissue Res,* 367**,** 59-72.

ESTEBAN-REDONDO, I. & INNES, E. A. (1997): Toxoplasma gondii infection in sheep and cattle. *Comp Immunol Microbiol Infect Dis,* 20**,** 191-6.

FARRELL, S. R. & THORPE, C. (2005): Augmenter of liver regeneration: a flavin-dependent sulfhydryl oxidase with cytochrome c reductase activity. *Biochemistry,* 44**,** 1532-41.

FARVER, O., VITU, E., WHERLAND, S., FASS, D. & PECHT, I. (2009): Electron transfer reactivity of the Arabidopsis thaliana sulfhydryl oxidase AtErv1. *J Biol Chem,* 284**,** 2098-105.

FASS, D. (2008): The Erv family of sulfhydryl oxidases. *Biochim Biophys Acta,* 1783**,** 557-66.

FIC, E., KEDRACKA-KROK, S., JANKOWSKA, U., PIROG, A. & DZIEDZICKA-WASYLEWSKA, M. (2010): Comparison of protein precipitation methods for various rat brain structures prior to proteomic analysis. *Electrophoresis,* 31**,** 3573-9.

FIDALGO, L. M. & GILLE, L. (2011): Mitochondria and trypanosomatids: targets and drugs. *Pharm Res,* 28**,** 2758-70.

FISCHER, M., HORN, S., BELKACEMI, A., KOJER, K., PETRUNGARO, C., HABICH, M., ALI, M., KUTTNER, V., BIEN, M., KAUFF, F., DENGJEL, J., HERRMANN, J. M. & RIEMER, J. (2013): Protein import and oxidative folding in the mitochondrial intermembrane space of intact mammalian cells. *Mol Biol Cell,* 24**,** 2160-70.

FLIS, V. V. & DAUM, G. (2013): Lipid transport between the endoplasmic reticulum and mitochondria. *Cold Spring Harb Perspect Biol,* 5.

FLOHE, L. (2012): The trypanothione system and the opportunities it offers to create drugs for the neglected kinetoplast diseases. *Biotechnol Adv,* 30**,** 294-301.

FREY, T. G. & MANNELLA, C. A. (2000): The internal structure of mitochondria. *Trends Biochem Sci,* 25**,** 319-24.

FRIEDMAN, J. R. & NUNNARI, J. (2014): Mitochondrial form and function. *Nature,* 505**,** 335-43.

FRY, M. & PUDNEY, M. (1992): Site of action of the antimalarial hydroxynaphthoquinone, 2-[trans-4-(4'-chlorophenyl) cyclohexyl]-3-hydroxy-1,4-naphthoquinone (566C80). *Biochem Pharmacol,* 43**,** 1545-53.

GABRIEL, K., MILENKOVIC, D., CHACINSKA, A., MULLER, J., GUIARD, B., PFANNER, N. & MEISINGER, C. (2007): Novel mitochondrial intermembrane space proteins as substrates of the MIA import pathway. *J Mol Biol,* 365**,** 612-20.

GARDNER, M. J., HALL, N., FUNG, E., WHITE, O., BERRIMAN, M., HYMAN, R. W., CARLTON, J. M., PAIN, A., NELSON, K. E., BOWMAN, S., PAULSEN, I. T., JAMES, K., EISEN, J. A., RUTHERFORD, K., SALZBERG, S. L., CRAIG, A., KYES, S., CHAN, M. S., NENE, V., SHALLOM, S. J., SUH, B., PETERSON, J., ANGIUOLI, S., PERTEA, M., ALLEN, J., SELENGUT, J., HAFT, D., MATHER, M. W., VAIDYA, A. B., MARTIN, D. M., FAIRLAMB, A. H., FRAUNHOLZ, M. J., ROOS, D. S., RALPH, S. A., MCFADDEN, G. I., CUMMINGS, L. M., SUBRAMANIAN, G. M., MUNGALL, C., VENTER, J. C., CARUCCI, D. J., HOFFMAN, S. L., NEWBOLD, C., DAVIS, R. W., FRASER, C. M. & BARRELL, B. (2002): Genome sequence of the human malaria parasite Plasmodium falciparum. *Nature,* 419**,** 498-511.

GERBER, J., MUHLENHOFF, U., HOFHAUS, G., LILL, R. & LISOWSKY, T. (2001): Yeast ERV2p is the first microsomal FAD-linked sulfhydryl oxidase of the Erv1p/Alrp protein family. *J Biol Chem,* 276**,** 23486-91.

GIETZ, R. D. & SCHIESTL, R. H. (2007a): High-efficiency yeast transformation using the LiAc/SS carrier DNA/PEG method. *Nat Protoc,* 2**,** 31-4.

GIETZ, R. D. & SCHIESTL, R. H. (2007b): Quick and easy yeast transformation using the LiAc/SS carrier DNA/PEG method. *Nat Protoc,* 2**,** 35-7.

GLICK, B. S., BRANDT, A., CUNNINGHAM, K., MULLER, S., HALLBERG, R. L. & SCHATZ, G. (1992): Cytochromes c1 and b2 are sorted to the intermembrane space of yeast mitochondria by a stop-transfer mechanism. *Cell,* 69**,** 809-22.

GOMEZ-EICHELMANN, M. C., HOLZ, G., JR., BEACH, D., SIMPSON, A. M. & SIMPSON, L. (1988): Comparison of several lizard Leishmania species and strains in terms of kinetoplast minicircle and maxicircle DNA sequences, nuclear chromosomes, and membrane lipids. *Mol Biochem Parasitol,* 27**,** 143-58.

GOODMAN, C. D., BUCHANAN, H. D. & MCFADDEN, G. I. (2017): Is the Mitochondrion a Good Malaria Drug Target? *Trends Parasitol,* 33**,** 185-193.

GOSSAGE, S. M., ROGERS, M. E. & BATES, P. A. (2003): Two separate growth phases during the development of Leishmania in sand flies: implications for understanding the life cycle. *Int J Parasitol,* 33**,** 1027-34.

GRAY, M. W., LANG, B. F. & BURGER, G. (2004): Mitochondria of protists. *Annu Rev Genet,* 38**,** 477-524.

GREENWOOD, B. M., FIDOCK, D. A., KYLE, D. E., KAPPE, S. H., ALONSO, P. L., COLLINS, F. H. & DUFFY, P. E. (2008): Malaria: progress, perils, and prospects for eradication. *J Clin Invest,* 118**,** 1266-76.

GROSS, E., SEVIER, C. S., VALA, A., KAISER, C. A. & FASS, D. (2002): A new FAD-binding fold and intersubunit disulfide shuttle in the thiol oxidase Erv2p. *Nat Struct Biol,* 9**,** 61-7.

GROSS, J. & BHATTACHARYA, D. (2009): Mitochondrial and plastid evolution in eukaryotes: an outsiders' perspective. *Nat Rev Genet,* 10**,** 495-505.

GRUMBT, B., STROOBANT, V., TERZIYSKA, N., ISRAEL, L. & HELL, K. (2007): Functional characterization of Mia40p, the central component of the disulfide relay system of the mitochondrial intermembrane space. *J Biol Chem,* 282**,** 37461-70.

GUO, P. C., MA, J. D., JIANG, Y. L., WANG, S. J., BAO, Z. Z., YU, X. J., CHEN, Y. & ZHOU, C. Z. (2012): Structure of yeast sulfhydryl oxidase erv1 reveals electron transfer of the disulfide relay system in the mitochondrial intermembrane space. *J Biol Chem,* 287**,** 34961-9.

HAINDRICH, A. C., BOUDOVA, M., VANCOVA, M., DIAZ, P. P., HORAKOVA, E. & LUKES, J. (2017): The intermembrane space protein Erv1 of Trypanosoma brucei is essential for mitochondrial Fe-S cluster assembly and operates alone. *Mol Biochem Parasitol,* 214**,** 47-51.

HANSEN, R. E. & WINTHER, J. R. (2009): An introduction to methods for analyzing thiols and disulfides: Reactions, reagents, and practical considerations. *Anal Biochem,* 394**,** 147-58.

HARBAUER, A. B., ZAHEDI, R. P., SICKMANN, A., PFANNER, N. & MEISINGER, C. (2014): The protein import machinery of mitochondria-a regulatory hub in metabolism, stress, and disease. *Cell Metab,* 19**,** 357-72.

HARNER, M., KORNER, C., WALTHER, D., MOKRANJAC, D., KAESMACHER, J., WELSCH, U., GRIFFITH, J., MANN, M., REGGIORI, F. & NEUPERT, W. (2011): The mitochondrial contact site complex, a determinant of mitochondrial architecture. *Embo j,* 30**,** 4356-70.

HEATH-ENGEL, H. M. & SHORE, G. C. (2006): Mitochondrial membrane dynamics, cristae remodelling and apoptosis. *Biochim Biophys Acta,* 1763**,** 549-60.

HECKLER, E. J., CRASSOUS, P. A., BASKARAN, P. & BEUVE, A. (2013): Protein disulfide-isomerase interacts with soluble guanylyl cyclase via a redox-based mechanism and modulates its activity. *Biochem J,* 452**,** 161-9.

HELL, K. (2008): The Erv1-Mia40 disulfide relay system in the intermembrane space of mitochondria. *Biochim Biophys Acta,* 1783**,** 601-9.

HERRMANN, J. M. & HELL, K. (2005): Chopped, trapped or tacked--protein translocation into the IMS of mitochondria. *Trends Biochem Sci,* 30**,** 205-11.

HERRMANN, J. M. & KOHL, R. (2007): Catch me if you can! Oxidative protein trapping in the intermembrane space of mitochondria. *J Cell Biol,* 176**,** 559-63.

HERWALDT, B. L. (1999): Leishmaniasis. *Lancet,* 354**,** 1191-9.

HIDE, M., RITLENG, A. S., BRIZARD, J. P., MONTE-ALLEGRE, A. & SERENO, D. (2008): Leishmania infantum: tuning digitonin fractionation for comparative proteomic of the mitochondrial protein content. *Parasitol Res,* 103**,** 989-92.

HILL, K., MODEL, K., RYAN, M. T., DIETMEIER, K., MARTIN, F., WAGNER, R. & PFANNER, N. (1998): Tom40 forms the hydrophilic channel of the mitochondrial import pore for preproteins [see comment]. *Nature,* 395**,** 516-21.

HOFHAUS, G., LEE, J.-E., TEWS, I., ROSENBERG, B. & LISOWSKY, T. (2003): The N-terminal cysteine pair of yeast sulfhydryl oxidase Erv1p is essential for in vivo activity and interacts with the primary redox centre. *European Journal of Biochemistry,* 270**,** 1528-1535.

HOFHAUS, G., STEIN, G., POLIMENO, L., FRANCAVILLA, A. & LISOWSKY, T. (1999): Highly divergent amino termini of the homologous human ALR and yeast scERV1 gene products define species specific differences in cellular localization. *European Journal of Cell Biology,* 78**,** 349-356.

HOFMANN, S., ROTHBAUER, U., MUHLENBEIN, N., BAIKER, K., HELL, K. & BAUER, M. F. (2005): Functional and mutational characterization of human MIA40 acting during import into the mitochondrial intermembrane space. *J Mol Biol,* 353**,** 517-28.

HOPPINS, S. & NUNNARI, J. (2009): The molecular mechanism of mitochondrial fusion. *Biochim Biophys Acta,* 1793**,** 20-6.

HSU, P. D., SCOTT, D. A., WEINSTEIN, J. A., RAN, F. A., KONERMANN, S., AGARWALA, V., LI, Y., FINE, E. J., WU, X., SHALEM, O., CRADICK, T. J., MARRAFFINI, L. A., BAO, G. & ZHANG, F. (2013): DNA targeting specificity of RNA-guided Cas9 nucleases. *Nat Biotechnol,* 31**,** 827-32.

HU, J., DONG, L. & OUTTEN, C. E. (2008): The redox environment in the mitochondrial intermembrane space is maintained separately from the cytosol and matrix. *J Biol Chem,* 283**,** 29126-34.

JACOT, D., WALLER, R. F., SOLDATI-FAVRE, D., MACPHERSON, D. A. & MACRAE, J. I. (2016): Apicomplexan Energy Metabolism: Carbon Source Promiscuity and the Quiescence Hyperbole. *Trends Parasitol,* 32**,** 56-70.

KALLERGI, E., ANDREADAKI, M., KRITSILIGKOU, P., KATRAKILI, N., POZIDIS, C., TOKATLIDIS, K., BANCI, L., BERTINI, I., CEFARO, C., CIOFI-BAFFONI, S., GAJDA, K. & PERUZZINI, R. (2012): Targeting and maturation of Erv1/ALR in the mitochondrial intermembrane space. *ACS Chem Biol,* 7**,** 707-14.

KAWANO, S., YAMANO, K., NAOE, M., MOMOSE, T., TERAO, K., NISHIKAWA, S., WATANABE, N. & ENDO, T. (2009): Structural basis of yeast Tim40/Mia40 as an oxidative translocator in the mitochondrial intermembrane space. *Proc Natl Acad Sci U S A,* 106**,** 14403-7.

KITA, K., NIHEI, C. & TOMITSUKA, E. (2003): Parasite mitochondria as drug target: diversity and dynamic changes during the life cycle. *Curr Med Chem,* 10**,** 2535-48.

KOCH, J. R. & SCHMID, F. X. (2014a): Mia40 combines thiol oxidase and disulfide isomerase activity to efficiently catalyze oxidative folding in mitochondria. *J Mol Biol,* 426**,** 4087-4098.

KOCH, J. R. & SCHMID, F. X. (2014b): Mia40 targets cysteines in a hydrophobic environment to direct oxidative protein folding in the mitochondria. *Nat Commun,* 5**,** 3041.

KOEHLER, C. M., JAROSCH, E., TOKATLIDIS, K., SCHMID, K., SCHWEYEN, R. J. & SCHATZ, G. (1998): Import of mitochondrial carriers mediated by essential proteins of the intermembrane space. *Science,* 279**,** 369-73.

KOEHLER, C. M. & TIENSON, H. L. (2009): Redox regulation of protein folding in the mitochondrial intermembrane space. *Biochim Biophys Acta,* 1793**,** 139-45.

KOJER, K., BIEN, M., GANGEL, H., MORGAN, B., DICK, T. P. & RIEMER, J. (2012): Glutathione redox potential in the mitochondrial intermembrane space is linked to the cytosol and impacts the Mia40 redox state. *Embo j,* 31**,** 3169-82.

KOJER, K., PELEH, V., CALABRESE, G., HERRMANN, J. M. & RIEMER, J. (2015): Kinetic control by limiting glutaredoxin amounts enables thiol oxidation in the reducing mitochondrial intermembrane space. *Mol Biol Cell,* 26**,** 195-204.

KOTLOFF, K. L., NATARO, J. P., BLACKWELDER, W. C., NASRIN, D., FARAG, T. H., PANCHALINGAM, S., WU, Y., SOW, S. O., SUR, D., BREIMAN, R. F., FARUQUE, A. S., ZAIDI, A. K., SAHA, D., ALONSO, P. L., TAMBOURA, B., SANOGO, D., ONWUCHEKWA, U., MANNA, B., RAMAMURTHY, T., KANUNGO, S., OCHIENG, J. B., OMORE, R., OUNDO, J. O., HOSSAIN, A., DAS, S. K., AHMED, S., QURESHI, S., QUADRI, F., ADEGBOLA, R. A., ANTONIO, M., HOSSAIN, M. J., AKINSOLA, A., MANDOMANDO, I., NHAMPOSSA, T., ACACIO, S., BISWAS, K., O'REILLY, C. E., MINTZ, E. D., BERKELEY, L. Y., MUHSEN, K., SOMMERFELT, H., ROBINS-BROWNE, R. M. & LEVINE, M. M. (2013): Burden and aetiology of diarrhoeal disease in infants and young children in developing countries (the Global Enteric Multicenter Study, GEMS): a prospective, case-control study. *Lancet,* 382**,** 209-22.

LAEMMLI, U. K. (1970): Cleavage of structural proteins during the assembly of the head of bacteriophage T4. *Nature,* 227**,** 680-5.

LAMBROS, C. & VANDERBERG, J. P. (1979): Synchronization of Plasmodium falciparum erythrocytic stages in culture. *J Parasitol,* 65**,** 418-20.

LANGE, H., LISOWSKY, T., GERBER, J., MUHLENHOFF, U., KISPAL, G. & LILL, R. (2001): An essential function of the mitochondrial sulfhydryl oxidase Erv1p/ALR in the maturation of cytosolic Fe/S proteins. *EMBO Rep,* 2**,** 715-20.

LARSSON, N. G. (2010): Somatic mitochondrial DNA mutations in mammalian aging. *Annu Rev Biochem,* 79**,** 683-706.

LEE, J., HOFHAUS, G. & LISOWSKY, T. (2000): Erv1p from Saccharomyces cerevisiae is a FAD-linked sulfhydryl oxidase. *FEBS Lett,* 477**,** 62-6.

LEVITAN, A., DANON, A. & LISOWSKY, T. (2004): Unique features of plant mitochondrial sulfhydryl oxidase. *J Biol Chem,* 279**,** 20002-8.

LI, W., MO, W., SHEN, D., SUN, L., WANG, J., LU, S., GITSCHIER, J. M. & ZHOU, B. (2005): Yeast model uncovers dual roles of mitochondria in action of artemisinin. *PLoS Genet,* 1**,** e36.

LIEDGENS, L. 2018. *Investigation of oxidative protein foldingin protist mitochondria and elucidation of the catalytic mechanism of glutaredoxins.* Doctor of Natural Sciences Dissertation, Ruperto Carola University of Heidelberg.

LISOWSKY, T. (1992): Dual function of a new nuclear gene for oxidative phosphorylation and vegetative growth in yeast. *Mol Gen Genet,* 232**,** 58-64.

LISOWSKY, T. (1994): ERV1 is involved in the cell-division cycle and the maintenance of mitochondrial genomes in Saccharomyces cerevisiae. *Curr Genet,* 26**,** 15-20.

LISOWSKY, T., LEE, J. E., POLIMENO, L., FRANCAVILLA, A. & HOFHAUS, G. (2001): Mammalian augmenter of liver regeneration protein is a sulfhydryl oxidase. *Dig Liver Dis,* 33**,** 173-80.

LITHGOW, T. & SCHNEIDER, A. (2010): Evolution of macromolecular import pathways in mitochondria, hydrogenosomes and mitosomes. *Philos Trans R Soc Lond B Biol Sci,* 365**,** 799-817.

LIU, L., JOHNSON, H. L., COUSENS, S., PERIN, J., SCOTT, S., LAWN, J. E., RUDAN, I., CAMPBELL, H., CIBULSKIS, R., LI, M., MATHERS, C. & BLACK, R. E. (2012): Global, regional, and national causes of child mortality: an updated systematic analysis for 2010 with time trends since 2000. *Lancet,* 379**,** 2151-61.

LONGEN, S., WOELLHAF, M. W., PETRUNGARO, C., RIEMER, J. & HERRMANN, J. M. (2014): The disulfide relay of the intermembrane space oxidizes the ribosomal subunit mrp10 on its transit into the mitochondrial matrix. *Dev Cell,* 28**,** 30-42.

LOOKE, M., KRISTJUHAN, K. & KRISTJUHAN, A. (2011): Extraction of genomic DNA from yeasts for PCR-based applications. *Biotechniques,* 50**,** 325-8.

LOZANO, R., NAGHAVI, M., FOREMAN, K., LIM, S., SHIBUYA, K., ABOYANS, V., ABRAHAM, J., ADAIR, T., AGGARWAL, R., AHN, S. Y., ALVARADO, M., ANDERSON, H. R., ANDERSON, L. M., ANDREWS, K. G., ATKINSON, C., BADDOUR, L. M., BARKER-COLLO, S., BARTELS, D. H., BELL, M. L., BENJAMIN, E. J., BENNETT, D., BHALLA, K., BIKBOV, B., BIN ABDULHAK, A., BIRBECK, G., BLYTH, F., BOLLIGER, I., BOUFOUS, S., BUCELLO, C., BURCH, M., BURNEY, P., CARAPETIS, J., CHEN, H., CHOU, D., CHUGH, S. S., COFFENG, L. E., COLAN, S. D., COLQUHOUN, S., COLSON, K. E., CONDON, J., CONNOR, M. D., COOPER, L. T., CORRIERE, M., CORTINOVIS, M., DE VACCARO, K. C., COUSER, W., COWIE, B. C., CRIQUI, M. H., CROSS, M., DABHADKAR, K. C., DAHODWALA, N., DE LEO, D., DEGENHARDT, L., DELOSSANTOS, A., DENENBERG, J., DES JARLAIS, D. C., DHARMARATNE, S. D., DORSEY, E. R., DRISCOLL, T., DUBER, H., EBEL, B., ERWIN, P. J., ESPINDOLA, P., EZZATI, M., FEIGIN, V., FLAXMAN, A. D., FOROUZANFAR, M. H., FOWKES, F. G., FRANKLIN, R., FRANSEN, M., FREEMAN, M. K., GABRIEL, S. E., GAKIDOU, E., GASPARI, F., GILLUM, R. F., GONZALEZ-MEDINA, D., HALASA, Y. A., HARING, D., HARRISON, J. E., HAVMOELLER, R., HAY, R. J., HOEN, B., HOTEZ, P. J., HOY, D., JACOBSEN, K. H., JAMES, S. L., JASRASARIA, R., JAYARAMAN, S., JOHNS, N., KARTHIKEYAN, G., KASSEBAUM, N., KEREN, A., KHOO, J. P., KNOWLTON, L. M., KOBUSINGYE, O., KORANTENG, A., KRISHNAMURTHI, R., LIPNICK, M., LIPSHULTZ, S. E., OHNO, S. L., et al. (2012): Global and regional mortality from 235 causes of death for 20 age groups in 1990 and 2010: a systematic analysis for the Global Burden of Disease Study 2010. *Lancet,* 380**,** 2095-128.

LUKES, J., GUILBRIDE, D. L., VOTYPKA, J., ZIKOVA, A., BENNE, R. & ENGLUND, P. T. (2002): Kinetoplast DNA network: evolution of an improbable structure. *Eukaryot Cell,* 1**,** 495-502.

MACRAE, J. I., DIXON, M. W., DEARNLEY, M. K., CHUA, H. H., CHAMBERS, J. M., KENNY, S., BOTTOVA, I., TILLEY, L. & MCCONVILLE, M. J. (2013): Mitochondrial metabolism of sexual and asexual blood stages of the malaria parasite Plasmodium falciparum. *BMC Biol,* 11**,** 67.

MANI, J., DESY, S., NIEMANN, M., CHANFON, A., OELJEKLAUS, S., PUSNIK, M., SCHMIDT, O., GERBETH, C., MEISINGER, C., WARSCHEID, B. & SCHNEIDER, A. (2015): Mitochondrial protein import receptors in Kinetoplastids reveal convergent evolution over large phylogenetic distances. *Nat Commun,* 6**,** 6646.

MANI, J., ROUT, S., DESY, S. & SCHNEIDER, A. (2017): Mitochondrial protein import - Functional analysis of the highly diverged Tom22 orthologue of Trypanosoma brucei. *Sci Rep,* 7**,** 40738.

MARTIN, J., MAHLKE, K. & PFANNER, N. (1991): Role of an energized inner membrane in mitochondrial protein import. Delta psi drives the movement of presequences. *J Biol Chem,* 266**,** 18051-7.

MATHER, M. W., HENRY, K. W. & VAIDYA, A. B. (2007): Mitochondrial drug targets in apicomplexan parasites. *Curr Drug Targets,* 8**,** 49-60.

MEHTA, A. & SHAHA, C. (2004): Apoptotic death in Leishmania donovani promastigotes in response to respiratory chain inhibition: complex II inhibition results in increased pentamidine cytotoxicity. *J Biol Chem,* 279**,** 11798-813.

MEIER, S., NEUPERT, W. & HERRMANN, J. M. (2005): Proline residues of transmembrane domains determine the sorting of inner membrane proteins in mitochondria. *J Cell Biol,* 170**,** 881-8.

MEISINGER, C., RYAN, M. T., HILL, K., MODEL, K., LIM, J. H., SICKMANN, A., MULLER, H., MEYER, H. E., WAGNER, R. & PFANNER, N. (2001): Protein import channel of the outer mitochondrial membrane: a highly stable Tom40-Tom22 core structure differentially interacts with preproteins, small tom proteins, and import receptors. *Mol Cell Biol,* 21**,** 2337-48.

MERMELEKAS, G., MAKRIDAKIS, M., KOECK, T. & VLAHOU, A. (2013): Redox proteomics: from residue modifications to putative biomarker identification by gel- and LC-MS-based approaches. *Expert Rev Proteomics,* 10**,** 537-49.

MESECKE, N., TERZIYSKA, N., KOZANY, C., BAUMANN, F., NEUPERT, W., HELL, K. & HERRMANN, J. M. (2005): A disulfide relay system in the intermembrane space of mitochondria that mediates protein import. *Cell,* 121**,** 1059-69.

MILLER, W. L. (2013): Steroid hormone synthesis in mitochondria. *Mol Cell Endocrinol,* 379**,** 62-73.

MISHRA, P. & CHAN, D. C. (2014): Mitochondrial dynamics and inheritance during cell division, development and disease. *Nat Rev Mol Cell Biol,* 15**,** 634-46.

MOTTA, M. C. (2008): Kinetoplast as a potential chemotherapeutic target of trypanosomatids. *Curr Pharm Des,* 14**,** 847-54.

NAING, C., WHITTAKER, M. A., NYUNT WAI, V. & MAK, J. W. (2014): Is Plasmodium vivax malaria a severe malaria?: a systematic review and meta-analysis. *PLoS Negl Trop Dis,* 8**,** e3071.

NAKAO, L. S., EVERLEY, R. A., MARINO, S. M., LO, S. M., DE SOUZA, L. E., GYGI, S. P. & GLADYSHEV, V. N. (2015): Mechanism-based proteomic screening identifies targets of thioredoxin-like proteins. *J Biol Chem,* 290**,** 5685-95.

NAOE, M., OHWA, Y., ISHIKAWA, D., OHSHIMA, C., NISHIKAWA, S., YAMAMOTO, H. & ENDO, T. (2004): Identification of Tim40 that mediates protein sorting to the mitochondrial intermembrane space. *J Biol Chem,* 279**,** 47815-21.

NEUPERT, W. & HERRMANN, J. M. (2007): Translocation of proteins into mitochondria. *Annu Rev Biochem,* 76**,** 723-49.

NIEMANN, M., WIESE, S., MANI, J., CHANFON, A., JACKSON, C., MEISINGER, C., WARSCHEID, B. & SCHNEIDER, A. (2013): Mitochondrial outer membrane proteome of Trypanosoma brucei reveals novel factors required to maintain mitochondrial morphology. *Mol Cell Proteomics,* 12**,** 515-28.

OCANA, K. A. & DAVILA, A. M. (2011): Phylogenomics-based reconstruction of protozoan species tree. *Evol Bioinform Online,* 7**,** 107-21.

OKAMOTO, K. & SHAW, J. M. (2005): Mitochondrial morphology and dynamics in yeast and multicellular eukaryotes. *Annu Rev Genet,* 39**,** 503-36.

OLSZEWSKA, A. & SZEWCZYK, A. (2013): Mitochondria as a pharmacological target: magnum overview. *IUBMB Life,* 65**,** 273-81.

PAGANI, M., FABBRI, M., BENEDETTI, C., FASSIO, A., PILATI, S., BULLEID, N. J., CABIBBO, A. & SITIA, R. (2000): Endoplasmic reticulum oxidoreductin 1-lbeta (ERO1-Lbeta), a human gene induced in the course of the unfolded protein response. *J Biol Chem,* 275**,** 23685-92.

PAINTER, H. J., MORRISEY, J. M., MATHER, M. W. & VAIDYA, A. B. (2007): Specific role of mitochondrial electron transport in blood-stage Plasmodium falciparum. *Nature,* 446**,** 88-91.

PEIKERT, C. D., MANI, J., MORGENSTERN, M., KASER, S., KNAPP, B., WENGER, C., HARSMAN, A., OELJEKLAUS, S., SCHNEIDER, A. & WARSCHEID, B. (2017): Charting organellar importomes by quantitative mass spectrometry. *Nat Commun,* 8**,** 15272.

PELEH, V., CORDAT, E. & HERRMANN, J. M. (2016): Mia40 is a trans-site receptor that drives protein import into the mitochondrial intermembrane space by hydrophobic substrate binding. *Elife,* 5.

PELEH, V., RIEMER, J., DANCIS, A. & HERRMANN, J. M. (2014): Protein oxidation in the intermembrane space of mitochondria is substrate-specific rather than general. *Microb Cell,* 1**,** 81-93.

PELEH, V., ZANNINI, F., BACKES, S., ROUHIER, N. & HERRMANN, J. M. (2017): Erv1 of Arabidopsis thaliana can directly oxidize mitochondrial intermembrane space proteins in the absence of redox-active Mia40. *BMC Biol,* 15**,** 106.

PELLEGRINI, L. & SCORRANO, L. (2007): A cut short to death: Parl and Opa1 in the regulation of mitochondrial morphology and apoptosis. *Cell Death Differ,* 14**,** 1275-84.

PEREIRA, K. S., SCHMIDT, F. L., BARBOSA, R. L., GUARALDO, A. M., FRANCO, R. M., DIAS, V. L. & PASSOS, L. A. (2010): Transmission of chagas disease (American trypanosomiasis) by food. *Adv Food Nutr Res,* 59**,** 63-85.

PETERS, J. M., CHEN, N., GATTON, M., KORSINCZKY, M., FOWLER, E. V., MANZETTI, S., SAUL, A. & CHENG, Q. (2002): Mutations in cytochrome b resulting in atovaquone resistance are associated with loss of fitness in Plasmodium falciparum. *Antimicrob Agents Chemother,* 46**,** 2435-41.

PONTE-SUCRE, A. (2016): An Overview of Trypanosoma brucei Infections: An Intense Host-Parasite Interaction. *Front Microbiol,* 7**,** 2126.

PRUDENCIO, M., RODRIGUEZ, A. & MOTA, M. M. (2006): The silent path to thousands of merozoites: the Plasmodium liver stage. *Nat Rev Microbiol,* 4**,** 849-56.

PUSNIK, M., MANI, J., SCHMIDT, O., NIEMANN, M., OELJEKLAUS, S., SCHNARWILER, F., WARSCHEID, B., LITHGOW, T., MEISINGER, C. & SCHNEIDER, A. (2012): An essential novel component of the noncanonical mitochondrial outer membrane protein import system of trypanosomatids. *Mol Biol Cell,* 23**,** 3420-8.

PUSNIK, M., SCHMIDT, O., PERRY, A. J., OELJEKLAUS, S., NIEMANN, M., WARSCHEID, B., LITHGOW, T., MEISINGER, C. & SCHNEIDER, A. (2011): Mitochondrial preprotein translocase of trypanosomatids has a bacterial origin. *Curr Biol,* 21**,** 1738-43.

RICH, P. R. & MARECHAL, A. (2010): The mitochondrial respiratory chain. *Essays Biochem,* 47**,** 1-23.

RIEMER, J., BULLEID, N. & HERRMANN, J. M. (2009): Disulfide formation in the ER and mitochondria: two solutions to a common process. *Science,* 324**,** 1284-7.

RISSLER, M., WIEDEMANN, N., PFANNSCHMIDT, S., GABRIEL, K., GUIARD, B., PFANNER, N. & CHACINSKA, A. (2005): The essential mitochondrial protein Erv1 cooperates with Mia40 in biogenesis of intermembrane space proteins. *J Mol Biol,* 353**,** 485-92.

ROY, M., REDDY, P. H., IIJIMA, M. & SESAKI, H. (2015): Mitochondrial division and fusion in metabolism. *Curr Opin Cell Biol,* 33**,** 111-8.

ROZHKOVA, A., STIRNIMANN, C. U., FREI, P., GRAUSCHOPF, U., BRUNISHOLZ, R., GRUTTER, M. G., CAPITANI, G. & GLOCKSHUBER, R. (2004): Structural basis and kinetics of inter- and intramolecular disulfide exchange in the redox catalyst DsbD. *Embo j,* 23**,** 1709-19.

RUDYK, O. & EATON, P. (2014): Biochemical methods for monitoring protein thiol redox states in biological systems. *Redox Biol,* 2**,** 803-13.

SAADATNIA, G. & GOLKAR, M. (2012): A review on human toxoplasmosis. *Scand J Infect Dis,* 44**,** 805-14.

SANDS, M., KRON, M. A. & BROWN, R. B. (1985): Pentamidine: a review. *Rev Infect Dis,* 7**,** 625-34.

SAZANOV, L. A. (2015): A giant molecular proton pump: structure and mechanism of respiratory complex I. *Nat Rev Mol Cell Biol,* 16**,** 375-88.

SCHARWEY, M., TATSUTA, T. & LANGER, T. (2013): Mitochondrial lipid transport at a glance. *J Cell Sci,* 126**,** 5317-23.

SCHEIBYE-KNUDSEN, M., FANG, E. F., CROTEAU, D. L., WILSON, D. M., 3RD & BOHR, V. A. (2015): Protecting the mitochondrial powerhouse. *Trends Cell Biol,* 25**,** 158-70.

SCHMIDT, O., PFANNER, N. & MEISINGER, C. (2010): Mitochondrial protein import: from proteomics to functional mechanisms. *Nat Rev Mol Cell Biol,* 11**,** 655-67.

SCHNEIDER, A., BURSAC, D. & LITHGOW, T. (2008): The direct route: a simplified pathway for protein import into the mitochondrion of trypanosomes. *Trends Cell Biol,* 18**,** 12-8.

SEN, N. & MAJUMDER, H. K. (2008): Mitochondrion of protozoan parasite emerges as potent therapeutic target: exciting drugs are on the horizon. *Curr Pharm Des,* 14**,** 839-46.

SHAPIRO, T. A., KLEIN, V. A. & ENGLUND, P. T. (1989): Drug-promoted cleavage of kinetoplast DNA minicircles. Evidence for type II topoisomerase activity in trypanosome mitochondria. *J Biol Chem,* 264**,** 4173-8.

SIDERIS, D. P., PETRAKIS, N., KATRAKILI, N., MIKROPOULOU, D., GALLO, A., CIOFI-BAFFONI, S., BANCI, L., BERTINI, I. & TOKATLIDIS, K. (2009): A novel intermembrane space-targeting signal docks cysteines onto Mia40 during mitochondrial oxidative folding. *J Cell Biol,* 187**,** 1007-22.

SIDERIS, D. P. & TOKATLIDIS, K. (2007): Oxidative folding of small Tims is mediated by site-specific docking onto Mia40 in the mitochondrial intermembrane space. *Mol Microbiol,* 65**,** 1360-73.

SIMPSON, A. G. & ROGER, A. J. (2004): The real 'kingdoms' of eukaryotes. *Curr Biol,* 14**,** R693-6.

SINGHA, U. K., HAMILTON, V., DUNCAN, M. R., WEEMS, E., TRIPATHI, M. K. & CHAUDHURI, M. (2012): Protein translocase of mitochondrial inner membrane in Trypanosoma brucei. *J Biol Chem,* 287**,** 14480-93.

SINGHA, U. K., PEPRAH, E., WILLIAMS, S., WALKER, R., SAHA, L. & CHAUDHURI, M. (2008): Characterization of the mitochondrial inner membrane protein translocator Tim17 from Trypanosoma brucei. *Mol Biochem Parasitol,* 159**,** 30-43.

SIRRENBERG, C., BAUER, M. F., GUIARD, B., NEUPERT, W. & BRUNNER, M. (1996): Import of carrier proteins into the mitochondrial inner membrane mediated by Tim22. *Nature,* 384**,** 582-5.

SIRRENBERG, C., ENDRES, M., FOLSCH, H., STUART, R. A., NEUPERT, W. & BRUNNER, M. (1998): Carrier protein import into mitochondria mediated by the intermembrane proteins Tim10/Mrs11 and Tim12/Mrs5. *Nature,* 391**,** 912-5.

SPECHT, S., LIEDGENS, L., DUARTE, M., STIEGLER, A., WIRTH, U., EBERHARDT, M., TOMAS, A., HELL, K. & DEPONTE, M. (2018): A single-cysteine mutant and chimeras of essential Leishmania Erv can complement the loss of Erv1 but not of Mia40 in yeast. *Redox Biol,* 15**,** 363-374.

SRIVASTAVA, I. K., ROTTENBERG, H. & VAIDYA, A. B. (1997): Atovaquone, a broad spectrum antiparasitic drug, collapses mitochondrial membrane potential in a malarial parasite. *J Biol Chem,* 272**,** 3961-6.

SRIVASTAVA, I. K. & VAIDYA, A. B. (1999): A mechanism for the synergistic antimalarial action of atovaquone and proguanil. *Antimicrob Agents Chemother,* 43**,** 1334-9.

STEIN, G. & LISOWSKY, T. (1998): Functional comparison of the yeast scERV1 and scERV2 genes. *Yeast,* 14**,** 171-80.

STEINER, H., ZOLLNER, A., HAID, A., NEUPERT, W. & LILL, R. (1995): Biogenesis of mitochondrial heme lyases in yeast. Import and folding in the intermembrane space. *J Biol Chem,* 270**,** 22842-9.

STEMMER, M., THUMBERGER, T., DEL SOL KEYER, M., WITTBRODT, J. & MATEO, J. L. (2015): CCTop: An Intuitive, Flexible and Reliable CRISPR/Cas9 Target Prediction Tool. *PLoS One,* 10**,** e0124633.

STERNBERG, S. H., REDDING, S., JINEK, M., GREENE, E. C. & DOUDNA, J. A. (2014): DNA interrogation by the CRISPR RNA-guided endonuclease Cas9. *Nature,* 507**,** 62-7.

STOJANOVSKI, D., BRAGOSZEWSKI, P. & CHACINSKA, A. (2012): The MIA pathway: a tight bond between protein transport and oxidative folding in mitochondria. *Biochim Biophys Acta,* 1823**,** 1142-50.

STOJANOVSKI, D., MULLER, J. M., MILENKOVIC, D., GUIARD, B., PFANNER, N. & CHACINSKA, A. (2008): The MIA system for protein import into the mitochondrial intermembrane space. *Biochim Biophys Acta,* 1783**,** 610-7.

STUART, K. & PANIGRAHI, A. K. (2002): RNA editing: complexity and complications. *Mol Microbiol,* 45**,** 591-6.

SUTHERLAND, C. J., TANOMSING, N., NOLDER, D., OGUIKE, M., JENNISON, C., PUKRITTAYAKAMEE, S., DOLECEK, C., HIEN, T. T., DO ROSARIO, V. E., AREZ, A. P., PINTO, J., MICHON, P., ESCALANTE, A. A., NOSTEN, F., BURKE, M., LEE, R., BLAZE, M., OTTO, T. D., BARNWELL, J. W., PAIN, A., WILLIAMS, J., WHITE, N. J., DAY, N. P., SNOUNOU, G., LOCKHART, P. J., CHIODINI, P. L., IMWONG, M. & POLLEY, S. D. (2010): Two nonrecombining sympatric forms of the human malaria parasite Plasmodium ovale occur globally. *J Infect Dis,* 201**,** 1544-50.

SZTOLSZTENER, M. E., BREWINSKA, A., GUIARD, B. & CHACINSKA, A. (2013): Disulfide bond formation: sulfhydryl oxidase ALR controls mitochondrial biogenesis of human MIA40. *Traffic,* 14**,** 309-20.

TERZIYSKA, N., GRUMBT, B., BIEN, M., NEUPERT, W., HERRMANN, J. M. & HELL, K. (2007): The sulfhydryl oxidase Erv1 is a substrate of the Mia40-dependent protein translocation pathway. *FEBS Lett,* 581**,** 1098-102.

TERZIYSKA, N., GRUMBT, B., KOZANY, C. & HELL, K. (2009): Structural and functional roles of the conserved cysteine residues of the redox-regulated import receptor Mia40 in the intermembrane space of mitochondria. *J Biol Chem,* 284**,** 1353-63.

TERZIYSKA, N., LUTZ, T., KOZANY, C., MOKRANJAC, D., MESECKE, N., NEUPERT, W., HERRMANN, J. M. & HELL, K. (2005): Mia40, a novel factor for protein import into the intermembrane space of mitochondria is able to bind metal ions. *FEBS Lett,* 579**,** 179-84.

TORGERSON, P. R., DEVLEESSCHAUWER, B., PRAET, N., SPEYBROECK, N., WILLINGHAM, A. L., KASUGA, F., ROKNI, M. B., ZHOU, X. N., FEVRE, E. M., SRIPA, B., GARGOURI, N., FURST, T., BUDKE, C. M., CARABIN, H., KIRK, M. D., ANGULO, F. J., HAVELAAR, A. & DE SILVA, N. (2015): World Health Organization Estimates of the Global and Regional Disease Burden of 11 Foodborne Parasitic Diseases, 2010: A Data Synthesis. *PLoS Med,* 12**,** e1001920.

TORRES-GUERRERO, E., QUINTANILLA-CEDILLO, M. R., RUIZ-ESMENJAUD, J. & ARENAS, R. (2017): Leishmaniasis: a review. *F1000Res,* 6**,** 750.

TRAGER, W. & JENSEN, J. B. (1976): Human malaria parasites in continuous culture. *Science,* 193**,** 673-5.

VAIDYA, A. B., AKELLA, R. & SUPLICK, K. (1989): Sequences similar to genes for two mitochondrial proteins and portions of ribosomal RNA in tandemly arrayed 6-kilobase-pair DNA of a malarial parasite. *Mol Biochem Parasitol,* 35**,** 97-107.

VAIDYA, A. B. & MATHER, M. W. (2009): Mitochondrial evolution and functions in malaria parasites. *Annu Rev Microbiol,* 63**,** 249-67.

VAN WILPE, S., RYAN, M. T., HILL, K., MAARSE, A. C., MEISINGER, C., BRIX, J., DEKKER, P. J., MOCZKO, M., WAGNER, R., MEIJER, M., GUIARD, B., HONLINGER, A. & PFANNER, N. (1999): Tom22 is a multifunctional organizer of the mitochondrial preprotein translocase. *Nature,* 401**,** 485-9.

VERCESI, A. E., BERNARDES, C. F., HOFFMANN, M. E., GADELHA, F. R. & DOCAMPO, R. (1991): Digitonin permeabilization does not affect mitochondrial function and allows the determination of the mitochondrial membrane potential of Trypanosoma cruzi in situ. *J Biol Chem,* 266**,** 14431-4.

VERCESI, A. E. & DOCAMPO, R. (1992): Ca2+ transport by digitonin-permeabilized Leishmania donovani. Effects of Ca2+, pentamidine and WR-6026 on mitochondrial membrane potential in situ. *Biochem J,* 284 (Pt 2)**,** 463-7.

VITU, E., BENTZUR, M., LISOWSKY, T., KAISER, C. A. & FASS, D. (2006): Gain of function in an ERV/ALR sulfhydryl oxidase by molecular engineering of the shuttle disulfide. *J Mol Biol,* 362**,** 89-101.

VOGTLE, F. N., BURKHART, J. M., RAO, S., GERBETH, C., HINRICHS, J., MARTINOU, J. C., CHACINSKA, A., SICKMANN, A., ZAHEDI, R. P. & MEISINGER, C. (2012): Intermembrane space proteome of yeast mitochondria. *Mol Cell Proteomics,* 11**,** 1840-52.

WALTHER, D. M. & RAPAPORT, D. (2009): Biogenesis of mitochondrial outer membrane proteins. *Biochim Biophys Acta,* 1793**,** 42-51.

WEBB, C. T., GORMAN, M. A., LAZAROU, M., RYAN, M. T. & GULBIS, J. M. (2006): Crystal structure of the mitochondrial chaperone TIM9.10 reveals a six-bladed alpha-propeller. *Mol Cell,* 21**,** 123-33.

WHO 2012a. Global report for research on infectious diseases of poverty 2012. Geneva.

WHO 2012b. Research Priorities for Chagas Disease, Human African Trypanosomiasis and Leishmaniasis. Geneva: World Health Organization.

WHO 2014. World malaria report 2014. Geneva: World Health Organization.

WHO 2015. Investing to overcome the global impact of neglected tropical diseases: third WHO report on neglected diseases 2015. Geneva: World Health Organization.

WHO 2016. Weekly epidemiological record. 22 ed. Geneva.

WHO 2017a. Report of the second WHO stakeholders meeting on rhodesiense human African trypanosomiasis. Geneva: World Health Organization

WHO 2017b. World malaria report 2017. Geneva: World Health Organization.

WHO 2018. Summary of global update on provision of preventive chemotherapy in 2017 and progress towards ensuring timely supplies and management *In:* BISWAS, D. G. (ed.) *Weekly epidemiological record.* World Health Organization.

WIEDEMANN, N. & PFANNER, N. (2017): Mitochondrial Machineries for Protein Import and Assembly. *Annu Rev Biochem,* 86**,** 685-714.

WOJDYLA, K. & ROGOWSKA-WRZESINSKA, A. (2015): Differential alkylation-based redox proteomics--Lessons learnt. *Redox Biol,* 6**,** 240-52.

WROBEL, L., TOPF, U., BRAGOSZEWSKI, P., WIESE, S., SZTOLSZTENER, M. E., OELJEKLAUS, S., VARABYOVA, A., LIRSKI, M., CHROSCICKI, P., MROCZEK, S., JANUSZEWICZ, E., DZIEMBOWSKI, A., KOBLOWSKA, M., WARSCHEID, B. & CHACINSKA, A. (2015): Mistargeted mitochondrial proteins activate a proteostatic response in the cytosol. *Nature,* 524**,** 485-8.

WU, C. K., DAILEY, T. A., DAILEY, H. A., WANG, B. C. & ROSE, J. P. (2003): The crystal structure of augmenter of liver regeneration: A mammalian FAD-dependent sulfhydryl oxidase. *Protein Sci,* 12**,** 1109-18.

YAMAUCHI, L. M., COPPI, A., SNOUNOU, G. & SINNIS, P. (2007): Plasmodium sporozoites trickle out of the injection site. *Cell Microbiol,* 9**,** 1215-22.

YUSUF, J. J. (2017): Review on Bovine Babesiosis and its Economical Importance. *Journal of Veterinary Medicine and Research,* 4**,** 9.

7 Supplementary information

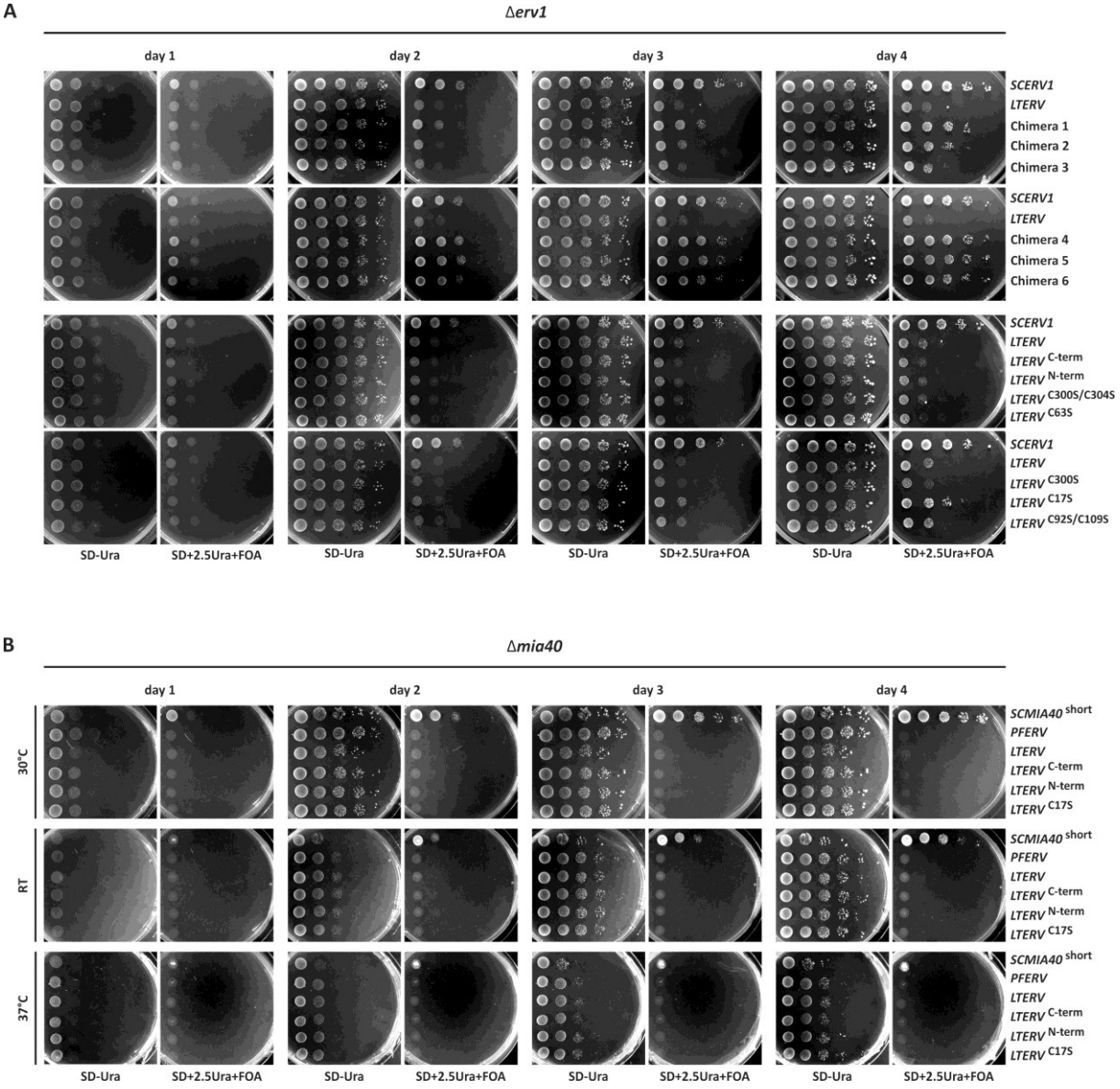

Supplementary figure 1 | Yeast *SCERV1* and *SCMIA40* complementation assays with chimeric, truncated, and mutant *LTERV*. Adapted from Specht *et al.* (2018).

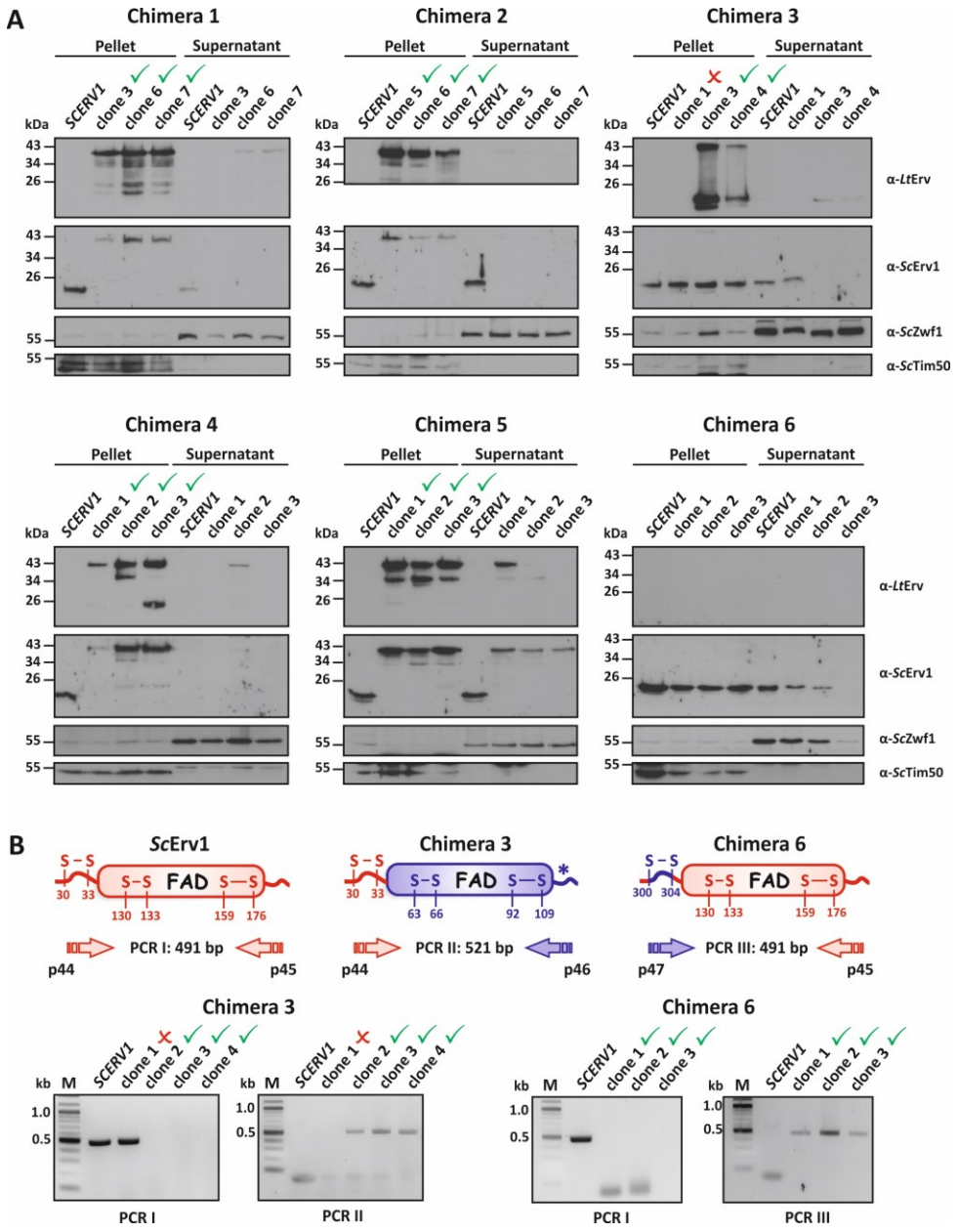

Supplementary figure 2 | Western blot and PCR analysis of Δ*erv1* yeast strains harbouring chimera 1-6. Adapted from Specht *et al.* (2018).

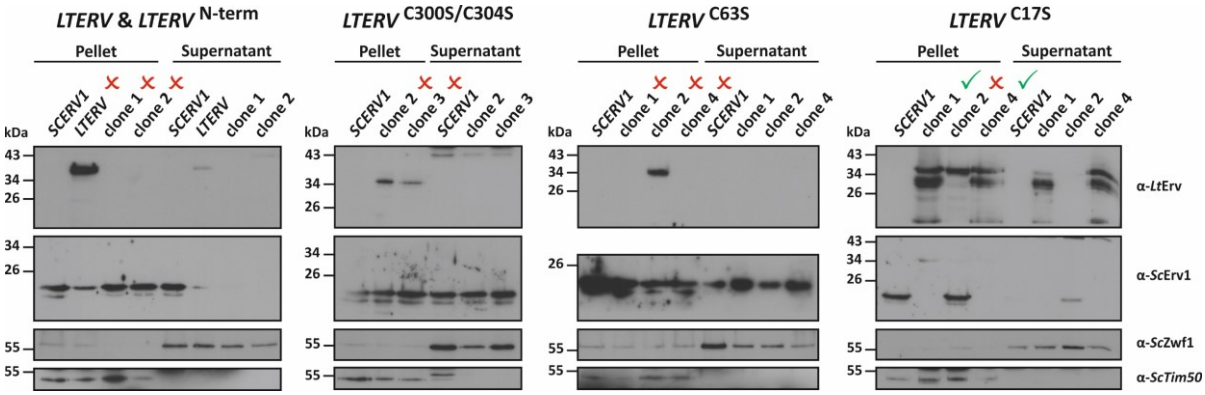

Supplementary figure 3 | Western blot analysis of Δ*erv1* yeast strains harbouring wildtype, truncated, and mutant *LTERV*. Adapted from Specht *et al.* (2018).

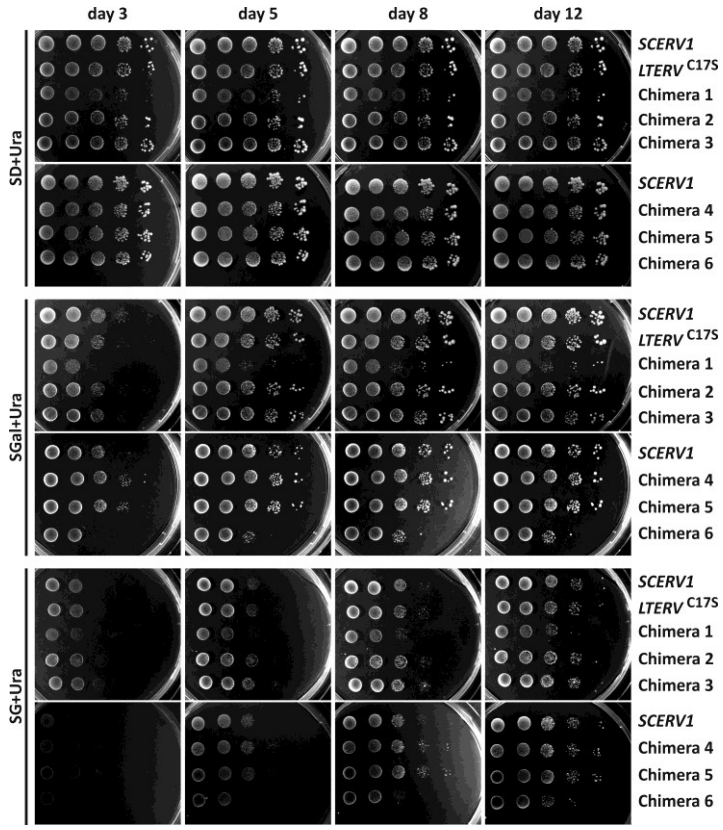

Supplementary figure 4 | Growth assays of Δ*erv1* yeast strains harbouring chimera 1-6 or *LTERV*^{C17S}. Adapted from Specht *et al.* (2018).